RELATIVE MOTION MODELING AND AUTONOMOUS NAVIGATION ACCURACY

K. T. Alfriend and S. R. Vadali

Texas Engineering Experiment Station
1470 William D. Fitch PKY
College Station, TX 77845-4645

15 Nov 2016

Final Report

AIR FORCE RESEARCH LABORATORY
Space Vehicles Directorate
3550 Aberdeen Ave SE
AIR FORCE MATERIEL COMMAND
KIRTLAND AIR FORCE BASE, NM 87117-5776

DTIC COPY
NOTICE AND SIGNATURE PAGE

This report is the result of contracted fundamental research deemed exempt from public affairs security and policy review in accordance with SAF/AQR memorandum dated 10 Dec 08 and AFRL/CA policy clarification memorandum dated 16 Jan 09. This report is available to the general public, including foreign nationals. Copies may be obtained from the Defense Technical Information Center (DTIC) (http://www.dtic.mil).

AFRL-RV-PS-TR-2016-0111 HAS BEEN REVIEWED AND IS APPROVED FOR PUBLICATION IN ACCORDANCE WITH ASSIGNED DISTRIBUTION STATEMENT.

//SIGNED//   //SIGNED//
T. ALAN LOVELL   PAUL HAUSGEN, Ph.D.
Program Manager   Technical Advisor, Spacecraft Component Technology

//SIGNED//
JOHN BEAUCHEMIN
Chief Engineer, Spacecraft Technology Division
Space Vehicles Directorate

This report is published in the interest of scientific and technical information exchange, and its publication does not constitute the Government's approval or disapproval of its ideas or findings.

REPORT DOCUMENTATION PAGE

Form Approved
OMB No. 0704-0188

Public reporting burden for this collection of information is estimated to average 1 hour per response, including the time for reviewing instructions, searching existing data sources, gathering and maintaining the data needed, and completing and reviewing this collection of information. Send comments regarding this burden estimate or any other aspect of this collection of information, including suggestions for reducing this burden to Department of Defense, Washington Headquarters Services, Directorate for Information Operations and Reports (0704-0188), 1215 Jefferson Davis Highway, Suite 1204, Arlington, VA 22202-4302. Respondents should be aware that notwithstanding any other provision of law, no person shall be subject to any penalty for failing to comply with a collection of information if it does not display a currently valid OMB control number. **PLEASE DO NOT RETURN YOUR FORM TO THE ABOVE ADDRESS.**

1. REPORT DATE (DD-MM-YYYY)	2. REPORT TYPE	3. DATES COVERED (From - To)
14-11-2016	Final Report	27-Dec-2012 – 31-Aug- 2016

4. TITLE AND SUBTITLE

Relative Motion Modeling and Autonomous Navigation Accuracy

5a. CONTRACT NUMBER
FA9453-13-C-0202

5b. GRANT NUMBER

5c. PROGRAM ELEMENT NUMBER
62601F

6. AUTHOR(S)

K. T. Alfriend and S. R. Vadali

5d. PROJECT NUMBER
8809

5e. TASK NUMBER
PPM00017978

5f. WORK UNIT NUMBER
EF008849

7. PERFORMING ORGANIZATION NAME(S) AND ADDRESS(ES)
Texas Engineering Experiment Station
1470 William D. Fitch PKY
College Station, TX 77845-4645

8. PERFORMING ORGANIZATION REPORT NUMBER

9. SPONSORING / MONITORING AGENCY NAME(S) AND ADDRESS(ES)
Air Force Research Laboratory
Space Vehicles Directorate
3550 Aberdeen Ave, SE
Kirtland AFB, NM 87117-5776

10. SPONSOR/MONITOR'S ACRONYM(S)
AFRL/RVSV

11. SPONSOR/MONITOR'S REPORT NUMBER(S)
AFRL-RV-PS-TR-2016-0111

12. DISTRIBUTION / AVAILABILITY STATEMENT
Approved for public release; distribution is unlimited.

13. SUPPLEMENTARY NOTES

14. ABSTRACT
This research developed a methodology for determining the required accuracy of the dynamic model based on system requirements, the relative navigation accuracy and thruster accuracy. A state transition matrix was developed to propagate satellite relative motion to include non-conservative forces and the effect of higher order gravitational terms. The models developed were validated using numerical simulations.

15. SUBJECT TERMS
Dynamic Model Expansion; Earth Gravitational Perturbation; Goddard Mission Analysis Tool; GMAT; Hamiltonian Methods; LEO Orbits; Lunar-solar Perturbations; Methodology Evaluation; 3-axis Stabilized Satellites

16. SECURITY CLASSIFICATION OF:			17. LIMITATION OF ABSTRACT	18. NUMBER OF PAGES	19a. NAME OF RESPONSIBLE PERSON
a. REPORT Unclassified	**b. ABSTRACT** Unclassified	**c. THIS PAGE** Unclassified	Unlimited	134	T. Alan Lovell / **19b. TELEPHONE NUMBER** (include area code)

Standard Form 298 (Rev. 8-98)
Prescribed by ANSI Std. 239.18

--- This Page Intentionally Left Blank ---

TABLE OF CONTENTS

LIST OF FIGURES

LIST OF TABLES

PREFACE

This final report represents the work conducted under Contract FA9453-13-C-0202 from 27 December, 2012 to 22 July, 2016. This project was directed by Principal Investigators (PIs) Dr. Kyle T. Alfriend and Dr. Srinivas R. Vadali of Texas A&M University. The PIs were assisted by Research Associates Dr. Hui Yan and Dr. Kohei Fujimoto, and PhD students, Bharat Mahajan and Lt Col Kirk W. Johnson.

The work presented in this report is a summary of the following set of papers, easily accessible in the open literature:

1. Yan, H., Vadali, S.R., and Alfriend, K.T., "State Transition Matrix for Relative Motion Including General Gravitational Perturbations," AAS 15-339, AAS/AIAA Space Flight Mechanics Meeting, Williamsburg, VA, Jan 11-14, 2015.
2. Yan, H., Vadali, S.R., and Alfriend, K.T., "A Recursive Formulation of the Satellite Perturbed Relative Motion Problem," AAS/AIAA Astrodynamics Meeting, San Diego, CA, Aug 2014.
3. Yan, H., Vadali, S.R., and Alfriend, K.T., "State Transition Matrix for Relative Motion Including J2 and Third-Body Perturbations," AAS 14-379, AAS/AIAA Space Flight Mechanics Meeting, Santa Fe, NM, January 2014.
4. Yan, H., Vadali, S.R., and Alfriend, K.T., "State Transition Matrix for Relative Motion including Higher-order Gravity Perturbations," AAS 13-793, AAS/AIAA Astrodynamics Meeting, Hilton Head, SC, Aug 12-15, 2013.
5. Mahajan, B., Vadali, S. R., and Alfriend, K. T., "Analytic Solution for Satellite Relative Motion with Zonal Gravity Perturbations," No. 15-705, *AAS/AIAA Astrodynamics Specialist Conference*, Vail, CO, August, 2015.
6. Mahajan, B., Vadali, S. R., and Alfriend, K. T., "Analytic Solution for Satellite Relative Motion: The Complete Zonal Gravitational Problem," No. 16-262, *26th AAS/AIAA Spaceflight Mechanics Meeting*, Napa, California, February, 2016.
7. Johnson, K. W., Vadali, S. R., and Alfriend, K. T., "Comparison of Orbit Element Sets for Modeling Perturbed Satellite Relative Motion," *26th AAS/AIAA Space Flight Mechanics Meeting*, Napa, California, 2016.
8. Fujimoto, K., Alfriend, K. T. and Vadali, S. R. "Bridging Dynamical Modeling Effort and Sensor Accuracy in Relative Spacecraft Navigation," Presented at the 2015 AAS/AIAA Astrodynamics Specialist Conference, Vail, CO, 2015.

ACKNOWLEDGMENTS

DISCLAIMER

(This Page Intentionally Left Blank)

1 SUMMARY

This report documents the work performed for the project entitled "Relative Motion Modeling and Autonomous Navigation Accuracy" being performed at Texas A&M University under contract to the Air Force Research Laboratory. The PIs of this project are Drs. Kyle T. Alfriend and Srinivas R. Vadali.

The objectives of this project are:

- To develop a methodology for determining the required accuracy of the dynamic model based on system requirements, the relative navigation accuracy and thruster accuracy.
- To extend the Gim-Alfriend state transition matrix (GA-STM) for relative motion to include non-conservative forces and the effect of higher order gravitational terms on the mean motion.
- Validate the developed models using numerical simulation.

In current practice, the dynamical model in a spacecraft navigation algorithm is often set *ad hoc* without explicit regard for the level of measurement, guidance, or control errors expected. The dynamic model for the relative motion of two satellites should be consistent with the accuracy of the relative navigation system and the control system, otherwise fuel will be wasted or unnecessary computation will be performed. For example, including more perturbations in the relative motion dynamic model that improve the predicted motion over a few orbits by a few centimeters provides no real improvement if the relative navigation accuracy is no better than 10's of centimeters. The purpose here is to develop a methodology that would simplify the workflow of designing navigation systems so that the trade space between navigation system parameters and dynamical model fidelity could be quickly surveyed in lieu of performing massive numerical simulations for numerous scenarios and system parameter variations. First, the cost of a particular dynamical model within the navigation algorithm was expressed as a combination of the computation cost and the maneuver impulse, Δv, cost to rectify the expected state error. A confidence value accompanies the Δv cost through its Mahalanobis distance with respect to the state estimate uncertainty. Then two methods are introduced to reduce the cost computation burden. First, the state transition matrices of different dynamical models were approximated as functions of the time derivatives of the kinematic states. Then, a simplified form of the linear sensitivity of maximum *a posteriori* state estimates with respect to errors in the state transition matrix was derived. The accuracy of these approximations is deemed sufficient through a Monte Carlo simulation for a wide range of formation geometries in low Earth orbit.

The GA-STM was the first development to include the effect of the absolute and differential effects of the equatorial bulge term, J_2, in the linearized equations for the relative motion of satellites. The second objective of this project is to improve the dynamic modeling of the relative motion by adding the effects of higher order gravitational perturbations, lunar-solar effects perturbations, and the non-conservative perturbations to the GA-STM. This has been achieved. The accuracy of the expanded GA-STM was evaluated using numerical simulations with the Goddard General Mission Analysis Tool (GMAT).

The results show that

- Including the effects of the higher order geopotential short period effects on the calculation of the relative initial conditions reduces the secular drift. The J_2^2 effects are the most dominant.
- Including the secular and long period effects of the lunar perturbations on the relative motion of high altitude satellites, e.g., geosynchronous, is important.
- The use of an exponential density model for the relative, not necessarily the absolute motion of the Chief or reference satellite, improves the accuracy of the relative motion.

Other developments are

- The evaluation of using other variables, such as Hoots variables, for the relative motion, and
- A generalized formulation for computing the effects of higher order geopotential terms on the relative motion.

The results of this program will improve the precise maintenance of satellite formations and provide an approach for selecting the appropriate dynamic model used for the type of relative motion mission. This will save costs in the analysis and formation design, and in the development of on-board software because the dynamic model will be consistent with the required performance and relative navigation system.

2 INTRODUCTION

Accurate analytic modeling of inter-satellite relative motion is indispensable for fast and reliable prediction, fuel-efficient formation maintenance, space situational awareness, and proximity operations. In contrast to numerical propagation, analytic or semi-analytic solutions not only effect faster long-term propagation of the system states, but also provide valuable insight for mission analysis and parametric studies. One of the main challenges underlying the development of a satellite relative motion theory for low and medium Earth orbits is the modeling of the effect of nonspherical Earth gravity and other perturbations such as differential drag, third-body gravitation and solar radiation pressure. For guidance, control, and navigation, the analytical model in the form of a state transition matrix (STM) is most desirable. In addition, the sensing or navigation modules of spacecraft use estimation theory to provide estimates of states, which are derived from Kalman filters. The complexity of the dynamic model implemented in a Kalman filter to estimate the relative motion of two satellites should be consistent with the accuracy of the relative navigation system and the control system, otherwise fuel will be wasted or unnecessary computation will be performed. For example, including more perturbations in the relative motion dynamic model that improve the predicted motion over a few orbits by a few centimeters provides no real improvement if the relative navigation accuracy is no better than 10's of centimeters.

This report presents work performed to address the two main issues raised above.

2.1 Objective

The objectives of this project are:

1. To extend GA-STM [1] for relative motion to include non-conservative forces and the effect of higher order gravitational terms.
2. To develop a methodology for determining the required accuracy of the dynamic model based on system requirements, the relative navigation accuracy and thruster accuracy.
3. Validate the developed models using the GMAT [2].

2.2 Tasks

The tasks undertaken under this contract are:

1. Dynamic Model for Earth gravitational perturbation: This task extends the GA-STM to include the mean and periodic effects of the higher order Earth gravitational perturbations, i.e., the zonal and tesseral harmonics.
2. Dynamic Model Expansion to include non-Earth gravitational perturbations: Inclusion of differential drag, luni-solar third body, and solar radiation pressure perturbations.
3. A method to determine consistency between the dynamic model, navigation accuracy and thruster accuracy.

2.3   Organization of the Report

Section 3 of the report presents the methods, assumptions, and procedures used. Section 3.1 of the report presents the research undertaken to develop an extended GA-STM for Earth gravitational perturbations. Section 3.2 of the report includes the development of the STM for non-Earth gravitational effects. The analysis and the development of a method to determine consistency between the dynamic model, navigation accuracy and thruster Accuracy is presented in Section 3.3. Section 4 presents the results and discussion. The report concludes with recommendations for future research, the subject of Section 5.

3 METHODS, ASSUMPTIONS, AND PROCEDURES

3.1 Dynamical Model for Earth Gravitational Perturbations

This section presents the development of relative motion theories to model zonal and tesseral harmonics. The principal tool used for developing analytical satellite theories is the method of averaging, either by formal perturbation theories [3, 4] or the perturbation approach of Kaula [5]. Lie-series based approaches can be used to determine long period and short period effects that are closed form in eccentricity (at least for the zonals) and the algorithm is extendable to compute effects up to any order. In contrast, Kaula's approach produces compact expressions for first-order short period effects due to the zonals and tesserals using eccentricity functions, which involve infinite-series in eccentricity. These methods and their applications are discussed briefly in the following subsections.

3.1.1 Principles of Averaging

The principles of averaging, as applied to satellite theory, are illustrated by using the zonal harmonics expansion of the geopotential. For the zonal problem, the geopotential in terms of spherical harmonics can be expressed as

$$U = \frac{\mu}{r}\left[1 - \sum_{n=2}^{\infty} J_n \left(\frac{R_e}{r}\right)^n P_n(sin(\phi))\right] \tag{1}$$

The symbols r, ϕ, R_e, μ, J_n and P_n represent the satellite radius, its geocentric latitude, radius of Earth, gravitational parameter, zonal geopotential coefficients, and the Legendre polynomial of the nth degree, respectively. The corresponding Hamiltonian can be expressed as a power series in J_2 using a combination of Delaunay and classical orbital elements. The Delaunay and classical elements are related: $L = \sqrt{\mu / a}$, $G = L\sqrt{1-e^2}$, $H = G \cos i$, $l = M$, $g = \omega$, and $h = \Omega$.

3.1.1.1 Deprit's Method

The Hamiltonian for the complete zonal problem can be written as

$$H = H_0 + J_2 H_1 + \frac{J_2^2}{2!} H_2 \tag{2}$$

where

$$H_0 = -\frac{1}{2}\frac{\mu^2}{L^2}$$

$$H_1 = \frac{\mu R_e^2}{a^3}\left(\frac{a}{r}\right)^3 P_2(\sin(\phi))$$

$$H_2 = \sum_{n=3}^{\infty} H_{2,n} = \sum_{n=3}^{\infty} \frac{2!}{J_2^2} J_n \frac{\mu R_e^n}{a^{n+1}}\left(\frac{a}{r}\right)^{n+1} P_n(\sin(\phi))$$

The above Hamiltonian H for the complete zonal problem can be normalized using Deprit's Lie-transform based canonical perturbation method. This approach works by separating the secular and periodic effects with the help of two successive Delaunay normalizations of the gravitational potential. The first normalization averages out the short period terms containing mean anomaly, l, and produces a short period generating function. The resulting singly-averaged Hamiltonian includes long period as well as secular terms. The second normalization is necessary to separate the long period terms containing the argument of perigee angle, g, to produce a doubly-averaged Hamiltonian (or Kamiltonian) consisting of only the secular terms. The Lie-transform based perturbation equations up to third-order used for separating the secular and periodic effects can be written as

$$H_0 = K_0$$
$$(H_0, W_1) + H_1 = K_1$$
$$(H_0, W_2) + (H_1 + K_1, W_1) + H_2 = K_2 \tag{3}$$
$$(H_0, W_3) + (2H_1 + K_1, W_2) + (H_2 + 2K_2, W_1) - ((K_1, W_1), W_1) + H_3 = K_3$$

where K_0, K_1, K_2, and K_3 are the Kamiltonians of successive orders and similarly, W_1, W_2, and W_3 are the generating functions of successive orders. The parentheses represent the Poisson brackets, which are evaluated in terms of the canonical Delaunay element set $D = [l, g, h, L, G, H]$. The total Kamiltonian, K, up to order 3 and the generating function, W, up to order 2 are respectively,

$$K = K_0 + J_2 K_1 + \frac{J_2^2}{2!} K_2 + \frac{J_2^3}{3!} K_3 + O(J_2^4) \tag{4}$$

$$W = W_1 + J_2 W_2 + \frac{J_2^2}{2!} W_3 + O(J_2^3)$$

Because J_2 is considered as the only first-order perturbation, the first-order Kamiltonian K_1 and short-period generating function W_1 obtained during the first normalization of H, have no contributions from the other zonals. The second-order perturbations in H_2 appear for the first time at the second order in the perturbation equations and involves computation of Poisson brackets only at the third-order. As a result, the second-order contributions $K_{2,n}$ to the total

Kamiltonian K_2 and $W_{2,n}$ to the total short-period generating function W_2 due to any zonal harmonic J_n ($n \geq 3$) can be computed as

$$K_{2,n} = \frac{1}{2\pi} \int_0^{2\pi} H_{2,n} \frac{r^2}{a^2\sqrt{1-e^2}} \, df$$

$$W_{2,n} = -\frac{1}{\frac{\partial H_0}{\partial L}} \left(K_{2,n}(l-f) - \int_p H_{2,n} \frac{r^2}{a^2\sqrt{1-e^2}} \, df \right)$$

(5)

The subscript p of the integral sign indicates that the integration is performed for the periodic part of the integrand only, i.e., terms involving cosine and sine functions of true or mean anomaly. By making use of definition of the perturbing potential, the above integrals can be written as

$$K_{2,n} = \frac{1}{2\pi} \frac{2!}{J_2^2} J_n \frac{\mu R_e^n}{a^{n+1}\sqrt{1-e^2}} \int_0^{2\pi} \left(\frac{a}{r}\right)^{n-1} P_n(\sin(\phi)) \, df$$

(6)

$$W_{2,n} = \sqrt{\frac{a^3}{\mu}} \left(K_{2,n}(f-l) + \frac{2!}{J_2^2} J_n \frac{\mu R_e^n}{a^{n+1}\sqrt{1-e^2}} \int_p \left(\frac{a}{r}\right)^{n-1} P_n(\sin(\phi)) \, df \right)$$

The above integrals can be computed in closed form for an arbitrary zonal to produce expressions for the single-averaged Hamiltonian and short period generating function. A similar procedure can be used to perform the second normalization to average out the long-period terms dependent on the perigee angle, g, to derive the long period generating function. Once the expressions for averaged Hamiltonian and generating functions are available, the secular as well as periodic effects on a satellite due to these perturbations can be easily computed. The secular variations of the orbital elements can be derived using Hamilton's canonical equations, which propagates the mean elements, $\mathcal{E}_m$ in time using the singly or doubly-averaged Hamiltonian. The periodic contributions to the mean elements up to second-order can be computed using the following near-identity transformation to get the osculating elements, $\mathcal{E}_o$:

$$\mathcal{E}_o = \mathcal{E}_m + J_2(\mathcal{E}_m, W_1) + \frac{J_2^2}{2!}\left(((\mathcal{E}_m, W_1), W_1) + (\mathcal{E}_m, W_2) \right) + O(J_2^3)$$

(7)

3.1.1.2 Kaula's method

Kaula's approach [4] treats the full geopotential expansion, including zonal and tesseral harmonics. The potential is expressed in terms of the classical elements as

$$U = \frac{\mu}{r} + \sum_{l=2}^{\infty} \sum_{m=0}^{l} \sum_{p=0}^{l} \sum_{q=-\infty}^{\infty} \frac{\mu}{a} \left(\frac{R_e}{a}\right)^l F_{lmp}(i) \, G_{lpq}(e) S_{lmpq}(\omega, M, \Omega, \theta_{GST})$$

(8)

The S functions contain the gravitational coefficients and the F and G functions are the inclination and eccentricity functions, respectively, and

$$S = \begin{array}{l} C_{lm}\cos\Theta + S_{lm}\sin\Theta, \text{ if } (l-m) \text{ even} \\ -S_{lm}\cos\Theta + C_{lm}\sin\Theta, \text{ if } (l-m) \text{ odd} \end{array} \tag{9}$$

where

$$\Theta = \Theta_{lmpq} = (l-2p)\omega + (l-2p+q)M + m(\Omega - \theta_{GST})$$

where l is the zonal degree, m is the tesseral order, p is the index of inclination function F, q is the power of the eccentricity function G and θ_{GST} is the Greenwich Sidereal Time. Explicit forms of the F and G functions have been tabulated in Kaula [5]. The averaged Hamiltonian for J_2 is obtained by setting in Eq. (8), $l = 2, m = 0, p = 1, q = 0$ and the averaged Hamiltonian for J_4 is the potential when $l = 4, m = 0, p = 2, q = 0$.

Kaula's linear solutions are useful for modeling short period corrections to the classical orbital elements, especially for orbits of small eccentricity. The series expansions in the G functions can be truncated at a suitable order for small eccentricities. According Kaula's theory [5], the first approximations to the perturbations of the orbital elements or the solutions of the Lagrange planetary equations for the geopotential model are expressed as

$$\Delta a_{lmpq} = 2\frac{\mu R_e^l}{na^{l+2}\dot\Theta}F_{lmp}G_{lpq}(l-2p+q)S_{lmpq} \tag{10}$$

$$\Delta e_{lmpq} = \frac{\mu R_e^l}{na^{l+3}e\dot\Theta}F_{lmp}G_{lpq}[\eta(l-2p+q)-(l-2p)]S_{lmpq} \tag{11}$$

$$\Delta i_{lmpq} = \frac{\mu R_e^l}{na^{l+3}\eta\sin i\dot\Theta}F_{lmp}G_{lpq}[(l-2p)\cos i - m]S_{lmpq} \tag{12}$$

$$\Delta\omega_{lmpq} = \frac{\mu R_e^l}{na^{l+3}\dot\Theta}\eta[e^{-1}F_{lmp}\frac{\partial G_{lpq}}{\partial e} - \cot i\frac{\partial F_{lmp}}{\partial i}G_{lpq}]\bar S_{lmpq} \tag{13}$$

$$\Delta\Omega_{lmpq} = \frac{\mu R_e^l}{na^{l+3}\eta\sin i\dot\Theta}\frac{\partial F_{lmp}}{\partial i}G_{lpq}\bar S_{lmpq} \tag{14}$$

$$\Delta M_{lmpq} = \frac{\mu R_e^l}{na^{l+3}\dot\Theta}[-\eta e^{-1}\frac{\partial G_{lpq}}{\partial e} + 2(l+1)G_{lpq}]F_{lmp}\bar S_{lmpq} \tag{15}$$

For near circular orbits, Kaula's solution to the J_2 problem is obtained by setting $q=0$ and $l-2p+q\neq 0$:

$$\Delta a_{sp} = \Delta a_{2000} + \Delta a_{2020} \approx -\frac{3J_2 R_e^2 \sin^2 i}{2a} \cos 2\lambda \tag{16}$$

$$\Delta i_{sp} = \Delta i_{2000} + \Delta i_{2020} \approx -\frac{3J_2 R_e^2 \sin 2i}{8a^2} \cos 2\lambda \tag{17}$$

$$\Delta \Omega_{sp} = \Delta \Omega_{2000} + \Delta \Omega_{2020} \approx -\frac{3J_2 R_e^2 \cos i}{4a^2} \sin 2\lambda \tag{18}$$

3.1.2 The Gim-Alfriend State Transition Matrix

An analytic satellite theory can be used to propagate multiple satellites using the results from the previous section. Relative motion between satellites can be discerned by differencing the orbital elements or the states of any two satellites in a formation. Even though this approach is reasonable and applicable to arbitrary formation sizes, the drawback is the computational time and the information exchange required. In addition, a direct analytic solution for the relative motion problem also benefits in formulating guidance and control algorithms for rendezvous and proximity operations. For formation control, especially for proximity operations, the differential orbital elements of a deputy can be represented as a first-order variation of the orbital elements of the reference or chief satellite. These differential orbital elements can be directly propagated in time in the presence of the gravitational perturbations using the differential perturbation effects. This approach originally used for computing the state transition matrix for the relative motion in the presence of J_2 perturbation up to first-order, is known as GA-STM. It directly propagates in time the relative states of the deputy in a curvilinear frame attached to the chief.

The GA-STM is composed of three different matrices: the geometric transformation matrix Σ, the relative mean-to-osculating transformation matrix D, and the relative mean STM φ. The relative mean STM propagates in time the relative mean elements of the deputy with respect to the chief, using the mean rates of the chief's orbital elements. The relative mean orbital elements are then converted into the relative osculating elements when operated on by D. Finally, the geometric transformation matrix transforms the relative osculating orbital elements into the curvilinear orbit frame. Using these three matrices, GA-STM, Φ, can be written as

$$\Phi(t, t_0) = \Sigma(t)D(t)\phi(t, t_0)D^{-1}(t_0)\Sigma^{-1}(t_0) \tag{19}$$

where the propagation of the relative position and velocity states in the curvilinear coordinate system is achieved from time t_0 to t.

3.1.2.1 The Geometric Transformation Matrix

The geometric transformation matrix converts the relative orbital elements into the relative position and velocity states in the curvilinear orbit frame. The curvilinear frame is defined with respect to an imaginary circle with its origin at the chief and its radius taken as the geocentric radius of the chief. The relative position with respect to the chief can be defined in terms of three

coordinates: x represents the difference in the radii of the two satellites, and y and z represent the curvilinear distances from the chief, along and normal to the imaginary circle, respectively. If $\boldsymbol{x}$ represents the relative states in the curvilinear frame and $\Delta\boldsymbol{e}$ represents the relative orbital elements, then the geometric transformation matrix is defined as

$$\boldsymbol{x}(t) = \Sigma(t)\Delta\boldsymbol{e}(t) \tag{20}$$

where $\boldsymbol{x} = [x, y, z, \dot{x}, \dot{y}, \dot{z}]^T$ and $\Delta\boldsymbol{e} = \boldsymbol{e}_d - \boldsymbol{e}_c$. The subscripts d and c indicate the deputy and chief, respectively, and the boldface letters represent vectors. The geometric transformation matrix can be computed by taking the first variation of the chief's radial distance and its direction cosine matrix. The first three rows of Σ represent the position equations and are given as follows [1]:

$$[\boldsymbol{x}]_c = [\delta\boldsymbol{R}_c]_c + C_{ci}\delta C_{ci}^T[\boldsymbol{R}_c]_c \tag{21}$$

where $[\boldsymbol{R}_c]_c = [R_c\ 0\ 0]^T$, $[\boldsymbol{x}]_c = [x\ y\ z]^T$, and $C_{ci} = R_3(f+\omega)R_1(i)R_3(\Omega)$.

The notation $[\ ]_c$ represents a vector with components expressed in the chief's orbital frame and the prefix δ represents the variation of the quantity. The symbol R represents the simple rotation matrix, with the subscript specifying the type of rotation. In a similar fashion, the relative velocity of the deputy in the curvilinear frame can also be computed by making use of the transport equation:

$$[\dot{\boldsymbol{x}} + \varpi \times \boldsymbol{x}]_c = [\delta V_c]_c + C_{ci}\delta C_{ci}^T[\boldsymbol{V}_c]_c \tag{22}$$

where $[\boldsymbol{V}_c]_c = [V_r\ V_t\ V_n]^T$. The symbols, V_r, V_t, and V_n represent the chief's velocity components in the radial, tangential and normal directions, respectively. The symbol ϖ represents the angular velocity of the chief satellite, which can be expressed in terms of the osculating orbital elements as

$$\varpi = \left[\frac{\dot{\Omega}\sin i}{\sin(f+\omega)} \quad 0 \quad \frac{\sqrt{\mu p}}{R_c^2} \right]^T \tag{23}$$

where $\dot{\Omega} = \frac{1}{nab\sin i}\frac{\partial R_p}{\partial i}$ and $R_p = J_2 H_1$.

The symbols, p, n, and b represent the parameter of the chief's orbit, mean motion, and the semiminor axis, respectively. The symbol R_p represents the perturbing potential and is needed to compute the nodal angle rate. In the case of original GA-STM, R_p consists of J_2 effects only, however the effects due to an arbitrary zonal harmonic can be incorporated by including the corresponding perturbing potential in R_p. The equations for relative position $\boldsymbol{x}$ and relative velocity $\dot{\boldsymbol{x}}$ can be expressed in terms of the orbital elements. Expressions for the elements of Σ in

terms of nonsingular and equinoctial elements for the first-order J_2 problem are given in [1]. The inverse of Σ is required to transform the initial relative osculating states in the curvilinear frame to the relative osculating orbital elements; it can either be computed numerically or by reversion, using symbolic algebra.

3.1.2.2 The Relative Mean-to-Osculating Transformation Matrix

The matrix D converts the relative mean elements into the relative osculating elements. It captures the short-period and long-period effects on the differential orbital elements and is defined as the Jacobian of the contact transformations as given in Eq. (7). The D matrix can be computed using the following relations

$$D = D_{SP} D_{LP} \tag{24}$$

where $D_{LP} = \left[\frac{\partial \mathcal{E}_{LP}}{\partial \mathcal{E}_m}\right]$ and $D_{SP} = \left[\frac{\partial \mathcal{E}_{SP}}{\partial \mathcal{E}_{LP}}\right]$.

In the above relations, the symbols $\mathcal{E}_m, \mathcal{E}_o, \mathcal{E}_{LP}$ represent the chief's mean elements, the osculating elements and the elements with short-period effects averaged out, respectively.

3.1.2.3 The Relative Mean STM

The relative mean STM, ϕ, propagates in time the relative mean differential elements of the deputy relative to those of the chief. It models the secular effects on the differential mean elements by using the first-order variation of the mean rates of the chief. The following equations define the relative mean STM:

$$\partial \mathcal{E}_m(t) = \phi(t, t_0) \partial \mathcal{E}_m(t_0) \tag{25}$$

where $\phi(t, t_0) = \frac{\partial \mathcal{E}_m(t)}{\partial \mathcal{E}_m(t_0)}$ and the symbols $\mathcal{E}_m(t)$ and $\mathcal{E}_m(t_0)$ represent the chief's mean elements at time t and initial time t_0, respectively.

3.1.3 Extended Relative Motion Model based on Nonsingular Elements

The addition of the higher-order corrections to the orbit theory allows one to extend the capabilities of the GA-STM. Brouwer's theory [3] incorporates the secular, short periodic, long periodic effects J_2, and the secular and long periodic effects of J_2^2 and J_3-J_6. For the geopotential, the magnitudes of J_2^2 and the higher coefficients are of the same order. These effects have been used to extend the GA-STM significantly. In addition, the short period of J_2^2 have also been incorporated. The nonsingular elements are: $[a, \lambda = M + \omega, i, q_1 = e\cos(\omega), q_2 = e\sin(\omega), h = \Omega]$.

3.1.3.1 Short Period Terms due to J_2^2

Kinoshita [6], in his third-order theory, provides an expression for the short-periodic generating function of O(J_2^2) valid for small eccentricity. His expressions for the mean-osculating transformation can be simplified considerably by setting eccentricity to zero and retaining second-order accuracy. These correction terms for the nonsingular elements are

$$q_1^{sp22} = \frac{J_2^2}{L^8}[\left(-\frac{21}{64}si^2 + \frac{51}{128}si^4\right)\cos 5\lambda +$$
$$\left(-\frac{9}{16} + \frac{173}{64}si^2 - \frac{449}{128}si^4\right)\cos 3\lambda + \left(\frac{81}{16} - \frac{75}{8}si^2 + \frac{231}{64}si^4\right)\cos \lambda] \tag{26}$$

$$q_2^{sp22} = \frac{J_2^2}{L^8}[\left(-\frac{21}{64}si^2 + \frac{51}{128}si^4\right)\sin 5\lambda +$$
$$\left(-\frac{9}{16} + \frac{155}{64}si^2 - \frac{395}{128}si^4\right)\sin 3\lambda + \left(\frac{63}{16} - \frac{21}{2}si^2 + \frac{465}{64}si^4\right)\sin \lambda] \tag{27}$$

$$\lambda^{sp22} = \frac{J_2^2}{L^8}[\left(\frac{9}{32} - \frac{3}{64}si^2 - \frac{39}{64}si^4\right)\sin 4\lambda + \left(-\frac{15}{4}si^2 + \frac{99}{32}si^4\right)\sin 2\lambda] \tag{28}$$

$$h^{sp22} = \frac{J_2^2}{L^8}ci[\left(-\frac{9}{32} - \frac{3}{32}si^2\right)\sin 4\lambda + \frac{9}{8}si^2 \sin 2\lambda] \tag{29}$$

$$L^{sp22} = \frac{J_2^2}{L^7}[\frac{15}{64}si^4 \cos 4\lambda + \left(\frac{15}{8}si^2 - \frac{27}{8}si^4\right)\cos 2\lambda$$
$$+ \left(\frac{9}{8} - \frac{45}{16}si^2 + \frac{141}{64}si^4\right)] \tag{30}$$

where $si = \sin i$, $ci = \cos i$. From these expressions, the corrections to the other elements are

$$a^{sp22} = 2L^{sp22}\sqrt{a}$$

$$i^{SP22} = \frac{L^{sp22}}{L}\cot i \tag{31}$$

$$\theta^{SP22} = \lambda^{sp22} + 2q_1^{sp22}\sin \lambda - 2q_2^{sp22}\cos \lambda$$

3.1.3.2 STM with Kaula's Theory for Zonal and Tesseral Harmonics

Assuming small eccentricity, the Kaula's corrections for the nonsingular elements are computed as [7]:

$$\Delta a_{lmpq} = 2\frac{\mu R_e^l}{na^{l+2}\dot{\Theta}}F_{lmp}G_{lpq}(l-2p+q)S_{lmpq}$$

$$\Delta\lambda_{lmpq} = \frac{\mu R_e^l}{na^{l+3}\dot{\Theta}}\bar{S}_{lmpq}\left[\left[\eta F_{lmp}\frac{\partial G_{lpq}}{\partial e}\left(\frac{e}{1+\eta}\right)-\cot i\frac{\partial F_{lmp}}{\partial i}G_{lpq}\eta^{-1}+\right.\right.$$
$$\left.\left. 2(l+1)F_{lmp}G_{lpq}\right]\right.$$

$$\Delta i_{lmpq} = \frac{\mu R_e^l}{na^{l+3}\eta\sin i\dot{\Theta}}F_{lmp}G_{lpq}[(l-2p)\cos i - m]S_{lmpq} \qquad (32)$$

$$\Delta q_{1lmpq} = \Delta e_{lmpq}\cos\omega - (e\Delta\omega)_{lmpq}\sin\omega$$

$$\Delta q_{2lmpq} = \Delta e_{lmpq}\sin\omega + (e\Delta\omega)_{lmpq}\cos\omega$$

$$\Delta\Omega_{lmpq} = \frac{\mu R_e^l}{na^{l+3}\eta\sin i\dot{\Theta}}\frac{\partial F_{lmp}}{\partial i}G_{lpq}\bar{S}_{lmpq}$$

For the numerical example, gravity coefficients of the 20x20 gravity field are obtained from the JGM-2 Model. The above equations are used to obtain the orbital elements of the chief and deputy, using their respective mean elements. The unit sphere approach is used to compute the relative motion variables in the local vertical local horizontal frame. Equivalent results from GMAT are also obtained for the 20x20 gravity field.

3.1.4   STM for the Complete Zonal Perturbation Problem

The nonspherical gravitational problem, including all the zonal harmonics is referred to as the complete zonal problem. This subsection describes in brief the methodology for deriving the STM for satellite relative motion that includes the perturbation effects, closed-form in eccentricity, due to zonal harmonics up to an arbitrary degree. The secular as well as the periodic effects up to second-order of any zonal harmonic on the orbital elements of a satellite are modeled using the Deprit's method. By making use of the GA-STM framework described in the previous subsection, these effects were then incorporated into a STM solution for the relative motion problem. Secular or mean rates up to 3rd order, long-period and short-period effects up to 2nd order for two different sets of orbital elements have been computed: the nonsingular set (nonsingular for zero eccentricity) and the equinoctial set. The nonsingular set is singular for equatorial orbits, but the equinoctial element set is completely nonsingular for equatorial and circular orbits. It is noted that the expressions for secular and periodic variations of the equinoctial elements are significantly larger than those for the nonsingular set.

A complete second-order analytic solution for an artificial satellite as well as a STM for relative motion incorporating the perturbation effects due to $J_2 - J_6$ has been computed for the

nonsingular element set [9]. Even for nonsingular elements, the expressions for secular and periodic effects, especially short-period effects at 2nd order, are too large and cumbersome for computations by hand. Therefore, the Maple symbolic algebra package was used to compute the STM in terms of nonsingular element sets. Because of the use of nonsingular elements, this version of relative motion STM has singularities for reference orbits that lie in the equatorial plane. Additionally, extending this STM beyond J_6 by computing expressions explicitly for each zonal proved to be a very time consuming and computer resource expensive process, even with the use of a symbolic algebra package.

To address these limitations, a slightly different approach was used to compute the STM in terms of equinoctial elements. This approach extended the earlier work done by Saedeleer [8], in which generalized expressions for first-order averaged Hamiltonian and generating function for the short-period effects, closed form in eccentricity, due to an arbitrary zonal harmonic were given. These formulae were originally derived for the classical orbital elements. Using the Deprit's method, generalized analytic formulae were derived for second-order secular and short-period and first-order long-period variations of the equinoctial elements due to an arbitrary zonal harmonic J_n (n ≥ 3). To derive the STM, analytic formulae for partial derivatives of the mean rates, short-period and long-period transformations with respect to equinoctial elements were also derived by hand. All these formulae are valid for any elliptic reference orbit without any singularities related to zero eccentricity or inclination values. Because J_2 causes the dominant effect, it is considered as a first-order perturbation while all the higher zonals as second-order perturbations. To validate the accuracy of the proposed STM, results were compared with direct numerical propagation using GMAT. The following subsection provides the analytic expressions for propagating a single satellite used to propagate the equinoctial elements of the chief. It is noted that the analytic propagation of the chief is needed to compute the STM for the relative motion.

3.1.4.1   Secular Effects

This subsection presents the secular effects on the equinoctial elements of an artificial satellite for the complete zonal problem. For any harmonic J_n (n ≥ 3), the generalized analytic formulae for second-order mean rates are provided here. For J_2, the expressions for secular rates up to third-order are explicitly computed using Maple. By using the analytic formulae, the contributions to the secular effects due to the zonal harmonics J_n (*n* ≥ 3) can be conveniently added to the J_2 secular rates without having to go through the process of two Delaunay normalizations of the perturbing potential. In order to derive the secular effects due to an arbitrary zonal, the closed-form expression for the doubly-averaged Hamiltonian or Kamiltonian $K_{2,n}$ is sought. Equation (6) provides the integrals necessary to be evaluated for finding expressions for $K_{2,n}$. Appendix A.1 provides helpful formulae for evaluating the integrals in Eq. (6).

Using the expressions for $K_{2,n}$, the formulae for the secular or mean rates of the orbital elements can be derived by using the Hamilton's canonical equations. It is noted that the Equinoctial elements are not canonical. Therefore, the secular rates of the Delaunay elements are computed first, which can then be used to compute the rates of the Equinoctial elements. Using the

canonical equations of motion, the formulae for the mean rates of Delaunay elements $\mathcal{D}$ due to even harmonics are computed as follows:

$$\dot{l}_n = \delta_n(a, e) \sum_{j=0}^{\lfloor \frac{n}{2} \rfloor} \beta_{j,n}(i) \sum_{\text{even } k=0}^{n-1} \frac{\alpha_{k,n}(e)}{2^k} \binom{n-2j}{\frac{n}{2}-j} \binom{k}{\frac{k}{2}} \frac{1}{L} \left\{ -3 + k\frac{\eta^2}{e^2} \right\}$$

$$\dot{g}_n = \delta_n(a, e) \sum_{j=0}^{\lfloor \frac{n}{2} \rfloor} \beta_{j,n}(i) \sum_{\text{even } k=0}^{n-1} \frac{\alpha_{k,n}(e)}{2^k} \binom{n-2j}{\frac{n}{2}-j} \binom{k}{\frac{k}{2}} \frac{1}{G} \left\{ -(2n-1) - k\frac{\eta^2}{e^2} + \frac{(n-2j)}{\tan^2(i)} \right\} \tag{33}$$

$$\dot{h}_n = \delta_n(a, e) \sum_{j=0}^{\lfloor \frac{n}{2} \rfloor} \beta_{j,n}(i) \sum_{\text{even } k=0}^{n-1} \frac{\alpha_{k,n}(e)}{2^k} \binom{n-2j}{\frac{n}{2}-j} \binom{k}{\frac{k}{2}} \frac{1}{H} \left\{ -\frac{(n-2j)}{\tan^2(i)} \right\}$$

$$\dot{L}_n = \dot{G}_n = \dot{H}_n = 0$$

where

$$\delta_n(a, e) = 2\frac{J_n}{J_2^2} \frac{\mu R_e^n}{2^n \eta^{2n-1} a^{n+1}}$$

$$\beta_{j,n}(i) = \frac{(-1)^j (2n-2j)! \sin^{n-2j}(i)}{j! \, (n-j)! \, (n-2j)! \, 2^{n-2j}}$$

$$\alpha_{k,n}(e) = e^k \binom{n-1}{k}$$

The total secular rates of the Delaunay elements, $\mathcal{D}$, are found by adding the secular rates due to J_2, $\mathcal{D}_{J_2}$, to the contributions of the higher degree zonal harmonics, $\mathcal{D}_n$, from the above formulae, as shown below:

$$\dot{\mathcal{D}} = \dot{\mathcal{D}}_{J_2} + \frac{J_2^2}{2!} \sum_{n=3}^{\infty} \dot{\mathcal{D}}_n \tag{34}$$

The Equinoctial elements (a, e, and i represent the three classical orbital elements: semimajor axis, eccentricity and inclination, respectively.) are

$$a = a$$

$$\Lambda = l + g + h$$

$$p_1 = \tan\left(\frac{i}{2}\right)\cos(h)$$

$$p_2 = \tan\left(\frac{i}{2}\right)\sin(h)$$

$$q_1 = e\cos(g + h)$$

$$q_2 = e\sin(g + h)$$

(35)

The Equinoctial elements of the reference satellite can be propagated from the initial time t_0 to time t as follows:

$$a(t) = a(t_0)$$

$$\Lambda(t) = \Lambda(t_0) + (\dot{l} + \dot{g} + \dot{h})(t - t_0)$$

$$p_1(t) = p_1(t_0)\cos(\dot{h}(t - t_0)) - p_2(t_0)\sin(\dot{h}(t - t_0))$$

$$p_2(t) = p_2(t_0)\cos(\dot{h}(t - t_0)) + p_1(t_0)\sin(\dot{h}(t - t_0))$$

$$q_1(t) = q_1(t_0)\cos((\dot{g} + \dot{h})(t - t_0)) - q_2(t_0)\sin((\dot{g} + \dot{h})(t - t_0))$$

$$q_2(t) = q_2(t_0)\cos((\dot{g} + \dot{h})(t - t_0)) + q_1(t_0)\sin((\dot{g} + \dot{h})(t - t_0))$$

(36)

3.1.4.2   Short Period Effects

Using the expansion formulae given in Appendix A.1, the analytic expression for the second-order short-period generating function $W_{2,n}$, closed form in eccentricity, corresponding to an arbitrary zonal J_n ($n \geq 3$) can be computed from Eq. (6). This expression for $W_{2,n}$ can be written succinctly as:

$$W_{2,n} = \mathcal{W}_1(a, e, i, f, l, g) + \mathcal{W}_2(a, e, i)\mathcal{W}_3(f, g)$$

(37)

where

$$\mathcal{W}_1(a, e, i, f, l, g) = \sqrt{\frac{a^3}{\mu}} K_{2,n}(f - l)$$

(38)

$$K_{2,n} = \delta_n(a,e) \sum_{j=0}^{\lfloor \frac{n}{2} \rfloor} \beta_{j,n}(i) \sum_{\substack{\text{even[odd]} \\ k=0}}^{n-1} \frac{\alpha_{k,n}(e)}{2^k} \left\{ \lambda_n \binom{n-2j}{\frac{n}{2}-j} \binom{k}{\frac{k}{2}} \right.$$

$$\left. + \sum_{p=0}^{\lfloor \frac{n-1}{2} \rfloor - j} \gamma_{p,j,n} \binom{k}{\frac{k-(n-2j-2p)}{2}} (\cos[\sin](n-2j-2p)g) \right\} \tag{39}$$

$$\beta_{j,n}(i) = \frac{(-1)^j (2n-2j)! \sin^{n-2j}(i)}{j!\,(n-j)!\,(n-2j)!\,2^{n-2j}} \tag{40}$$

$$\mathcal{W}_2(a,e,i) = \delta'_n(a,e) \sum_{j=0}^{\lfloor \frac{n}{2} \rfloor} \beta_{j,n}(i) \sum_{k=0}^{n-1} \frac{\alpha_{k,n}(e)}{2^k} \tag{41}$$

$$\mathcal{W}_3(f,g) = \lambda_n \binom{n-2j}{\frac{n}{2}-j} C(f)$$

$$+ \sum_{p=0}^{\lfloor \frac{n-1}{2} \rfloor - j} \gamma_{p,j,n} \left\{ \sum_{s=0}^{\lfloor \frac{k-1}{2} \rfloor} \binom{k}{s} \left(\frac{\sin[-\cos]((k-2s+c)f+cg)}{k-2s+c} \right) \right.$$

$$\left. + \sum_{\substack{s=0 \\ s \neq s^*}}^{\lfloor \frac{k-1}{2} \rfloor} \binom{k}{s} \left(\frac{\sin[\cos]((k-2s-c)f-cg)}{k-2s-c} \right) + \lambda_k \binom{k}{\frac{k}{2}} \frac{\sin[-\cos](cf+cg)}{c} \right\} \tag{42}$$

In the above equations, the square-bracketed terms applies for odd harmonics and $c = n - 2j - 2p$. The formulae for second-order short period contributions due to any zonal harmonic J_n ($n \geq 3$) can now be derived by evaluating the Poisson brackets with equinoctial elements. The formulae for these short-period contributions are derived by hand in this work and are given as below:

$$(a, W_{2,n}) = -2\sqrt{\frac{a}{\mu}} \left[\sqrt{\frac{a^3}{\mu}} K_{2,n} \left(\frac{\partial f}{\partial l} - 1 \right) + \mathcal{W}_2 \left(\frac{\partial \mathcal{W}_3}{\partial f} \right) \frac{\partial f}{\partial l} \right] \tag{43}$$

$$(\Lambda, W_{2,n}) = \frac{3}{\sqrt{\mu a}}\mathcal{W}_1 + \sqrt{\frac{a^3}{\mu}}\left\{(f-l)K_{2,n}^{LGH} + K_{2,n}f_{LG}\right\}$$

$$- \frac{\mathcal{W}_2}{\eta\sqrt{\mu a}}\left\{\frac{\cos(i)}{1+\cos(i)}(n-2j) + (2n-1) + \frac{k\eta^2}{1+\eta}\right\}\mathcal{W}_3 + \mathcal{W}_2\left(\frac{\partial\mathcal{W}_3}{\partial f}\right)f_{LG} \qquad (44)$$

$$(p_1, W_{2,n}) = \frac{1}{\eta\sqrt{\mu a}}\frac{\cos(i)}{1+\cos(i)}\left[-\sin(h)\left\{\sqrt{\frac{a^3}{\mu}}(f-l)(-K_{2,n}(n-2j)) - \mathcal{W}_2(n-2j)\mathcal{W}_3\right\}\right.$$

$$\left. - \cos(h)\left\{\sqrt{\frac{a^3}{\mu}}(f-l)\frac{\partial K_{2,n}}{\partial g} + \mathcal{W}_2\frac{\partial\mathcal{W}_3}{\partial g}\right\}\right] \qquad (45)$$

$$(p_2, W_{2,n}) = \frac{1}{\eta\sqrt{\mu a}}\frac{\cos(i)}{1+\cos(i)}\left[\cos(h)\left\{\sqrt{\frac{a^3}{\mu}}(f-l)(-K_{2,n}(n-2j)) - \mathcal{W}_2(n-2j)\mathcal{W}_3\right\}\right.$$

$$\left. - \sin(h)\left\{\sqrt{\frac{a^3}{\mu}}(f-l)\frac{\partial K_{2,n}}{\partial g} + \mathcal{W}_2\frac{\partial\mathcal{W}_3}{\partial g}\right\}\right] \qquad (46)$$

$$(q_1, W_{2,n}) = -\sin(g+h)\left\{\sqrt{\frac{a^3}{\mu}}(f-l)K_{2,n}^{eGH} - \sqrt{\frac{a^3}{\mu}}\frac{\partial f}{\partial e}\frac{\eta}{\sqrt{\mu a}}K_{2,n}\right.$$

$$\left. - \left(\frac{\partial\mathcal{W}_2}{\partial e}\frac{\eta}{\sqrt{\mu a}} + \frac{e}{\eta\sqrt{\mu a}}\frac{1}{1+\cos(i)}\mathcal{W}_2^i\right)\mathcal{W}_3 - \frac{\partial f}{\partial e}\frac{\eta}{\sqrt{\mu a}}\mathcal{W}_2\frac{\partial\mathcal{W}_3}{\partial f}\right\}$$

$$- \cos(g+h)\left\{\mathcal{W}_1^{lge} + \mathcal{W}_{23}^{lge}\right\} \qquad (47)$$

$$(q_2, W_{2,n}) = \cos(g+h)\left\{\sqrt{\frac{a^3}{\mu}}(f-l)K_{2,n}^{eGH} - \sqrt{\frac{a^3}{\mu}}\frac{\partial f}{\partial e}\frac{\eta}{\sqrt{\mu a}}K_{2,n}\right.$$

$$\left. - \left(\frac{\partial\mathcal{W}_2}{\partial e}\frac{\eta}{\sqrt{\mu a}} + \frac{e}{\eta\sqrt{\mu a}}\frac{1}{1+\cos(i)}\mathcal{W}_2^i\right)\mathcal{W}_3 - \frac{\partial f}{\partial e}\frac{\eta}{\sqrt{\mu a}}\mathcal{W}_2\frac{\partial\mathcal{W}_3}{\partial f}\right\}$$

$$- \sin(g+h)\left\{\mathcal{W}_1^{lge} + \mathcal{W}_{23}^{lge}\right\} \qquad (48)$$

In the above equations, frequently occurring expressions are replaced by defining new terms to save space. The definition of these terms are provided in Appendix A.2. The expressions for short-period corrections up to second-order due to J_2 are computed explicitly by using the Maple software. The osculating equinoctial elements $\mathcal{E}_o$ can be computed by using the following near-identity transformations:

$$\mathcal{E}_o = \mathcal{E}_{LP} + J_2 \left(\mathcal{E}_{LP}, W_1^{SP}\right) + \frac{J_2^2}{2!} \left(\left(\left(\mathcal{E}_{LP}, W_1^{SP}\right), W_1^{SP}\right) + \left(\mathcal{E}_{LP}, W_2^{SP}\right)\right) + O(J_2^3)$$

(49)

$$\mathcal{E}_{LP} = \mathcal{E}_o - J_2 \left(\mathcal{E}_o, W_1^{SP}\right) + \frac{J_2^2}{2!} \left(\left(\left(\mathcal{E}_o, W_1^{SP}\right), W_1^{SP}\right) - \left(\mathcal{E}_o, W_2^{SP}\right)\right) + O(J_2^3)$$

In the above equations, W_1^{SP} represents the first-order generating function due to J_2 and W_2^{SP} represents the complete second-order generating function due to J_2 and higher zonals. The second of the above equations is the inverse near-identity transformation.

3.1.4.3 *Long Period Effects*

Once short-period effects are averaged out, a second Delaunay normalization of the singly-averaged Hamiltonian is required to compute the long-period generating function. Since the long-period generating function is not a function of l, the perturbation equations given in Eq. (3) simplify because the first Poisson bracket involving H_0 vanishes. As a result, the first-order long-period generating function W_1^{LP} can be computed using the following second-order perturbation equation

$$\left(H_1 + K_1, W_1^{LP}\right) + H_2 = K_2$$

(50)

In the above equation, H_2 represents the second-order singly-averaged Hamiltonian that includes long-period terms dependent on g due to the zonals J_n ($n \geq 3$), K_2 is the second-order Kamiltonian with only the secular terms. Because the J_2 potential has no long-period terms dependent on g, $H_1 = K_1$. The Poisson bracket in the above equation can be evaluated to result in the following equation for $W_{1,n}^{LP}$ for an arbitrary zonal hamronic J_n ($n \geq 3$).

$$W_{1,n}^{LP} = \frac{1}{2\frac{\partial K_1}{\partial G}} \int_{lp} K_{2,n} \, \mathrm{d}g$$

(51)

The subscript lp on the integral sign denotes the integration of the long-periodic terms of the integrand only. The first-order Kamiltonian K_1 has contributions from J_2 only and its value is given as [9].

$$K_1 = -\frac{1}{4} \frac{R_e{}^2 \mu \left(3 \cos^2(i) - 1\right)}{a^3 \eta^3}$$

(52)

Substituting the above value for K_1 and the formulae for $K_{2,n}$, the formulae for the first-order long-period generating function for even zonal harmonics (n ≥ 3) can be written as

$$W_{1,n}^{LP} = \sin(i)\mathcal{W}_1(a,e,i)\mathcal{W}_2(g) \tag{53}$$

where

$$\mathcal{W}_1(a,e,i) = \delta_n^{LP}(a,e)\sum_{j=0}^{\lfloor\frac{n}{2}\rfloor}\beta_{j,n}^{LP}(i)\sum_{\text{even[odd]}\;k=0}^{n-1}\frac{\alpha_{k,n}(e)}{2^k} \tag{54}$$

$$\mathcal{W}_2(g) = \sum_{p=0}^{\lfloor\frac{n-1}{2}\rfloor-j}\gamma_{p,j,n}\left(\begin{array}{c}k\\\frac{k-(n-2j-2p)}{2}\end{array}\right)\frac{(-\sin[\cos](n-2j-2p)g)}{(n-2j-2p)} \tag{55}$$

$$\delta_n^{LP}(a,e) = \frac{2}{3}\frac{a^{7/2}\eta^4}{\sqrt{\mu}R_e^2}\delta_n(a,e) \tag{56}$$

$$\beta_{j,n}^{LP}(i) = \frac{(-1)^j(2n-2j)!\sin^{n-2j-1}(i)}{(1-5\cos^2(i))j!\,(n-j)!\,(n-2j)!\,2^{n-2j}} \tag{57}$$

Using the above expression for the long-period generating function, the analytic formulae for the long-period effects due to any zonal harmonic J_n (n ≥ 3) can be computed by evaluating the Poisson brackets for the equinoctial elements. These formulae for the first-order long-period effects are derived and given as follows:

$$\left(a, W_{1,n}^{LP}\right) = 0 \tag{58}$$

$$\left(\Lambda, W_{1,n}^{LP}\right) = \sin(i)\frac{W_1(a,e,i)}{\sqrt{\mu a}}\left[-\frac{2n-5}{\eta} - \frac{\eta k}{1+\eta} + \frac{10\cos(i)(1-\cos(i))}{\eta(1-5\cos^2(i))}\right.$$
$$\left. +\frac{n-2j}{\eta}\left(\frac{-\cos(i)}{2\cos^2\left(\frac{i}{2}\right)}\right)\right]W_2(g) \tag{59}$$

$$\left(p_1, W_{1,n}^{LP}\right) = \frac{\cos(i)}{2\eta\sqrt{\mu a}\cos^2\left(\frac{i}{2}\right)}\left[\sin(h)W_1\left\{(n-2j) - \frac{10\sin^2(i)}{1-5\cos^2(i)}\right\}W_2 - \cos(h)W_1 W_4\right] \tag{60}$$

$$\left(p_2, W_{1,n}^{LP}\right) = \frac{\cos(i)}{2\eta\sqrt{\mu a}\cos^2\left(\frac{i}{2}\right)}\left[-\cos(h)W_1\left\{(n-2j) - \frac{10\sin^2(i)}{1-5\cos^2(i)}\right\}W_2 - \sin(h)W_1 W_4\right] \tag{61}$$

$$\left(q_1, W_{1,n}^{LP}\right) = \sin(i)\frac{\sin(g+h)}{\eta\sqrt{\mu a}}\left[W_1\left\{e(2n-5) - \frac{5e\sin(2i)\tan\left(\frac{i}{2}\right)}{1-5\cos^2(i)} + \frac{e\cos(i)(n-2j)}{2\cos^2\left(\frac{i}{2}\right)}\right\}W_2\right.$$
$$\left. +\eta^2 W_3 k W_2\right] + \sin(i)\frac{\eta}{\sqrt{\mu a}}\cos(g+h)W_3 W_4 \tag{62}$$

$$\left(q_2, W_{1,n}^{LP}\right) = -\sin(i)\frac{\cos(g+h)}{\eta\sqrt{\mu a}}\left[W_1\left\{e(2n-5) - \frac{5e\sin(2i)\tan\left(\frac{i}{2}\right)}{1-5\cos^2(i)} + \frac{e\cos(i)(n-2j)}{2\cos^2\left(\frac{i}{2}\right)}\right\}W\right.$$
$$\left. +\eta^2 W_3 k W_2\right] + \sin(i)\frac{\eta}{\sqrt{\mu a}}\sin(g+h)W_3 W_4 \tag{63}$$

It is noted that the order of terms in a product in the above equations must be preserved because of presence of the summation indices. The long-period effects can be added to the mean Equinoctial elements $\mathcal{E}_m$ to compute Equinoctial elements with short-periods effects averaged out, $\mathcal{E}_{LP}$, using the following near-identity transformation up to second-order.

$$\mathcal{E}_{LP} = \mathcal{E}_m + J_2\left(\mathcal{E}_m, W_1^{LP}\right) + \frac{J_2^2}{2!}\left(\left(\left(\mathcal{E}_m, W_1^{LP}\right), W_1^{LP}\right) + \left(\mathcal{E}_m, W_2^{LP}\right)\right) + O(J_2^3)$$
$$\mathcal{E}_m = \mathcal{E}_{LP} - J_2\left(\mathcal{E}_{LP}, W_1^{LP}\right) + \frac{J_2^2}{2!}\left(\left(\left(\mathcal{E}_{LP}, W_1^{LP}\right), W_1^{LP}\right) - \left(\mathcal{E}_{LP}, W_2^{LP}\right)\right) + O(J_2^3) \tag{64}$$

3.1.4.4 STM for the Perturbed Relative Motion

The perturbations effects computed in the previous subsections due to an arbitrary zonal harmonic J_n (n ≥ 3) were incorporated into the GA-STM framework by computing the partial derivatives of the formulae for mean rates, long-period and short-period effects with respect to the equinoctial elements. These analytic formulae for the partial derivatives are derived by hand and implemented in a MATLAB code, however they not included in this report to save space. The partial derivatives of the mean rates are incorporated into the differential mean STM, whereas the partial derivatives of the long-period and short-period formulae are used to update the D_{LP} and D_{SP} matrices of the GA-STM as defined in the previous subsections. To update the geometric transformation matrix given in Subsection 3.1.2.1, the chief's nodal angle rate formulae must be updated to include the effects of higher zonals by using the following perturbing potential (This equation is not numbered.)

$$R_p = J_2 H_1 + \frac{J_2^2}{2!} H_2 \tag{65}$$

3.1.5 Gim-Alfriend State Transition Matrix in Terms of Hoots Elements

This portion of the study reformulated the GA-STM for linearized satellite relative motion in terms of Hoots elements [10]. The Hoots elements are $y_1 = r$, $y_2 = \dot{r}$, $y_3 = r\dot{f}$, $y_4 = \sin i/2 \sin u$, $y_5 = \sin i/2 \cos u$, and $y_6 = u + h$, where r is the orbit radius, f is the true anomaly, i is the inclination, h is the right ascension of the ascending node, $u = f + g$ is the argument of latitude, and g is the argument of perigee. The Hoots elements are completely nonsingular for all eccentricities and inclinations.

3.1.5.1 Sensitivity Matrix D

The sensitivity matrix $D(t)$ is defined as $D = \partial \underline{y}/\partial \underline{y}''$, the Jacobian of the osculating elements with respect to the mean elements. Considering the osculating elements as a vector of nonlinear functions of the mean elements, and expanding the elements for a deputy satellite as a Taylor series about the reference or chief satellite, yields the following:

$$\underline{y}_d(t) = \underline{y}_c(t) + \frac{\partial \underline{y}}{\partial \underline{y}''}\bigg|_{\underline{y}''_c} \left(\underline{y}''_d(t) - \underline{y}''_c(t)\right) + \cdots \tag{66}$$

This shows that D can function as a linearized operator for relative motion, mapping the differences in mean Hoots elements into differential osculating Hoots elements:

$$\delta \underline{y}(t) = D(t)\left[\underline{y}''_d(t) - \underline{y}''_c(t)\right] \tag{67}$$

Importantly, this relationship can be inverted at the initial time, providing a way to convert the osculating initial conditions to mean relative initial conditions:

$$\delta \underline{y}''(t_0) = D^{-1}(t_0)\left[\underline{y}_d(t_0) - \underline{y}_c(t_0)\right] \tag{68}$$

Given correction terms $\underline{y} - \underline{y}''$ from the mean-to-osculating transformation of a particular perturbation theory, we can compute the sensitivity matrix as $D = I_{6\times6} + \frac{\partial(\underline{y}-\underline{y}'')}{\partial \underline{y}''}$, where I is the identity matrix. If the perturbation theory uses successive transformations (for example, long-period and short-period corrections), then we can apply the D operators in succession:

$$D = D^{SP}D^{LP} = \frac{\partial \underline{y}}{\partial \underline{y}'}\frac{\partial \underline{y}'}{\partial \underline{y}''} = \left(I_{6\times6} + \frac{\partial(\underline{y}-\underline{y}')}{\partial \underline{y}'}\right)\left(I_{6\times6} + \frac{\partial(\underline{y}'-\underline{y}'')}{\partial \underline{y}''}\right) \tag{69}$$

It is possible to compute D based on the first-order J_2-only corrections from Hoots theory (equivalent to Brouwer theory, but with singularities removed and certain other improvements) as $D = I_{6\times6} + D^{(lp)} + D^{(sp)}$, where $D^{(lp)} = \frac{\partial(\underline{y}'-\underline{y}'')}{\partial \underline{y}''}$, $D^{(sp)} = \frac{\partial(\underline{y}-\underline{y}')}{\partial \underline{y}'}$, and the product $D^{(sp)}D^{(lp)}$ has been neglected as second-order in J_2. Once the correction terms $\underline{y}' - \underline{y}''$ and $\underline{y} - \underline{y}'$ are expressed in terms of only the Hoots elements, forming matrices $D^{(lp)}$ and $D^{(sp)}$ is a straightforward matter of taking partial derivatives. Note that using mean elements $\underline{y}''$, rather than intermediate elements $\underline{y}'$, as inputs when computing $D^{(sp)}$ would constitute yet another approximation, introducing error of second order in J_2.

3.1.5.2 Mean State Transition Matrix $\overline{\varphi}_{\underline{y}}$

Considering the state $\underline{y}''(t)$ as a vector function of the initial conditions, and expanding the state for a deputy satellite as a Taylor series about the chief, yields the following:

$$\underline{y}''_d(t) = \underline{y}''_c(t) + \left.\frac{\partial \underline{y}''(t)}{\partial \underline{y}''(t_0)}\right|_{\underline{y}''_c(t_0)}\left(\underline{y}''_d(t_0) - \underline{y}''_c(t_0)\right) + \cdots \tag{70}$$

$$\text{or } \delta \underline{y}''(t) = \left.\frac{\partial \underline{y}''(t)}{\partial \underline{y}''(t_0)}\right|_{\underline{y}''_c(t_0)}\delta \underline{y}''(t_0) + \cdots \tag{71}$$

This shows that $\overline{\varphi}_{\overline{y}}(t, t_0) = \left.\frac{\partial \underline{y}''(t)}{\partial \underline{y}''(t_0)}\right|_{\underline{y}''_c(t_0)}$ is the linearized relative state transition matrix (STM), so that (neglecting terms of second order in the relative coordinates) $\delta \underline{y}''(t) = \overline{\varphi}_{\overline{y}}(t, t_0) \delta \underline{y}''(t_0)$. Finding the partial derivatives of $\underline{y}''(t)$ with respect to the initial conditions is most conveniently accomplished through a change of variables to a set of elements $\underline{x}$: $x_1 = a$, $x_2 = e \sin l$, $x_3 = e \cos l$, $x_4 = \sin i/2 \sin h$, $x_5 = \sin i/2 \cos h$, and $x_6 = l + g + h$, where e is eccentricity and l is mean anomaly. Then we can say that

$$\frac{\partial \underline{y}''(t)}{\partial \underline{y}''(t_0)} = \frac{\partial \underline{y}''(t)}{\partial \underline{x}''(t)} \frac{\partial \underline{x}''(t)}{\partial \underline{x}''(t_0)} \frac{\partial \underline{x}''(t_0)}{\partial \underline{y}''(t_0)} \tag{72}$$

Hoots found the partial derivatives of $\underline{y}$ with respect to $\underline{x}$, and these can be assembled into $\mathcal{J} = \frac{\partial \underline{y}}{\partial \underline{x}}$, the geometric transformation between the two sets, which has the same form whether computed using mean, intermediate, or osculating elements (i.e., $\frac{\partial \underline{y}''}{\partial \underline{x}''} = \frac{\partial \underline{y}'}{\partial \underline{x}'} = \frac{\partial \underline{y}}{\partial \underline{x}}$). The vector $\underline{x}$ is expressed in terms of the initial conditions as

$$x_1''^{(t)} = x_1''^{(t_0)}$$

$$x_2''(t) = x_2''(t_0) \cos\left[(n'' + \dot{l}_p'')(t - t_0)\right] + x_3''(t_0) \sin\left[(n'' + \dot{l}_p'')(t - t_0)\right]$$

$$x_3''(t) = -x_2''(t_0) \sin\left[(n'' + \dot{l}_p'')(t - t_0)\right] + x_3''(t_0) \cos\left[(n'' + \dot{l}_p'')(t - t_0)\right]$$

$$\tag{73}$$

$$x_4''(t) = x_4''(t_0) \cos\left[\dot{h}_p''(t - t_0)\right] + x_5''(t_0) \sin\left[\dot{h}_p''(t - t_0)\right]$$

$$x_5''(t) = -x_4''(t_0) \sin\left[\dot{h}_p''(t - t_0)\right] + x_5''(t_0) \cos\left[\dot{h}_p''(t - t_0)\right]$$

$$x_6''(t) = x_6''(t_0) + \left(n'' + \dot{l}_p'' + \dot{g}_p'' + \dot{h}_p''\right)(t - t_0)$$

where $n = \sqrt{\mu/a^3}$ is the mean motion (so that $n'' = \sqrt{\mu/x_1''(t_0)^3}$) and the subscript p indicates the secular rates due to perturbations (which can be found from Brouwer theory [3]). Let $\overline{\varphi}_{\underline{x}}(t,t_0) = \frac{\partial \underline{y}''(t)}{\partial \underline{y}''(t_0)}$. Then

$$\overline{\varphi}_{\underline{y}}(t,t_0) = \mathcal{J}(t)\overline{\varphi}_{\underline{x}}(t,t_0)\mathcal{J}^{-1}(t_0) \tag{74}$$

where all initial conditions are for the chief satellite. Note that $\underline{x}$ and $\overline{\varphi}_{\underline{x}}(t,t_0)$ are nonlinear functions of the perturbed mean secular rates and will have to be re-derived to account for $J_2{}^2$ or higher zonal harmonics.

3.1.5.3 *Relative Transformation Map Σ*

Reference [1] reports expressions for the spherical curvilinear coordinates of a deputy satellite's relative position $\underline{r}(t)$ and velocity $\underline{v}(t)$ in terms of the chief's osculating nonsingular elements $(a, u, i, q_1 = e \cos g, q_2 = e \sin g,$ and $h)$ and the deputy's relative osculating nonsingular elements $(\delta a, \delta u, \delta i, \delta q_1, \delta q_2,$ and $\delta h)$. These can be easily mapped into expressions in terms of chief and relative classical orbit elements using the variations, $\delta q_1 = \cos g\, \delta e - e \sin g\, \delta g$, $\delta q_2 = \sin g\, \delta e + e \cos g\, \delta g$, $\delta u = \delta g + \delta f$, and $\delta f = \frac{\partial f}{\partial e}\delta e + \frac{\partial f}{\partial l}\delta l$. Some terms in $\underline{v}(t)$ depend on the perturbed rates of change in u and h, which can be found from Gauss's Variational Equations in terms of the perturbing acceleration vector due to the Earth's gravitational zonal harmonics. The expressions for $\underline{r}(t)$ and $\underline{v}(t)$ can then be transformed into Hoots elements via the following relationships (all derived from the definitions of the Hoots elements given above): $\sin u = \frac{y_4}{\sin i/2}$, $\cos u = \frac{y_5}{\sin i/2}$, $\sin f = \frac{y_2\eta}{nae}$, $\cos f = \frac{1}{e}\left(\frac{a\eta^2}{y_1} - 1\right)$, $a = \frac{y_1{}^2 y_3{}^2}{\mu\eta^2}$, $\sin i/2 = \sqrt{y_4{}^2 + y_5{}^2}$, and $\cos i/2 = \sqrt{1 - y_4{}^2 - y_5{}^2}$, where $\eta = \sqrt{1 - e^2}$. Solving these relations for the final variable, e, yields a 4th-order polynomial whose only root on $e \in [0,1)$ is $e = \frac{1}{\mu}\sqrt{y_1{}^2 y_3{}^4 + y_1{}^2 y_2{}^2 y_3{}^2 - 2\mu y_1 y_3{}^2 + \mu^2}$. The differential elements are transformed using a linearized map containing the partial derivatives of the classical orbit elements with respect to the Hoots elements. Finally, the coefficients of the differential Hoots elements are formed into matrix $\Sigma(t)$, so that

$$[\underline{r}(t)^T \quad \underline{v}(t)^T]^T = \Sigma(t)\delta\underline{y}(t) \tag{75}$$

The portion of the transformation due to the perturbing acceleration can be partitioned into a separate map $B(t)$, so that $\Sigma(t) = A(t) + B(t)$.

3.2 Dynamical Model Expansion: Non-Earth Gravitational Perturbations

The dominant perturbation on satellite motion for objects in LEO is the equatorial bulge term, J_2. Atmospheric drag affects objects up to about 1000 km altitude. At higher altitudes, particularly, geosynchronous altitude, the perturbations resulting due to the moon and sun can be as large as the Earth gravitational effects and need to be evaluated. Also, at these altitudes the solar radiation effects, which are not a function of altitude, can also have a significant effect. At altitudes under 1000 km atmospheric drag effects can be significant and need to be considered. The effect of these perturbations on the relative emotion of satellites are addressed in this chapter. Lunar and solar effects are addressed in Section 3.2.1, solar radiation effects are covered in Section 3.2.2 and atmospheric drag in Section 3.2.3. These effects are incorporated into the Gim-Alfriend STM.

3.2.1 Dynamic Model Expansion: Third Body Perturbations

The effects of lunar perturbations on satellites have been studied extensively, using perturbation methods and averaging. The first lunisolar disturbing function was developed for the secular and long periodic terms in the 1950s by Kozai [11] and expanded by Musen et al [12]. Kaula [5] investigated a general method to represent the disturbing potentials in terms of orbital elements. The advantage of this approach is that specific terms can be studied in a convenient and general manner. For example, for the secular motion, the averaged Hamiltonian is the potential obtained by setting the coefficients depending on the satellite mean anomaly and argument of perigee to zero. The method was revisited by Giacaglia [13] and a treatment is presented in Vallado [14]. Although this infinite series summation method provides a general formulation, efficient numerical implementations require recursive formulations [15]. Kozai [11] developed an alternative method to compute the lunisolar perturbations. The disturbing function was expressed in terms of the orbital elements of the satellite and the polar geocentric coordinates of the Sun and the Moon. From the disturbing function form, the short periodic terms can be eliminated by taking the average with respect to the mean anomaly of satellite motion. The summation of the terms in the potential is carried up to order five. Prado [16] applied a double averaging technique to obtain the third-body disturbing potential using the formulation of the restricted three-body problem. Since the short periodic terms are removed from the model, it is convenient for the study of long-term orbit stability and leads to fast computations. Recently, the accuracy of the doubly-averaged model has been improved by including the lunar orbit's eccentricity and inclination in the studies presented in References [17-19].

Since the perturbed relative motion problem is very complex, our effort has focused on simplifying the dynamic models of relative motion. This section considers the third-body perturbation to extend the fidelity of the GA STM, based on the previous work by Roscoe, Vadali and Alfriend [12, 21]. The second-order effect of the averaged lunar perturbation is modeled with nonsingular elements. For nonlinear simulations, the relative motion of the Moon with respect to the Earth is incorporated from ephemerides data obtained from the Jet Propulsion Laboratory's HORIZONS website. The initial conditions for the averaged model are determined by a least squares method developed in Reference [18]. The nonlinear solution is validated by the General Mission Analysis Tool (GMAT) [2].

3.2.1.1 *Averaged Disturbing Potential*

In the following, the subscript "m" refers to the variable related to the Moon and the symbols "S" and "C", written with subscripts, stand for sine and cosine functions, respectively. The disturbing potential due to the Moon is

$$R = \frac{\mu_m G(m_e + m_m)}{\sqrt{r^2 + r_m^2 - 2rr_m \cos S}} \tag{76}$$

where $\mu_m = m_m/(m_e + m_m)$, G is the gravitational constant, m_e is the mass of Earth mass, m_m is the mass of the Moon, r is the distance from Earth to a satellite, and r_m is the Earth-Moon distance. The included angle between the vectors r and r_m, denoted by S, can be obtained from the dot product of the unit vectors r and r_m.

In the Earth centered inertial (ECI) frame, the unit vector $\hat{r}_m$ can be expressed in terms of the components

$$\begin{aligned}
\hat{x}_m &= C_{\Omega_m} C_{\theta_m} - S_{\Omega_m} S_{\theta_m} C_{i_m} \\
\hat{y}_m &= S_{\Omega_m} C_{\theta_m} + C_{\Omega_m} S_{\theta_m} C_{i_m} \\
\hat{z}_m &= S_{\theta_m} S_{i_m}
\end{aligned} \tag{77}$$

The ECI components can be expressed in the perifocal frame as

$$\begin{aligned}
\hat{x}_{m_p} &= \left(C_\Omega C_\omega - S_\Omega S_\omega C_i\right)\hat{x}_m + \left(S_\Omega C_\omega + C_\Omega S_\omega C_i\right)\hat{y}_m + S_\omega S_i \hat{z}_m \\
\hat{y}_{m_p} &= \left(-C_\Omega S_\omega - S_\Omega S_\omega C_i\right)\hat{x}_m + \left(-S_\Omega S_\omega + C_\Omega C_\omega C_i\right)\hat{y}_m + C_\omega S_i \hat{z}_m \\
\hat{z}_{m_p} &= S_\Omega S_i \hat{x}_m - C_\Omega S_i \hat{y}_m + C_i \hat{z}_m
\end{aligned} \tag{78}$$

In the perifocal frame, the unit vector $\hat{r}$ has components

$$\begin{aligned}
\hat{x}_p &= \cos f \\
\hat{y}_p &= \sin f \\
\hat{z}_p &= 0
\end{aligned} \tag{79}$$

where f is the true anomaly. From Eqs. (77-79), we have

$$\cos S = \alpha \cos f + \beta \sin f \tag{80}$$

where

$$\alpha = (C_{\Delta\Omega} C_\omega - S_{\Delta\Omega} S_\omega C_i)C_{\theta_m} + \left(C_{\Delta\Omega} S_\omega C_i C_{i_m} + S_{\Delta\Omega} C_\omega C_{i_m} + S_\omega S_i S_{i_m}\right)S_{\theta_m}$$

$$\beta = -(C_{\Delta\Omega}S_\omega + S_{\Delta\Omega}C_\omega C_i)C_{\theta_m} + (C_{\Delta\Omega}C_\omega C_i C_{i_m} - S_{\Delta\Omega}S_\omega C_{i_m} + C_\omega S_i S_{i_m})S_{\theta_m}$$

$$\Delta\Omega = \Omega - \Omega_m$$

Equation (76) is expanded in terms of the Legendre polynomials as

$$R = \frac{\mu_m G(m_0 + m_m)}{r_m} \sum_{n=2}^{\infty} \left(\frac{r}{r_m}\right)^2 P_n(\cos S) \tag{81}$$

Taking only the first term in the summation, the approximate disturbing potential is obtained as

$$R = \frac{\mu_m G(m_0 + m_m)}{r_m} \sum_{n=2}^{\infty} \left(\frac{r}{r_m}\right)^2 P_n(\cos S)$$

$$R = \frac{\mu_m n_m^2 a^2}{2} \left(\frac{a_m}{r_m}\right)^2 \left(\frac{r}{a}\right)^2 (3\cos^2 S - 1) \tag{82}$$

The time-averaged potential is defined by the relation

$$\langle F \rangle = \frac{1}{2\pi} \int_0^{2\pi} (F) dM$$

where M is the mean anomaly and F is an arbitrary potential function. Taking the first average over the mean anomaly of the satellite orbit [7] yields the averaged potential

$$\langle R_2 \rangle = \frac{\mu_m n_m^2 a^2}{2} \left(\frac{a_m}{r_m}\right)^3 \left\{ \left(1 + \frac{3}{2}e^2\right)\left[\frac{3}{2}(\alpha^2 + \beta^2 - 1)\right] + \frac{15}{4}e^2(\alpha^2 - \beta^2) \right\} \tag{83}$$

The identities $\langle S_{\theta_m}^2 \rangle = \langle C_{\theta_m}^2 \rangle = \frac{1}{2}$ and $\langle S_{\theta_m} C_{\theta_m} \rangle = 0$ have been used to derive the above equation.

The second average is taken with respect to the lunar period. Considering the lunar orbit's eccentricity, we have from [20], $\langle (\frac{a_m}{r_m})^3 \rangle = (1 - e_m^2)^{-\frac{3}{2}}$. Hence, the second average of Eq. (83) is

$$\langle\langle R_2 \rangle\rangle = \frac{\mu_m n_m^2 a^2}{16} (1 - e_m^2)^{-\frac{3}{2}} \left[(6 + 9e^2)A + 15e^2 B - 12e^2 - 8 \right] \tag{84}$$

where

$$A = C_{\Delta\Omega}^2\big(1 + C_i^2 C_{i_m}^2\big) + S_{\Delta\Omega}^2\big(C_i^2 + C_{i_m}^2\big) + S_i^2 S_{i_m}^2 + \frac{1}{2} S_{2i_m} S_{2i} C_{\Delta\Omega}$$

$$B = \left[C_{\Delta\Omega}^2\big(1 - C_i^2 C_{i_m}^2\big) + S_{\Delta\Omega}^2\big(C_{i_m}^2 - C_i^2\big) - S_i^2 S_{i_m}^2 - \frac{1}{2} S_{2i_m} S_{2i} C_{\Delta\Omega} \right] C_{2\omega}$$
$$- \big(S_{2\Delta\Omega} C_i S_{i_m}^2 - S_{\Delta\Omega} S_i S_{2i_m}\big) S_{2\omega}$$

3.2.1.2   Secular and Long Period Rates

Lagrange's planetary equations can be obtained for the double-averaged potential as

$$\dot{a} = 0$$

$$\dot{e} = -\frac{\eta}{na^2 e}\frac{\partial \langle\langle R_2\rangle\rangle}{\partial \omega}$$

$$\dot{i} = \frac{1}{na^2 \eta \sin i}\left[\cos i\, \frac{\partial \langle\langle R_2\rangle\rangle}{\partial \omega} - \frac{\partial \langle\langle R_2\rangle\rangle}{\partial \Omega}\right] \tag{85}$$

$$\dot{\Omega} = \frac{1}{na^2 \eta \sin i}\frac{\partial \langle\langle R_2\rangle\rangle}{\partial i}$$

$$\dot{\omega} = \frac{\eta}{na^2 e}\frac{\partial \langle\langle R_2\rangle\rangle}{\partial e} - \frac{\cos i}{na^2 \eta \sin i}\frac{\partial \langle\langle R_2\rangle\rangle}{\partial i}$$

$$\dot{M} = n - \frac{\eta^2}{na^2 e}\frac{\partial \langle\langle R_2\rangle\rangle}{\partial e} - \frac{2}{na}\frac{\partial \langle\langle R_2\rangle\rangle}{\partial a}$$

where n is the mean motion and $\eta = \sqrt{1 - e^2}$. The required partial derivatives are

$$\frac{\partial \langle\langle R_2\rangle\rangle}{\partial a} = \frac{\mu_m n_m^2 a}{8}\big[(6 + 9e^2)A + 15e^2 B - 12e^2 - 8\big] \tag{86}$$

$$\frac{\partial \langle\langle R_2\rangle\rangle}{\partial e} = \frac{3\mu_m n_m^2 a^2 e}{8}[3A + 5B - 4] \tag{87}$$

$$\frac{\partial \langle\langle R_2\rangle\rangle}{\partial i} = \frac{\mu_m n_m^2 a^2}{16}\left[(6 + 9e^2)\frac{\partial A}{\partial i} + 15e^2\frac{\partial B}{\partial i}\right] \tag{88}$$

$$\frac{\partial \langle\langle R_2\rangle\rangle}{\partial \Omega} = \frac{\mu_m n_m^2 a^2}{16}\left[(6 + 9e^2)\frac{\partial A}{\partial \Omega} + 15e^2\frac{\partial B}{\partial \Omega}\right] \tag{89}$$

$$\frac{\partial \langle\langle R_2\rangle\rangle}{\partial \omega} = \frac{\mu_m n_m^2 a^2}{16}\left[(6 + 9e^2)\frac{\partial A}{\partial \omega} + 15e^2\frac{\partial B}{\partial \omega}\right] \tag{90}$$

$$\frac{\partial A}{\partial i} = \big(S_{i_m}^2 - C_{\Delta\Omega}^2 C_{i_m}^2 - S_{\Delta\Omega}^2\big)S_{2i} + S_{2i_m} C_{2i} C_{\Delta\Omega} \tag{91}$$

$$\frac{\partial A}{\partial \Omega} = \big(C_{i_m}^2 - C_i^2 C_{i_m}^2 - S_i^2\big)S_{2\Delta\Omega} - \frac{1}{2}S_{2i_m} S_{2i} S_{\Delta\Omega} \tag{92}$$

$$\frac{\partial A}{\partial \omega} = 0 \tag{93}$$

$$\frac{\partial B}{\partial i} = \left[C_{\Delta\Omega}^2 C_{i_m}^2 S_{2i} + S_{\Delta\Omega}^2 S_{2i} - S_{2i} S_{i_m}^2 - S_{2i_m} C_{2i} C_{\Delta\Omega} \right] C_{2\omega} \tag{94}$$
$$+ \left(S_{2\Delta\Omega} S_i S_{i_m}^2 + S_{\Delta\Omega} C_i S_{2i_m} \right) S_{2\omega}$$

$$\frac{\partial B}{\partial \Omega} = \left[S_{2\Delta\Omega} \left(C_i^2 C_{i_m}^2 - S_{i_m}^2 - C_i^2 \right) + \frac{1}{2} S_{2i_m} S_{2i} S_{\Delta\Omega} \right] C_{2\omega} \tag{95}$$
$$- \left(2 C_{2\Delta\Omega} C_i S_{i_m}^2 - C_{\Delta\Omega} S_i S_{2i_m} \right) S_{2\omega}$$

$$\frac{\partial B}{\partial \omega} = -2 \left[C_{\Delta\Omega}^2 \left(1 - C_i^2 C_{i_m}^2 \right) + S_{\Delta\Omega}^2 \left(C_{i_m}^2 - C_i^2 \right) - S_i^2 S_{i_m}^2 - \frac{1}{2} S_{2i_m} S_{2i} C_{\Delta\Omega} \right] S_{2\omega} \tag{96}$$
$$- 2 \left(S_{2\Delta\Omega} C_i S_{i_m}^2 - S_{\Delta\Omega} S_i S_{2i_m} \right) C_{2\omega}$$

The doubly-averaged lunar perturbation model is obtained by substituting Eq. (84) into the Lagrange's planetary equations (85).

3.2.1.3 Extended GA STM Including Third Body Perturbations

The development of the STM for long period effects of the 3rd body perturbations is now addressed, hence, set $D(t)$ as the identity matrix.

3.2.1.3.1 Secular and Long Period Terms

The STM of the current set of orbit elements with respect to the initial orbit elements, $\bar{\phi}_e$, considering only the secular and long period terms, can be calculated from the following relationships:

$$a = a_0$$
$$\lambda = \lambda_0 + \dot{\lambda} \Delta t$$
$$i = i_0 + \dot{i} \Delta t$$
$$q_1 = e \cos \omega = \left(1 - \frac{15}{16} \frac{\mu_m n_m^2}{n} \eta \frac{\partial B}{\partial \omega} \Delta t \right) \left(q_{10} \cos \Delta \omega - q_{20} \sin \Delta \omega \right) \tag{97}$$
$$q_2 = e \sin \omega = \left(1 - \frac{15}{16} \frac{\mu_m n_m^2}{n} \eta \frac{\partial B}{\partial \omega} \Delta t \right) \left(q_{10} \sin \Delta \omega + q_{20} \cos \Delta \omega \right)$$
$$\Omega = \Omega_0 + \dot{\Omega} \Delta t$$

where the subscript "0" means the initial state and $\Delta \omega = \dot{\omega}(t - t_0)$. The STM is obtained by assuming that the orbit element rates $\dot{\Omega}, \dot{\omega}$, and $\dot{\lambda}$ are constant and that $\Delta \omega$ is small. The details of the derivations are presented in Appendix B.

3.2.1.3.2 Geometric Transformation Matrix

The relative motion is best visualized in a local vertical local horizontal (LVLH) frame centered on the chief or a curvilinear system [2]. The $\Sigma(t)$ matrix is used to transform the osculating elements to LVLH coordinates. The normal acceleration is

$$U_h = \frac{h \sin i}{r \sin \theta} \dot{\Omega} \tag{98}$$

From Lagrange equations

$$\dot{\Omega} = \frac{1}{na^2 \eta \sin i} \frac{\partial R_2}{\partial i} \tag{99}$$

3.2.1.4 *Nonlinear Simulation Model and Initial Conditions*

The ECI reference epoch is set at the J2000 epoch. The *XY* plane is the plane of the Earth's orbit at the reference epoch. The *X* axis points to the ascending node of the instantaneous plane of the Earth's orbit and Earth's mean equator at the reference epoch. The *Z* axis is perpendicular to the *XY* plane in the directional sense of the Earth's North Pole at the reference epoch. The *Y* axis is determined by the right-hand rule. The simulations include the gravitational perturbations and the lunar perturbations. The high fidelity ephemerides data for the lunar motion are obtained from the Jet Propulsion Laboratory's HORIZONS website; the data is then interpolated using the method described in Reference 23.

Lagrange's planetary equations provide the rates of change of the classical orbital elements due to the doubly-averaged lunar perturbation. However, because the disturbing potential has been averaged, these now represent the rates of a new set of "lunar"-averaged orbital elements, rather than the instantaneous osculating elements. If equation (85) is applied without correcting the initial conditions for these differences, the results will become increasingly inaccurate as the equations are propagated forward in time. In the absence of an accurate conversion between the osculating and averaged elements, a least squares method is used to correct the initial conditions.

In our problem

$$\Delta x = (a_{osc0} - a_{ls}, \theta_{osc0} - \theta_{ls}, i_{osc0} - i_{ls}, q_{1osc0} - q_{1ls0}, q_{2osc0} - q_{2ls0}, \Omega_{osc0} - \Omega_{ls0}) \tag{100}$$

$$\tilde{y} = (a_{ls}, \theta_{ls}, i_{ls}, q_{1l}s, q_{2ls}, \Omega_{ls}) \tag{101}$$

$$f(\hat{x}) = (a_{osc}, \theta_{osc}, i_{osc}, q_{1osc}, q_{2osc}, \Omega_{osc}) \tag{102}$$

where the subscript "*osc*" stands for osculating elements and "*ls*" represents long and secular averaged elements, while "0" refers to initial values.

3.2.2 Dynamic Model Expansion: Solar Radiation Effects

Solar radiation pressure (SRP) is a nonconservative perturbation. For high altitude orbits, solar radiation pressure can be the dominant perturbative force, particularly for satellites with large area to mass ratio. By intentionally aligning a satellite's orientation with respect to the sun, this perturbative force can be used to maneuver the vehicle. For many years, the focus of SRP studies was confined to the minimization of its effects on spacecraft. More recently, considerable effort has been put into the development of applications to exploit the SRP effects for purposes of interplanetary propulsion, namely with solar sails [22]. Zeng, et al. [23] presented a time-optimal trajectory design for a novel dual-satellite sailcraft to accomplish mid or far-term interstellar missions

Application of SRP for formation flying has been investigated by various researchers. Williams and Wang [24] considered a satellite formation with a solar wing and it was shown that a solar torque can be generated roughly along the orbit direction. This torque can prevent the secular out-of-plane growth in a low-Earth orbit formation that is caused by differential nodal drift. Kumar, et al. [25] and Gong, et al. [26] demonstrated the feasibility of using SRP for maintaining the desired satellite formation for different scenarios.

In this section the GA STM is extended to include the differential SRP for relative motion. The SRP model is developed and the short and long period dynamics due to SRP are presented. Only the SRP perturbation is considered. The differential SRP is primarily caused by the differential area-to mass ratio (AMR) perturbations. The contribution here is that a new variable AMR is introduced to the GA STM to deal with the AMR perturbations. Numerical results show relative position errors are significantly reduced after the differential SRP is included in the GA STM.

3.2.2.1 Solar Radiation Pressure Model

The acceleration due to SRP is [14, 27]

$$\hat{a} = \frac{PA \cos \phi_{inc}}{m} \left\{ 2 \left[\frac{C_d}{3} + C_s \cos \phi_{inc} \right] \hat{n} + \left(1 - C_s\right) \hat{s} \right\} \tag{103}$$

where P is the solar radiation pressure (P=4.56e-6 N/m^2), A is the cross sectional area, m is mass, ϕ_{inc} is the incident angle, $\hat{n}$ is the unit vector of the cross sectional plate, $\hat{s}$ is the unit vector from the satellite to the Sun, and C_a, C_d, C_s are the coefficients of absorption, diffuse and specular reflectivity, respectively. Notice $C_a + C_d + C_s = 1$ and assume the satellite is spherical

$$\hat{a} = \frac{PA}{m} k \hat{s} = P k C_B \hat{s} \tag{104}$$

where $k = 1 + C_s + \frac{2}{3} C_d$ and the area-mass-ratio is $C_B = \frac{A}{m}$.

The components of the acceleration in the radial, transverse and normal direction are

$$U_r = -PkC_B \left(\bar{U}_r \cos\theta + \bar{U}_t \sin\theta \right)$$
$$U_t = -PkC_B \left(\bar{U}_t \cos\theta - \bar{U}_r \sin\theta \right) \tag{105}$$
$$U_h = -PkC_B \bar{U}_h$$

and

$$\bar{U}_r = \cos\Omega\cos\lambda_e + \sin\Omega\sin\lambda_e\cos\varepsilon$$
$$\bar{U}_t = -\sin\Omega\cos i\cos\lambda_e + \cos\Omega\cos i\sin\lambda_e\cos\varepsilon + \sin i\sin\lambda_e\sin\varepsilon \tag{106}$$
$$\bar{U}_h = \sin\Omega\sin i\cos\lambda_e - \cos\Omega\sin i\sin\lambda_e\cos\varepsilon + \cos i\sin\lambda_e\sin\varepsilon$$

3.2.2.2 Secular, Long Period Rates and Short Period Terms
3.2.2.2.1 Secular and Long Period Rates

Substituting Eq. (106) into the nonsingular Gauss equation yields

$$\frac{da}{dt} = \frac{2a^2}{h}\left[(q_1\sin\theta - q_2\cos\theta)U_r + \frac{p}{r}U_t\right]$$

$$\frac{d\theta}{dt} = \frac{h}{r^2} - \frac{r\sin\theta\cos i}{h\sin i}U_h$$

$$\frac{di}{dt} = \frac{r\cos\theta}{h}U_h$$

$$\frac{dq_1}{dt} = \frac{p}{h}\left\{\sin\theta U_r + \left[\left(1+\frac{r}{p}\right)\cos\theta + \frac{r}{p}q_1\right]U_t + \frac{r}{p}q_2\sin\theta\cot i U_h\right\} \tag{107}$$

$$\frac{dq_2}{dt} = \frac{p}{h}\left\{-\cos\theta U_r + \left[\left(1+\frac{r}{p}\right)\sin\theta + \frac{r}{p}q_2\right]U_t - \frac{r}{p}q_1\sin\theta\cot i U_h\right\}$$

$$\frac{d\Omega}{dt} = \frac{r\sin\theta}{h\sin i}U_h$$

$$\frac{dC_B}{dt} = 0$$

Assuming small eccentricity gives

$$\theta = \lambda + 2q_1 \sin \lambda - 2q_2 \cos \lambda$$

$$\frac{r}{a} = 1 - q_1 \cos \lambda - q_2 \sin \lambda$$

(108)

$$\sin \theta = -q_2 + \sin \lambda + q_1 \sin 2\lambda - q_2 \cos 2\lambda$$

$$\cos \theta = -q_1 + \cos \lambda + q_1 \cos 2\lambda + q_2 \sin 2\lambda$$

Substituting Eq. (108) into Eq. (107) gives

$$\dot{a} = \frac{2}{n} PkC_B \left\{ \bar{U}_r \sin \lambda - \bar{U}_t \cos \lambda + \left(\bar{U}_r q_1 - \bar{U}_t q_2 \right) \sin 2\lambda - \left(\bar{U}_r q_2 + \bar{U}_t q_1 \right) \cos 2\lambda \right\}$$

$$\dot{i} = \frac{1}{2na} PkC_B \bar{U}_h \left\{ 3q_1 - 2\cos \lambda - q_1 \cos 2\lambda - q_2 \sin 2\lambda \right\}$$

$$\dot{\Omega} = \frac{1}{2na \sin i} PkC_B \bar{U}_h \left\{ 3q_2 - 2\sin \lambda - q_1 \sin 2\lambda + q_2 \cos 2\lambda \right\}$$

$$\dot{q}_1 = -\frac{PkC_B}{na} \left\{ \frac{3}{2} \bar{U}_t + \frac{1}{2} \bar{U}_t \cos 2\lambda + \frac{1}{2} \bar{U}_r \sin 2\lambda + \frac{1}{4} \left(\bar{U}_r q_1 + 3 \bar{U}_t q_2 \right) \sin \lambda \right.$$

$$\left. + \frac{1}{4} \left(5 \bar{U}_r q_2 - 3 \bar{U}_t q_1 \right) \cos \lambda + \frac{3}{4} \left(\bar{U}_t q_2 - \bar{U}_r q_1 \right) \sin 3\lambda + \frac{3}{4} \left(\bar{U}_r q_2 + \bar{U}_t q_1 \right) \cos 3\lambda \right\} + \dot{\Omega} q_2 \cos i$$

(109)

$$\dot{q}_2 = -\frac{PkC_B}{na} \left\{ -\frac{3}{2} \bar{U}_r + \frac{\bar{U}_t}{2} \sin 2\lambda + \frac{\bar{U}_r}{2} \cos 2\lambda + \frac{1}{4} \left(3 \bar{U}_r q_2 - 5 \bar{U}_t q_1 \right) \sin \lambda \right.$$

$$\left. - \frac{1}{4} \left(3 \bar{U}_r q_1 + \bar{U}_t q_2 \right) \cos \lambda + \frac{3}{4} \left(\bar{U}_r q_2 + \bar{U}_t q_1 \right) \sin 3\lambda + \frac{3}{4} \left(\bar{U}_r q_1 - \bar{U}_t q_2 \right) \cos 3\lambda \right\} - \dot{\Omega} q_1 \cos i$$

$$\dot{\lambda} = n + \frac{PkC_B}{2na} \left\{ -3 \left(\bar{U}_r q_1 + \bar{U}_t q_2 \right) + 4 \bar{U}_t \sin \lambda + 4 \bar{U}_r \cos \lambda + \left(\bar{U}_r q_1 - \bar{U}_t q_2 \right) \cos 2\lambda \right.$$

$$\left. + \left(\bar{U}_r q_2 + \bar{U}_t q_1 \right) \sin 2\lambda \right\} - \dot{\Omega} \cos i$$

$$\dot{C}_B = 0$$

Averaging Eq. (109) by the mean argument of latitude over one orbit and ignoring the shadow effects yields the long period and secular rates [28].

$$\dot{\bar{a}} = 0$$

$$\dot{\bar{i}} = \frac{3PkC_B}{2na}\bar{U}_h q_1$$

$$\dot{\bar{\Omega}} = \frac{3PkC_B}{2na\sin i}\bar{U}_h q_2$$

$$\dot{\bar{q}}_1 = -\frac{3PkC_B}{2na}\bar{U}_t \qquad\qquad (110)$$

$$\dot{\bar{q}}_2 = \frac{3PkC_B}{2na}\bar{U}_r$$

$$\dot{\bar{\lambda}} = n - \frac{3PkC_B}{2na}\left(\bar{U}_r q_1 + \bar{U}_t q_2\right) - \frac{3\cos i}{2na\sin i}PkC_B\bar{U}_h q_2$$

$$\dot{\bar{C}}_B = 0$$

3.2.2.2.2 Short Period Terms

According to the method of averaging the zero order terms of the right sides of Eq. (109) should keep the same formulations, but in terms of the mean elements. Subtracting Eq. (110) from the zero order expansion of Eq. (109) and integrating the remaining terms, the short period terms are [28]

$$\delta a = -\frac{2PkC_B}{n^2}\left[\bar{U}_r\cos\lambda + \bar{U}_t\sin\lambda + \frac{1}{2}\left(\bar{U}_r q_1 - \bar{U}_t q_2\right)\cos 2\lambda + \frac{1}{2}\left(\bar{U}_r q_2 + \bar{U}_t q_1\right)\sin 2\lambda\right]$$

$$\delta i = -\frac{PkC_B\bar{U}_h}{2n^2 a}\left[2\sin\lambda + \frac{1}{2}q_1\sin 2\lambda - \frac{1}{2}q_2\cos 2\lambda\right]$$

$$\delta\Omega = \frac{PkC_B\bar{U}_h}{2n^2 a\sin i}\left[2\cos\lambda + \frac{1}{2}q_1\cos 2\lambda + \frac{1}{2}q_2\sin 2\lambda\right]$$

$$\delta q_1 = -\frac{PkC_B}{4n^2 a}\left\{\bar{U}_t\sin 2\lambda - \bar{U}_r\cos 2\lambda - \left(\bar{U}_r q_1 + 3\bar{U}_t q_2\right)\cos\lambda + \left(5\bar{U}_r q_2 - 3\bar{U}_t q_1\right)\sin\lambda\right.$$

$$\left. - \left(-\bar{U}_r q_1 + \bar{U}_t q_2\right)\cos 3\lambda + \left(\bar{U}_r q_2 + \bar{U}_t q_1\right)\sin 3\lambda\right\} + q_2\cos i\,\delta\Omega \qquad (111)$$

$$\delta q_2 = -\frac{PkC_B}{4n^2 a}\left\{-\bar{U}_t\cos 2\lambda + \bar{U}_r\sin 2\lambda - \left(3\bar{U}_r q_2 - 5\bar{U}_t q_1\right)\cos\lambda - \left(3\bar{U}_r q_1 + \bar{U}_t q_2\right)\sin\lambda\right.$$

$$\left. - \left(\bar{U}_r q_2 + \bar{U}_t q_1\right)\cos 3\lambda + \left(\bar{U}_r q_1 - \bar{U}_t q_2\right)\sin 3\lambda\right\} - q_1\cos i\,\delta\Omega$$

$$\delta\lambda = \frac{PkC_B}{n^2 a}\left[\bar{U}_r\sin\lambda - \bar{U}_t\cos\lambda + \left(\bar{U}_r q_1 - \bar{U}_t q_2\right)\sin 2\lambda - \left(\bar{U}_r q_2 + \bar{U}_t q_1\right)\cos 2\lambda\right] - \delta\Omega\cos i$$

$$\delta C_B = 0$$

The elements on the right sides of Eqs. (110-111) are the averaged or mean elements.

3.2.2.3 Extended GA STM Including SRP Perturbations
3.2.2.3.1 Differential Mean Elements

The STM or the partial derivative matrix of the current orbit elements with respect to the initial orbital elements in the mean space is represented by $\bar{\Phi}_e\left(t,t_0\right) = \dfrac{\partial \mathbf{e}}{\partial \mathbf{e}_0}$. Assume the secular and long period rates are constant. The mean propagation equations are

$$
\begin{aligned}
a &= a_0 + \dot{\bar{a}}\left(t - t_0\right) \\
\lambda &= \lambda_0 + \dot{\bar{\lambda}}\left(t - t_0\right) \\
i &= i_0 + \dot{\bar{i}}\left(t - t_0\right) \\
q_1 &= q_{10} + \dot{\bar{q}}_1\left(t - t_0\right) \\
q_2 &= q_{20} + \dot{\bar{q}}_2\left(t - t_0\right) \\
\Omega &= \Omega_0 + \dot{\bar{\Omega}}\left(t - t_0\right) \\
C_B &= C_{B0} + \dot{\bar{C}}_B\left(t - t_0\right)
\end{aligned}
\tag{112}
$$

The expressions for $\bar{\phi}_e$ are presented in Appendix C.

3.2.2.3.2 Mean to Osculating Transformation

The osculating elements are obtained as functions of the mean elements

$$
\mathbf{e} = \bar{\mathbf{e}} + \delta\mathbf{e}
\tag{113}
$$

where $\bar{\mathbf{e}}$ are the mean elements and $\delta\mathbf{e}$ are the short period terms as shown in Eq. (112) and Eq. (113), respectively. Taking derivatives with respect to the mean elements for Jacobian matrix, we have the mean to osculating transformation matrix or *D* matrix, as shown in the Appendix C.

3.2.2.3.3 Geometric Transformation

The Sigma matrix, Σ, is used to transform osculating elements to LVLH coordinates. Although the solar radiation pressure or atmospheric drag is a nonconservative perturbation, the velocity components have the same formulations as those of two-body problem. The normal accelerations are given in Eq. (105).

3.2.3 Dynamic Model Expansion: Drag Perturbations

Atmospheric drag is one of the major perturbations that influence satellite motion, especially for satellites in low earth orbit (LEO). Extensive modeling has been accurately built up for the gravitational field, but analytical treatment of atmospheric drag is very difficult since atmospheric density is fluctuated and tabular due to solar activity. It is well known the dynamic

system with drag is nonlinear and nonconservative and the analytical solutions of the dynamic system are unavailable. The best we can do is to derive approximate analytical solutions with desired accuracy.

Brouwer and Hori [29] obtained the analytical solutions for gravity and drag perturbations using von Zeipel transformations in Brouwer [3] on the basis of an exponential density model. The density function was expanded into a series of the ratio of the eccentricity to the density scale height. The resulting theory is limited to Earth satellite orbits with small eccentricities. Lane, et al. [30] improved the Brouwer-Hori work. By using a power law density model, the expansion of the density function was avoided so that a better convergence for low perigee heights is achieved. Hoots [31] further improved Lane's theory by eliminating small eccentricity divisors in the differential equations. Moreover he applied an averaging method so that the differential equations, rid of the mean anomaly, could be integrated more easily.

The differential drag has been used for controlling relative positions between satellites [32-33]. For formation flying, the difference between the effective cross sectional areas leads to the differential drag, either by change satellite attitude or by using deployable drag panels. Most papers about differential drag for formation control are based on CW equations or more accurately based on Schweighart and Sedwick equations [34] in which the differential drag is projected into the LVLH frame or along-track direction.

Reid and Misra [35] revised the Schweighart and Sedwick equations to include differential drag and extend the equations for reference orbits with small eccentricity. Recently Kumar, et al [36] examined the feasibility of formation maintenance using environmental forces, especially solar radiation pressure and aerodynamic forces. It is assumed that the satellites are equipped with solar flaps or aerodynamic flaps. By appropriate rotation of these flaps, it is possible to influence the relative motion between satellites in a formation.

Most authors considered the differential drag as a means to control satellite formations. Mishne [37] introduced mean rates due to drag into relative motion, which is a basis for control. Carter and Humi tried to include the aerodynamic forces into the analytical solutions of relative motion. Carter and Humi modified the Clohessy-Wiltshire equations to include the effects of atmospheric drag in two separate papers. The relative motion equations developed included a drag force that was proportional to linear velocity [38]. Then the relative motion equations developed included the effects of a more realistic drag model, one where drag is proportional to the square of velocity [39]. Based on these simplifying assumptions, a set of linear differential equations were obtained which can be solved in terms of integrals. This enables the representation of the solution of the problem in terms of a state-transition matrix. Palmerini et al. [40-41] showed the performance based on the Carter and Humi solutions is more efficient than CW equations if the aerodynamic perturbations are modeled into the analytical solutions.

In this report we extend the GA STM [1] to include differential drag. The exponential formulation is selected as the density model. The method of averaging is used for setting up the STM for mean element propagation. The short period terms are ignored. The extended GA STM includes parameter variables that allow modeling different ballistic coefficients.

3.2.3.1   Drag Perturbations

The satellite accelerations due to atmospheric drag are given by

$$\mathbf{U} = -\tfrac{1}{2} C_D C_B \rho v \mathbf{v} \tag{114}$$

Assume a non-rotating atmosphere, the acceleration in the normal direction is zero and the radial and tangential components are

$$
\begin{aligned}
U_r &= -\tfrac{1}{2} k \rho v v_r \\
U_t &= -\tfrac{1}{2} k \rho v v_t \\
U_h &= 0
\end{aligned}
\tag{115}
$$

where

$$
\begin{aligned}
k &= C_D C_B \\
v_r &= \sqrt{\tfrac{\mu}{p}} e \sin f \\
v_t &= \sqrt{\tfrac{\mu}{p}} \left(1 + e \cos f \right) \\
v &= \sqrt{\tfrac{\mu}{p}} \left(1 + 2e \cos f + e^2 \right)^{\frac{1}{2}}
\end{aligned}
$$

and ρ is the atmospheric density, v is the speed of the satellite relative to the atmosphere, $\mathbf{v}$ is a velocity vector in the direction motion, C_D is the dimensionless drag coefficient.

The atmospheric density model in Eq. (114) is

$$\rho = \rho_p e^{-\beta(r - r_p)} \tag{116}$$

where r_p is perigee altitude and β is the inverse of the atmospheric scale height.

3.2.3.2   Secular, Long and Short Period Terms from Drag Perturbations

Since the normal perturbed acceleration is zero, the extended nonsingular Gauss equation becomes

$$\frac{da}{dt} = \frac{2a^2}{h}\left[\left(q_1 \sin\theta - q_2 \cos\theta\right)U_r + \frac{p}{r}U_t\right]$$

$$\frac{d\lambda}{dt} = n - \frac{1}{na}\left[U_r\left(\frac{2r}{a} + \frac{\eta}{1+\eta}e\cos f\right) - U_t\frac{\eta}{1+\eta}\left(1+\frac{r}{p}\right)e\sin f\right]$$

$$\frac{di}{dt} = 0$$

$$\frac{dq_1}{dt} = \frac{p}{h}\left\{\sin\theta U_r + \left[\left(1+\frac{r}{p}\right)\cos\theta + \frac{r}{p}q_1\right]U_t\right\} \qquad (117)$$

$$\frac{dq_2}{dt} = \frac{p}{h}\left\{-\cos\theta U_r + \left[\left(1+\frac{r}{p}\right)\sin\theta + \frac{r}{p}q_2\right]U_t\right\}$$

$$\frac{d\Omega}{dt} = 0$$

$$\frac{dC_B}{dt} = 0$$

Assuming small eccentricity, we have approximately

$$\theta = \lambda + 2q_1 \sin\lambda - 2q_2 \cos\lambda$$

$$\frac{r}{a} = 1 - q_1 \cos\lambda - q_2 \sin\lambda$$

$$\sin\theta = -q_2 + \sin\lambda + q_1 \sin 2\lambda - q_2 \cos 2\lambda \qquad (118)$$

$$\cos\theta = -q_1 + \cos\lambda + q_1 \cos 2\lambda + q_2 \sin 2\lambda$$

With small eccentricity assumption, expanding Eq. (116) to the second order by Taylor series

$$\rho = \rho_p \exp\left(-\xi e\right)\left[1 + \frac{1}{4}\xi^2 e^2 + \xi\left(q_1 \cos\lambda + q_2 \sin\lambda\right) + \frac{1}{4}\xi^2\left(q_1^2 - q_2^2\right)\cos 2\lambda + \frac{1}{2}\xi^2 q_1 q_2 \sin 2\lambda\right] \quad (119)$$

where $\xi = \beta a$.

Substituting Eq. (115) and Eqs. (118-119) into (117) gives

$$\dot{a} = -na^2 C_D C_B \rho_p \exp(-\xi e)[1 + \frac{1}{4}\xi^2 e^2 + (\xi + 3)(q_1 \cos\lambda + q_2 \sin\lambda) +$$

$$\frac{1}{4}\xi^2 (q_1^2 - q_2^2)\cos 2\lambda + \frac{1}{2}\xi^2 q_1 q_2 \sin 2\lambda]$$

$$\dot{\lambda} = n + \frac{1}{2}naC_D C_B \rho_p \exp(-\xi e)(q_1 \sin\lambda - q_2 \cos\lambda)$$

$$\dot{i} = 0$$

$$\dot{q}_1 = -\frac{1}{2}naC_D C_B \rho_p \exp(-\xi e)[(1+\xi)q_1 + \left(2 + \frac{3}{4}\xi^2 q_1^2 + \frac{1}{4}\xi^2 q_2^2\right)\cos\lambda +$$

$$\frac{1}{2}\xi^2 q_1 q_2 \sin\lambda + (\xi + 3)(q_1 \cos 2\lambda + q_2 \sin 2\lambda) + \tag{120}$$

$$\frac{1}{4}\xi^2 (q_1^2 - q_2^2)\cos 3\lambda + \frac{1}{2}\xi^2 q_1 q_2 \sin 3\lambda]$$

$$\dot{q}_2 = -\frac{1}{2}naC_D C_B \rho_p \exp(-\xi e)[(1+\xi)q_2 + \left(2 + \frac{1}{4}\xi^2 q_1^2 + \frac{3}{4}\xi^2 q_2^2\right)\sin\lambda +$$

$$\frac{1}{2}\xi^2 q_1 q_2 \cos\lambda + (\xi + 3)(q_1 \sin 2\lambda - q_2 \cos 2\lambda) +$$

$$\frac{1}{4}\xi^2 (q_1^2 - q_2^2)\sin 3\lambda - \frac{1}{2}\xi^2 q_1 q_2 \cos 3\lambda]$$

$$\dot{\Omega} = 0$$

$$\dot{C}_B = 0$$

Averaging Eq. (120) over the mean argument of latitude over one orbit, we obtain the long period and secular rates

$$\dot{a} = -na^2 C_D C_B \rho_p \exp(-\xi e)\left(1 + \frac{1}{4}\xi^2 e^2\right)$$

$$\dot{\lambda} = n - \frac{3}{2}\frac{n}{a}\dot{a}\Delta t$$

$$\dot{i} = 0$$

$$\dot{q}_1 = -\frac{1}{2}naC_D C_B \rho_p \exp(-\xi e)(1+\xi)q_1 \tag{121}$$

$$\dot{q}_2 = -\frac{1}{2}naC_D C_B \rho_p \exp(-\xi e)(1+\xi)q_2$$

$$\dot{\Omega} = 0$$

$$\dot{C}_B = 0$$

The zero order terms of the right sides of Eq. (120) should keep the same formulations, but in terms of the mean elements. Subtracting Eq. (121) from the zero order expansion of Eq. (120) and integrating the remaining terms the short period terms are

$$\delta a = -a^2 C_D C_B \rho_p \exp(-\xi e)[(\xi+3)(q_1 \sin\lambda - q_2 \cos\lambda) +$$

$$\frac{1}{8}\xi^2(q_1^2 - q_2^2)\sin 2\lambda - \frac{1}{4}\xi^2 q_1 q_2 \cos 2\lambda]$$

$$\delta\lambda = \frac{1}{2}aC_D C_B \rho_p \exp(-\xi e)(q_1 \cos\lambda + q_2 \sin\lambda) - \frac{3}{2}\int \frac{n}{a}\delta a\, dt$$

$$\delta i = 0$$

$$\delta q_1 = -\frac{1}{2}aC_D C_B \rho_p \exp(-\xi e)[\left(2 + \frac{3}{4}\xi^2 q_1^2 + \frac{1}{4}\xi^2 q_2^2\right)\sin\lambda -$$

$$\frac{1}{2}\xi^2 q_1 q_2 \cos\lambda + \frac{1}{2}(\xi+3)(q_1 \sin 2\lambda - q_2 \cos 2\lambda) +$$

$$\frac{1}{12}\xi^2(q_1^2 - q_2^2)\sin 3\lambda - \frac{1}{6}\xi^2 q_1 q_2 \cos 3\lambda]$$

$$\delta q_2 = -\frac{1}{2}aC_D C_B \rho_p \exp(-\xi e)[-\left(2 + \frac{1}{4}\xi^2 q_1^2 + \frac{3}{4}\xi^2 q_2^2\right)\cos\lambda +$$

$$\frac{1}{2}\xi^2 q_1 q_2 \sin\lambda - \frac{1}{2}(\xi+3)(q_1 \cos 2\lambda + q_2 \sin 2\lambda) -$$

$$\frac{1}{12}\xi^2(q_1^2 - q_2^2)\cos 3\lambda - \frac{1}{6}\xi^2 q_1 q_2 \sin 3\lambda]$$

$$\delta\Omega = 0$$

$$\delta C_B = 0$$

(122)

The long period and secular rates Eq. (121) are obtained through the second order expansion of the density function; however, a more accurate method to obtain the mean rates is to use modified Bessel functions of the first kind [14]:

$$\dot{a} = -a^2 nk\rho_p f_1$$

$$\dot{e} = -ank\eta^2 \rho_p f_2$$

$$\dot{i} = 0$$

$$\dot{\Omega} = 0$$

$$\dot{\omega} = 0$$

$$\dot{M} = n_0 - \frac{3}{2}\frac{n_0}{a_0}\dot{a}t$$

(123)

where

$$f_1 = \left[I_0 + 2eI_1 + \tfrac{3}{4}e^2 \left(I_0 + I_2 \right) \right] \exp\left(-\beta ae \right)$$

$$f_2 = \left[I_1 + \tfrac{1}{2}e\left(I_0 + I_2 \right) + \tfrac{1}{8}e^2 \left(3I_1 + I_3 \right) \right] \exp\left(-\beta ae \right)$$

$I_n \left(\beta ae \right)$ are modified Bessel functions of the first kind,

$$I_n (z) = \frac{1}{2\pi} \int_0^{2\pi} e^{z\cos\theta} \cos\left(n\theta \right) d\theta \tag{124}$$

or

$$I_n (z) = \sum_{k=0}^{\infty} \frac{1}{(n+k)!k!} \left(\frac{z}{2} \right)^{n+2k} \tag{125}$$

3.2.3.3 *Extended GA STM Including Drag Perturbations*
3.2.3.3.1   Extended GA STM for Differential Mean Elements

It can be shown that the solution difference is very small between Eq. (121) and Eq. (123) for small eccentricity. Here we use Eq. (123) to set up the mean STM. Assume the constant mean rates

$$a = a_0 + \dot{a}_D \Delta t$$

$$\lambda = \lambda_0 + \left(n - \frac{3}{4}\frac{n}{a}\dot{a}_D\Delta t \right)\Delta t$$

$$i = i_0$$

$$q_1 = e\cos\omega = \left(e_0 + \dot{e}\Delta t \right)\cos\omega_0 = \left(1 + \frac{\dot{e}}{e_0}\Delta t \right)q_{10} = \left(1 + f_3\Delta t \right)q_{10} \tag{126}$$

$$q_2 = e\sin\omega = \left(e_0 + \dot{e}\Delta t \right)\sin\omega_0 = \left(1 + \frac{\dot{e}}{e_0}\Delta t \right)q_{20} = \left(1 + f_3\Delta t \right)q_{20}$$

$$\Omega = \Omega_0$$

$$C_B = C_{B0}$$

where

$$f_3 = -anC_DC_B\eta^2\rho_p\frac{f_2}{e} \tag{127}$$

From Eq. (125), we have

$$I_n = \frac{\beta ae}{2n}\left(I_{n-1} - I_{n+1}\right) \tag{128}$$

We can remove the zero eccentricity in the function f_3

$$f_3 = -\tfrac{1}{2}anC_DC_B\eta^2\rho_P\left[(1+a\beta)I_0 + (1-a\beta)I_2 + \tfrac{1}{4}e(3I_1 + I_3)\right]\exp(-\beta ae) \tag{129}$$

Taking the derivative of Eq. (126) with respect to the initial mean elements, we have the mean STM, as shown in Appendix D.

3.2.3.3.2 Mean to Osculating Element Transformation

Taking the derivative of Eq. (122) with respect to the mean elements yields the D_D matrix, as shown in Appendix D.

3.2.3.3.3 Geometric Transformation Matrix

Since U_h, the normal acceleration caused by drag perturbations, is zero, substituting in Eq. (126) gives the geometric transformation matrix.

3.2.3.4 Drag and Gravity Combined Perturbations
3.2.3.4.1 Extended GA STM for Mean Elements

The combined mean element propagation

$$
\begin{aligned}
a &= a_0 + \dot{a}_D\Delta t \\
\lambda &= \lambda_0 + \left(n + \dot{\lambda}_G - \frac{3}{4}\frac{n}{a}\dot{a}_D\Delta t\right)\Delta t \\
i &= i_0 \\
q_1 &= (1 + f_3\Delta t)\left(q_{10}\cos(\Delta\omega_G) - q_{20}\sin(\Delta\omega_G)\right) \\
q_2 &= (1 + f_3\Delta t)\left(q_{10}\sin(\Delta\omega_G) + q_{20}\cos(\Delta\omega_G)\right) \\
\Omega &= \Omega_0 + \dot{\Omega}_G \\
C_B &= C_{B0}
\end{aligned} \tag{130}
$$

Taking the derivatives of Eq. (130) with respect to the initial mean elements, gives the mean STM for drag and gravity combined perturbations.

3.2.3.4.2 Mean to Osculating Element Transformation

The mean to osculating transformation is

$$D = D_G + D_D \tag{131}$$

The drag perturbations do not change the geometric transformation matrix.

3.2.3.5 *Correction for Coupling Effects from Combined Perturbations*

The complexity of the oblateness and drag interactions was illustrated by Brouwer and Hori [30]. Green [41] expanded the combined perturbations to the second order and considered the crossing terms to be the coupling effects. The simple way to deal this problem is to use osculating height for air density when calculating mean drag functions [10, 42-43]. This is because the osculating height variations due to the Earth oblateness for LEO satellites can be several kilometers, which greatly influence the atmospheric density.

The correction for the height or radial distance [4] is

$$\delta r = \frac{1}{2} J_2 \frac{R_e^2}{p} \left(1 - \frac{3}{2} \sin^2 i \right) \left(1 + 2 \frac{r}{a\eta} + \frac{e \cos f}{1 + \eta} \right) - \frac{1}{4} J_2 \frac{R_e^2}{p} \sin^2 i \cos 2\theta \tag{132}$$

Notice the variables on the right sides of Eq. (132) are the mean variables. The corrected density is

$$\rho = \rho_p e^{-\beta(r + \delta r - r_p)} \tag{133}$$

Substituting Eq. (132) into (133) then Eq. (130) gives the mean rates for the combined perturbations.

3.2.4 Semi-Analytic Extended GA STM Including Drag and Gravity Perturbations

Accurate modeling of drag perturbations can be achieved by the use of semi-analytic schemes. Arsenault et al [44] suggested using a lower-order numerical integration scheme for drag perturbations. Hoots [10] applied the Gauss-Legendre formula to integrate the averaged drag functions.

Since the short period terms are averaged out, we use the lower order integration methods to propagate the mean elements. The Euler method is an example:

$$x_n = x_{n-1} + f(x_{n-1}, t_{n-1}) h \tag{134}$$

where *h* is the step size. The GA STM semi-analytic propagation is achieved using the steps outlined by Eqs. (135-137). The differential orbital elements at the initial time t_0 are obtained from the initial relative state vector as

$$\delta\mathbf{e}(t_0) = D^{-1}(t_0)\Sigma^{-1}(t_0)\mathbf{X}(t_0) \tag{135}$$

The averaged elements of the chief and deputy are propagated for an arbitrary time period $[t_0, t_N]$ by using the Euler method with *n* steps

$$
\begin{aligned}
\mathbf{e}_C(t_n) &= \mathbf{e}_C(t_{n-1}) + f\left(\mathbf{e}_C(t_{n-1}), t_{n-1}\right)h \\
\mathbf{e}_D(t_n) &= \mathbf{e}_D(t_{n-1}) + f\left(\mathbf{e}_D(t_{n-1}), t_{n-1}\right)h \\
\mathbf{e}_C(t_0) &= \mathbf{e}(t_0) \\
\mathbf{e}_D(t_0) &= \mathbf{e}(t_0) + \delta\mathbf{e}(t_0) \\
\mathbf{e}_C(t_N) &= \mathbf{e}_C(t_n) \\
\mathbf{e}_D(t_N) &= \mathbf{e}_D(t_n)
\end{aligned}
\tag{136}
$$

Finally, the relative state vector at the desired final time is obtained as

$$\mathbf{X}(t_N) = \Sigma(t_N)D(t_N)\left(\mathbf{e}_D(t_N) - \mathbf{e}_C(t_N)\right) \tag{137}$$

where **e** is the vector of the averaged elements and the subscripts *C* and *D* indicate the chief and deputy satellites, respectively. An alternative option is to use integration methods with variable step sizes, such as ODE45 in MATLAB. The averaged semi-major axis and eccentricity values are obtained by the Legendre-Gauss-Lobatto integration rule over one orbit using the rates

$$
\begin{aligned}
\dot{a}_d &= -\frac{a^2 k}{T}\sum_{i=0}^{N}\rho_i\left(1+e\cos E_i\right)^{\frac{3}{2}}\left(1-e\cos E_i\right)^{-\frac{1}{2}} w_i \\
\dot{e}_d &= -\frac{a\eta^2 k}{T}\sum_{i=0}^{N}\rho_i\left(1+e\cos E_i\right)^{\frac{1}{2}}\left(1-e\cos E_i\right)^{-\frac{1}{2}}\cos E_i w_i
\end{aligned}
\tag{138}
$$

ρ is the atmospheric density model, which in general is represented by a complex model, such as a tabular data model, here the exponential model is used as an example.

3.3 Dynamic Model, Navigation Accuracy and Thruster Accuracy Consistency

Although the guidance, navigation, and control (GNC) subsystems are commonly grouped together in the spacecraft design process, in practice, there are still inefficiencies caused by a lack of interdependency between them. Notably, the dynamical model in the navigation algorithm is often set *ad hoc* without explicit regard for the level of measurement, guidance, or control errors expected. We understand qualitatively that the "best" dynamical model will meet

some user-defined criteria on state uncertainty and maneuver cost while minimizing computational effort. For example, it is operationally suboptimal to implement a high-fidelity gravity model when the measurement hardware is known to be wildly inaccurate [46]. On the other hand, maneuvers executed to cancel out the effects of known yet ignored perturbations, if frequent enough, would deplete on-board fuel very quickly and shorten mission lifespan. A quantitative study is thus warranted, preferably via an analytical approach, on the consistency of GNC hardware subsystems versus dynamical modeling algorithms.

In this chapter, we tackle a subset of this problem: namely, we develop methods to quickly survey the trade space between navigation system parameters and dynamical model fidelity. We focus our efforts on forces that have precise deterministic physical models, e.g., the Earth's gravity, such that modeling errors may be regarded as biases. Our contributions are as follows. First, we show that a change in the dynamical model may be related to its corresponding change in STM via an explicitly defined vector function. This result not only allows us to compute the state transition matrix for multiple dynamical models efficiently, but also demonstrates that the change in the STM is typically on the order of 10^0 % over tens of orbit periods of the chief satellite. As such, as our second contribution, the linear sensitivity relating dynamical model fidelity to maximum *a posteriori* state estimate bias is derived. Although the dynamical model error cannot be factored out as a linear operator like the observation covariance or cadence, we may still gain approximate yet quick design insight into choosing an appropriate dynamical model for a set of given navigation system requirements. Finally, the cost of employing a particular dynamical model will be characterized through a maneuver metric first proposed by Schaub and Alfriend [47]. That is, the state deviation of the estimated trajectory from the reference is analytically transformed into a Δv via Gauss' planetary equations. The three results presented will simplify the workflow of designing GNC systems by mitigating the need to conduct a large-scale numerical validation of system performance.

3.3.1   Relating Dynamical Model and State Transition Matrix Fidelity

Suppose $\boldsymbol{x}(t; \boldsymbol{x}_0)$ is the trajectory given by a high-fidelity dynamical model $\dot{\boldsymbol{x}}(t; \boldsymbol{x}_0)$ that we regard as truth, and $\boldsymbol{x}_F(t; \boldsymbol{x}_0)$ is that given by the approximated dynamics $\dot{\boldsymbol{x}}_F(t; \boldsymbol{x}_0)$. The semicolon separates the time variable t from the initial conditions $\boldsymbol{x}_0$, which are treated as parameters. We define a scaling function $\boldsymbol{m}(t)$ such that

$$\mathbf{m}^i(t)\,\dot{\mathbf{x}}_F^i(t; \mathbf{x}_0) = \dot{\mathbf{x}}^i(t; \mathbf{x}_0) \tag{139}$$

for all *t* and all *i*, where the superscript indicates a vector or matrix index. We assume that the vectors are expressed in an inertial reference frame.

The state transition matrix (STM) of the true dynamics is given by

$$\Phi^{ij}(t; \mathbf{x}_0) = \frac{\partial \mathbf{x}^i}{\partial \mathbf{x}_0^j} \tag{140}$$

Then, for $\Phi^{ij}_F \neq 0$,

$$\frac{\Phi^{ij}}{\Phi^{ij}_F} = \frac{\partial \mathbf{x}^i/\partial \mathbf{x}^j_0}{\partial \mathbf{x}^i_F/\partial \mathbf{x}^j_{F,0}} \approx \frac{\left[\mathbf{x}^i(t; \mathbf{x}_0 + \mathbf{e}^j) - \mathbf{x}^i(t; \mathbf{x}_0)\right]/\varepsilon}{\left[\mathbf{x}^i_F(t; \mathbf{x}_0 + \mathbf{e}^j) - \mathbf{x}^i_F(t; \mathbf{x}_0)\right]/\varepsilon} = \frac{\mathbf{x}^i(t; \mathbf{x}_0 + \mathbf{e}^j) - \mathbf{x}^i(t; \mathbf{x}_0)}{\mathbf{x}^i_F(t; \mathbf{x}_0 + \mathbf{e}^j) - \mathbf{x}^i_F(t; \mathbf{x}_0)} \tag{141}$$

where $\mathbf{e}^j$ is a small variation along the j-direction with magnitude $\varepsilon \ll 1$. Now,

$$\mathbf{x}^i(t; \mathbf{x}_0) = \int_0^t \dot{\mathbf{x}}^i(\tau; \mathbf{x}_0)\mathrm{d}\tau + \mathbf{x}^i_0 = \int_0^t \mathbf{m}^i(\tau)\dot{\mathbf{x}}^i_F(\tau, \mathbf{x}_0)\mathrm{d}\tau + \mathbf{x}^i_0 \tag{142}$$

Applying integration by parts,

$$\mathbf{x}^i(t; \mathbf{x}_0) = \left[\mathbf{m}^i(\tau)\mathbf{x}^i_F(\tau; \mathbf{x}_0)\right]_0^t - \int_0^t \dot{\mathbf{m}}^i(\tau)\mathbf{x}^i_F(\tau; \mathbf{x}_0)\mathrm{d}\tau + \mathbf{x}^i_0 \tag{143}$$

$\int_0^t \dot{\mathbf{m}}^i(\tau)\mathbf{x}_F(\tau, \mathbf{x}_0)\mathrm{d}\tau \approx \mathbf{0}$ is a good assumption to order $10^0\,\%$ or better over 10^0 days for many Earth orbiters. Therefore,

$$\mathbf{x}^i(t; \mathbf{x}_0) \approx \mathbf{m}^i(t)\mathbf{x}^i_F(t; \mathbf{x}_0) - \mathbf{m}^i(0)\mathbf{x}^i_0 + \mathbf{x}^i_0 \tag{144}$$

$\mathbf{m}(0; \mathbf{x}_0) \approx \mathbf{m}(0; \mathbf{x}_0 + \mathbf{e}^j) \approx \mathbf{1}$ is, again, a good assumption to order $10^0\,\%$ or better. Thus, we can rewrite Eq. (141) as

$$\frac{\Phi^{ij}}{\Phi^{ij}_F} \approx \frac{\mathbf{m}^i(t)\left[\mathbf{x}^i_F(t; \mathbf{x}_0 + \mathbf{e}^j) - \mathbf{x}^i_F(t; \mathbf{x}_0)\right]}{\mathbf{x}^i_F(t; \mathbf{x}_0 + \mathbf{e}^j) - \mathbf{x}^i_F(t; \mathbf{x}_0)} = \mathbf{m}^i(t) \tag{145}$$

As such, one may compute the STM of the approximated dynamics $\Phi_F(t; \mathbf{x}_0)$ solely through the solution flow of the true dynamics $\mathbf{x}(t; \mathbf{x}_0)$, its corresponding STM $\Phi(t; \mathbf{x}_0)$, and the function $\mathbf{m}(t)$, which is readily available via $\mathbf{x}_F(t; \mathbf{x}_0)$. That is, for some t such that $\mathbf{m}^i(t) \neq 0$,

$$\Phi^{ij}_F(t; \mathbf{x}_0) = \frac{\Phi^{ij}(t; \mathbf{x}_0)}{\mathbf{m}^i(t)} \tag{146}$$

Since there is no need to solve ODEs for each component in Φ_F, the method above significantly speeds up the propagation of the secondary, assuming it is within the linear dynamical regime of the primary. Furthermore, the scaling function $\mathbf{m}(t)$ provides insight into the accuracy of the approximated STM with respect to the truth. The difference between the true and approximated STMs $\Delta\Phi$ is given as

$$\Delta\Phi(t; \mathbf{x}_0) = \Phi_F(t; \mathbf{x}_0) - \Phi(t; \mathbf{x}_0) = [M(t) - I]\Phi(t; \mathbf{x}_0) \tag{147}$$

where $M(t)$ is a matrix with $\mathbf{m}(t)$ along its diagonal and I is the identity matrix.

For instance, consider the simple 1-dimensional case

$$\dot{x} = x$$

$$\dot{x}_F = mx$$

(148)

where m is held constant. Then, the solution flow for the true dynamics is given as $x(t; x_0) = x_0 e^{t-t_0}$. Next,

$$x_F = \int_{t_0}^{t} mx_0 e^{\tau-t_0} \, d\tau + x_0 = mx_0 e^{t-t_0} = mx$$

(149)

such that $\Phi_F = m\Phi$ as derived.

3.3.2 Linear Sensitivity Analysis Between Dynamical Model Fidelity and Maximum *A Posteriori* State Estimates

We now derive below such a function for the batch least squares.

Nominally [48],

$$\hat{\mathbf{x}}_0 = \Lambda^{-1}\mathbf{N}$$

$$P_0 = \Lambda^{-1}$$

(150)

$$\Lambda = \sum_{i}^{N}(H_i^{\mathrm{T}}R_i^{-1}H_i) + \bar{P}_0$$

$$\mathbf{N} = \sum_{i}^{N}(H_i^{\mathrm{T}}R_i^{-1}\mathbf{y}_i) + \bar{P}_0^{-1}\bar{\mathbf{x}}_0$$

(151)

$$H_i = \tilde{H}_i\Phi(t_i; \mathbf{x}_0)$$

(152)

where $\hat{\mathbf{x}}_0$ and P_0 are the state deviation estimate and associated covariance at epoch, respectively, Λ is the information matrix, $\mathbf{N}$ is the normal vector, R_i is the observation covariance, $\bar{P}_0$ is the *a priori* covariance, $\mathbf{y}_i$ is the observation deviation vector from the reference trajectory, $\tilde{H}_i$ is the linear observation-state relationship, and $\Phi(t_i; \mathbf{x}_0) \stackrel{\text{def}}{=} \Phi_i$ is the STM. Subscripts indicate values for the i-th observation, and the summation is over all N observations. We assume that the observations are uncorrelated in time; thus, both the information matrix and normal vector may be accumulated as a summation.

Now, suppose we have an approximate dynamical model such that the new trajectory is given as

$$\mathbf{x}_{\mathrm{F}}(t_i; \mathbf{x}_0) = \mathbf{x}(t_i; \mathbf{x}_0) + \Delta\mathbf{x}(t_i; \mathbf{x}_0), \Phi_{\mathrm{F}}(t_0; \mathbf{x}_0) = \Phi(t_i; \mathbf{x}_0) + \Delta\Phi(t_i; \mathbf{x}_0)$$
$$\Leftrightarrow \mathbf{x}_{\mathrm{F},i} = \mathbf{x}_i + \Delta\mathbf{x}_i, \Phi_{\mathrm{F},i} = \Phi_i + \Delta\Phi_i \qquad (153)$$

Then, let

$$\hat{\mathbf{x}}_{\mathrm{F}} = (\Lambda_{\mathrm{F}})^{-1}\, \mathbf{N}_{\mathrm{F}}, P_{\mathrm{F}} = (\Lambda_{\mathrm{F}})^{-1} \qquad (154)$$

denote the state deviation estimate and associated covariance, respectively, obtained from the approximate model. The goal is to express analytically $\Delta\hat{\boldsymbol{x}}_0 = \hat{\boldsymbol{x}}_{\mathrm{F},0} - \hat{\boldsymbol{x}}_0$, $\Delta P_0 = P_{\mathrm{F},0} - P_0$. First, simply plug in

$$\Lambda_{\mathrm{F}} = \sum\left[(\Phi_i + \Delta\Phi_i)^{\mathrm{T}} \tilde{H}_i^{\mathrm{T}} R_i^{-1} \tilde{H}_i(\Phi_i + \Delta\Phi_i)\right] \approx \Lambda + \sum\left[\Delta H_i^{\mathrm{T}} R_i^{-1} H_i + H_i^{\mathrm{T}} R_i^{-1}\Delta H_i\right] \quad (155)$$

where $\Delta H_i = \hat{H}_i \Delta\Phi_i$ and any second-order terms are ignored. Similarly,

$$\mathbf{N}_{\mathrm{F}} = \sum\left[(\Phi_i + \Delta\Phi_i)^{\mathrm{T}} \tilde{H}_i^{\mathrm{T}} R_i^{-1} \mathbf{y}_{\mathrm{F},i}\right] + \bar{P}_0^{-1}\bar{\mathbf{x}}_0 \qquad (156)$$

Now, given $\boldsymbol{y}_{F,i} = \boldsymbol{y}_i + \Delta\boldsymbol{y}_i \approx \boldsymbol{y}_i - \tilde{H}_i\Delta\boldsymbol{x}_i$ since $\boldsymbol{Y}_i - \boldsymbol{G}(\boldsymbol{x}_{\mathrm{F},i}) = \boldsymbol{Y}_i - \boldsymbol{G}(\boldsymbol{x}_i) + \Delta\boldsymbol{y}_i \Leftrightarrow \Delta\boldsymbol{y}_i = \boldsymbol{G}(\boldsymbol{x}_i) - \boldsymbol{G}(\boldsymbol{x}_{\mathrm{F},i})$,

$$\mathbf{N}_{\mathrm{F}} = \mathbf{N} + \sum\left[\Delta H_i^{\mathrm{T}} R_i^{-1} \mathbf{y}_i - H_i^{\mathrm{T}} R_i^{-1} \tilde{H}_i\Delta\mathbf{x}_i\right] \qquad (157)$$

So,

$$\left\{\Lambda + \sum\left[\Delta H_i^{\mathrm{T}} R_i^{-1} H_i + H_i^{\mathrm{T}} R_i^{-1}\Delta H_i\right]\right\}\hat{\mathbf{x}}_{\mathrm{F},i} = \mathbf{N} + \sum\left[\Delta H_i^{\mathrm{T}} R_i^{-1} \mathbf{y}_i - H_i^{\mathrm{T}} R_i^{-1} \tilde{H}_i\Delta\mathbf{x}_i\right] \quad (158)$$

$$\hat{\mathbf{x}}_{\mathrm{F}} = [\Lambda + L]^{-1}\,(\mathbf{N} + \boldsymbol{\eta}) \qquad (159)$$

where

$$L = \sum\left[\Delta H_i^{\mathrm{T}} R_i^{-1} H_i + H_i^{\mathrm{T}} R_i^{-1}\Delta H_i\right], \boldsymbol{\eta} = \sum\left[\Delta H_i^{\mathrm{T}} R_i^{-1} \mathbf{y}_i - H_i^{\mathrm{T}} R_i^{-1} \tilde{H}_i\Delta\mathbf{x}_i\right] \quad (160)$$

Note that for some square matrix Q such that $Q^n \to 0$ $(n \to \infty)$,

$$(I + Q)^{-1} \approx I - Q \qquad (161)$$

Then, for some square matrices A and B with the same dimensions and A is semi-positive definite,

$$(A + B)^{-1} \approx A^{-1} - A^{-1}BA^{-1} \tag{162}$$

if $(A^{-1}BA^{-1})^n \to 0$ $(n \to \infty)$. Substituting $A = \Lambda$ and $B = L$,

$$\hat{\mathbf{x}}_F \approx (\Lambda^{-1} - \Lambda^{-1}L\Lambda^{-1})(\mathbf{N} + \boldsymbol{\eta}) \approx P\mathbf{N} + P\boldsymbol{\eta} - PLP\mathbf{N} \tag{163}$$

where $P = \Lambda^{-1}$ and again ignoring second-order and higher terms. So,

$$\begin{cases} \Delta\hat{\mathbf{x}} = P\boldsymbol{\eta} - PLP\mathbf{N} = P\boldsymbol{\eta} + \Delta P\mathbf{N} \\ \Delta P = -PLP \end{cases} \tag{164}$$

These expressions show that, unlike the measurement covariance matrix (if assumed constant over all observations) or the measurement cadence, the effects of STM bias cannot be factored out from the normal equation. Nonetheless, if we substitute Eq. (159) into the expression for Λ_F,

$$\Lambda_F = \sum \left[\Phi_i^{\mathrm{T}} M_i \tilde{H}_i^{\mathrm{T}} R_i^{-1} \tilde{H}_i M_i \Phi_i \right] \tag{165}$$

But $M_i \tilde{H}^{\mathrm{T}} R_i^{-1} \tilde{H}_i M_i < (m_i^M)^2 \tilde{H}_i^{\mathrm{T}} R_i^{-1} \tilde{H}_i$ where m_i^M is the component of $\boldsymbol{m}(t_i) \stackrel{\text{def}}{=} \boldsymbol{m}_i$ with the maximum absolute value. Thus,

$$\Lambda_F - \Lambda < \left[\left(m_M^M \right)^2 - 1 \right] \Lambda = \left[m_M^M - 1 \right] \left[m_M^M + 1 \right] \Lambda. \tag{166}$$

where m_M^M is the maximum of m_i^M over all observations. If $m_M^M - 1$ is on the order of 10^{-3} as in Fig. 43, then the difference in the information matrix between the two models is also, at most, on the order of 10^{-3}. In conclusion, a small bias in the STM has an equally small effect on the information matrix, and thus the estimated covariance.

Although we omit the details of the derivation for brevity, we may derive similar results for the Kalman filter such that, for the i-th observation,

$$\Delta\hat{\mathbf{x}}_i = \Delta\bar{\mathbf{x}}_i + \Delta K_i(\mathbf{y}_i - \tilde{H}\bar{\mathbf{x}}_i) - K_i\tilde{H}(\Delta\bar{\mathbf{x}}_i + \Delta\mathbf{x}_i)$$
$$\Delta P_i = (I - K_i\tilde{H})\Delta\bar{P}_i - \Delta K_i\tilde{H}\bar{P}_i = (I - K_i\tilde{H})\Delta\bar{P}_i(I - K_i\tilde{H})^{\mathrm{T}} \tag{167}$$

where

$$\Delta\bar{\mathbf{x}}_i = \Delta\Phi\hat{\mathbf{x}}_{i-1} + \Phi\Delta\hat{\mathbf{x}}_{i-1}$$
$$\Delta\bar{P}_i = \Delta\Phi P_{i-1}\Phi^{\mathrm{T}} + \Phi P_{i-1}\Delta\Phi^{\mathrm{T}} + \Phi\Delta P_{i-1}\Phi^{\mathrm{T}}$$
$$\Delta K_i = (I - K_i\tilde{H})\Delta\bar{P}\tilde{H}^{\mathrm{T}}(\tilde{H}\bar{P}\tilde{H}^{\mathrm{T}} + R)^{-1}$$

4   RESULTS AND DISCUSSION

4.1   Gravitational Perturbations
4.1.1   Kinoshita and Kaula Models

Figure 1 shows the errors in the three components as well as the r.m.s. error in the relative position obtained from the Kinoshita theory when compared with a numerical simulation. The effects included are J_2, augmented with those due to the mean and long periodic effects of J_2^2, J_4, and J_6.
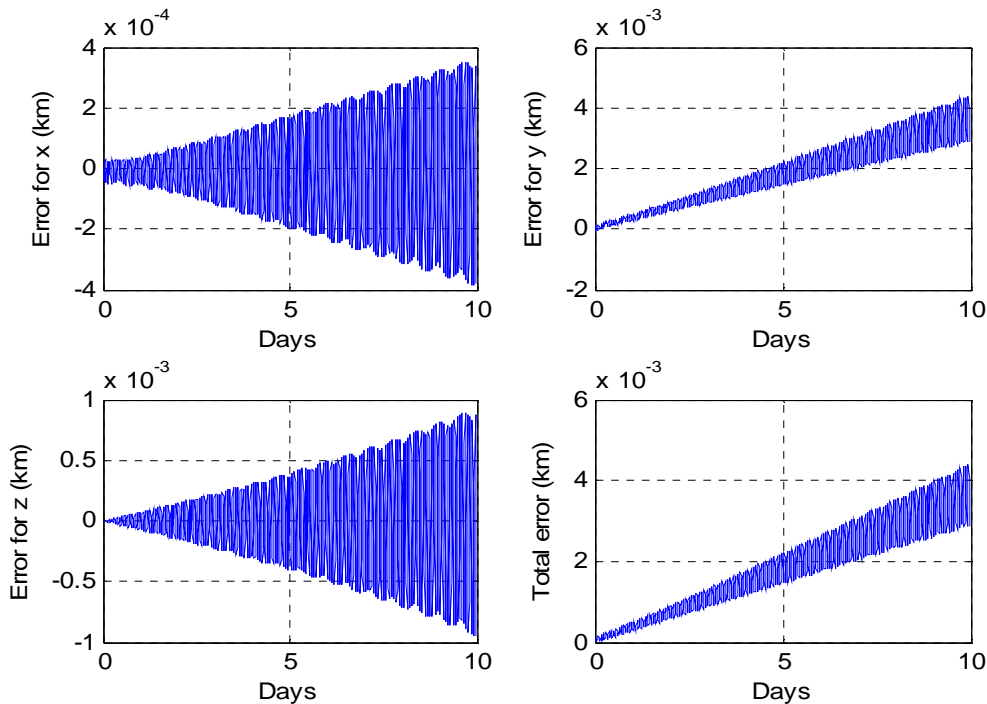

Figure 1. Modeling J_2, J_2^2, J_4, J_6 (mean and long-periodic effects)

Effects of the J_2^2 Short-periodic terms

Figure 2 shows the effects of including the short periodic contributions from J_2^2.   It shows the errors resulting from modeling J_2 (mean, short and long periodic) and including J_2^2 mean, long and short periodic effects. Figure 2 shows that the errors are uniformly lower in all the three axes with respect to those in Figure 1. Hence, modeling the J_2^2 short-periodic terms, albeit for e=0, is beneficial and improves the accuracy of the relative motion STM. Figures 3-5 show the differences between the augmented Kaula and GMAT solutions in the radial, along-track and cross-track directions.
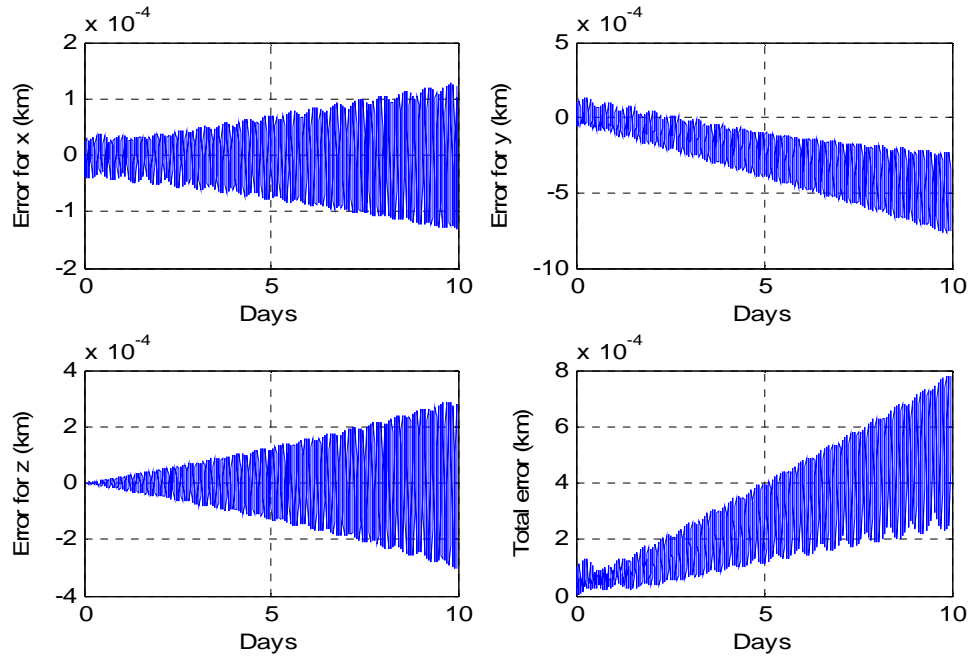
Figure 2. Error from first order of J_2, J_4 and J_6 modeling plus J_2^2 mean rate and short period
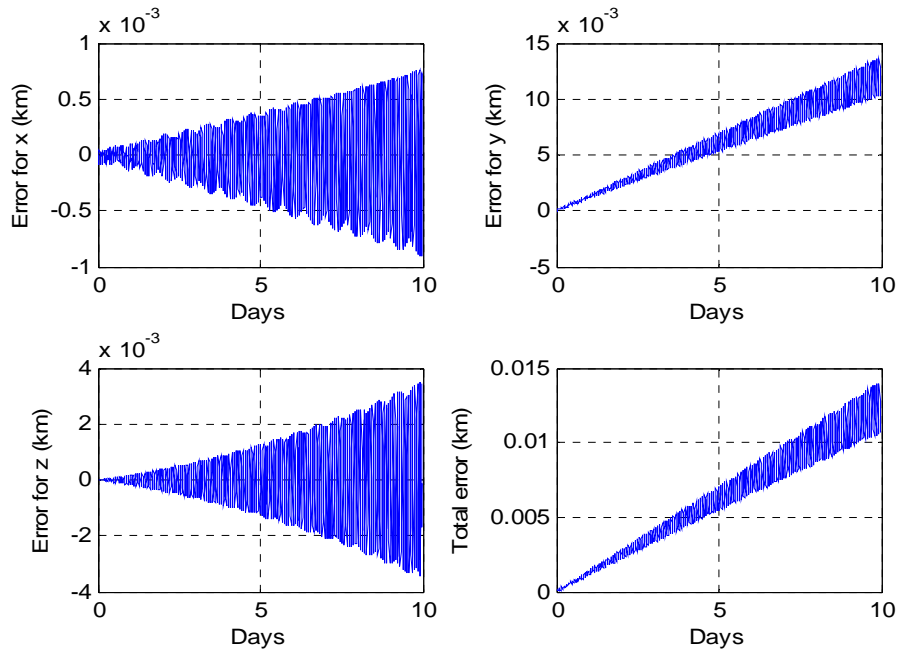

Figure 3. Difference between the Kaula and GMAT with 20x20 gravity field without J_{22} secular and short period terms
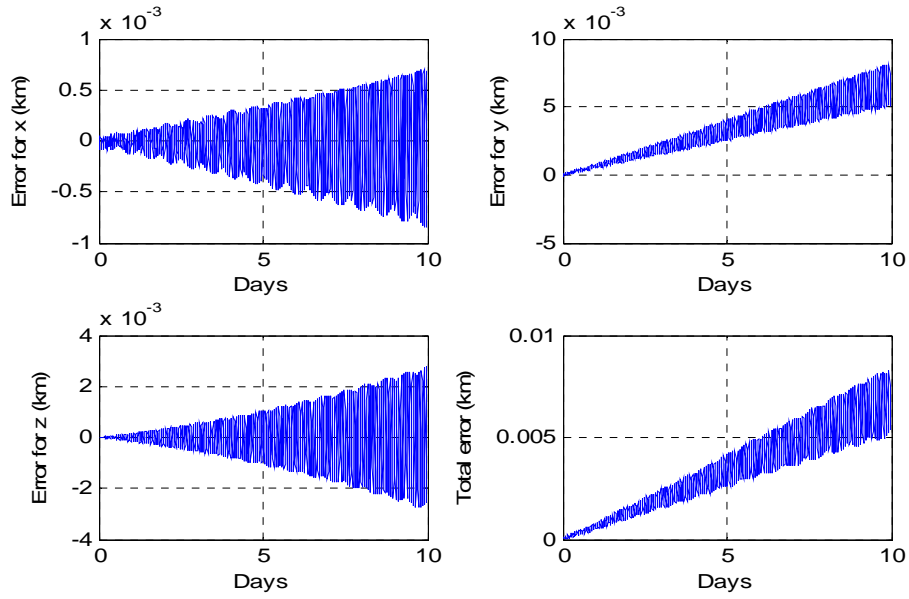
Figure 4. Difference between the Kaula and GMAT with 20x20 gravity field with $J_2{}^2$ secular terms and without $J_2{}^2$ short period terms
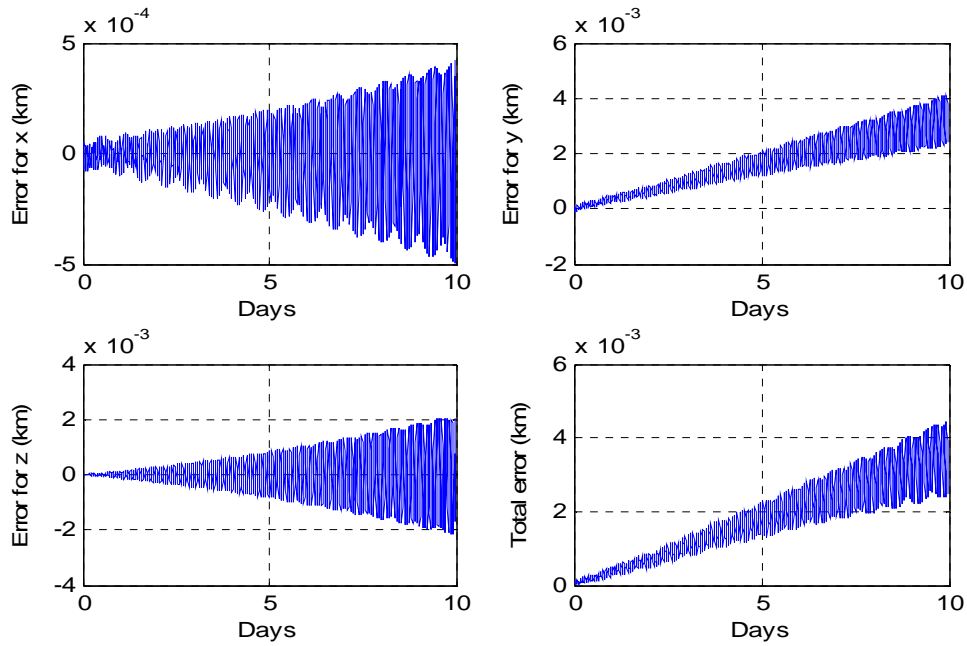

Figure 5. Difference between Kaula and GMAT with 20x20 gravity field with $J_2{}^2$ secular and short period terms

Table 1. Root mean square error for the Extended GA-STM propagation (10 days)

Effects modeled for determining the initial conditions	Modeling Perturbations in the extended GA STM for propagation	ICs obtained from the classical Kaula model (km)
J_2 only	J_2 only	0.009433
J_2, J_2^2	J_2, J_2^2	0.006497
J_2, J_2^2, J_2^2 sp	J_2, J_2^2	0.004661
J_2, J_2^2, J_2^2 sp, J_3	J_2, J_2^2 and J_3	0.006539
J_2, J_2^2, J_2^2 sp, J_3, J_4	J_2, J_2^2, J_3, J_4	0.005952
J_2, J_2^2, J_2^2 sp, J_3, J_4, J_5	$J_2, J_2^2, J_3, J_4, J_5$	0.006566
J_2, J_2^2, J_2^2 sp, J_3, J_4, J_5, J_6	$J_2, J_2^2, J_3, J_4, J_5, J_6$	0.005540

4.1.2   GA-STM with Hoots Variables

The Hoots version of the GA-STM can be evaluated via MATLAB simulation. Its error (versus a numerically integrated trajectory) can be compared with the results from directly differencing the analytically propagated trajectories of both chief and deputy satellites. These numerically computed differences can then be mapped into relative space, forming a rough lower bound on the error for closed-form relative motion approximations (such as the GA-STM).

In Figure 6, the satellites are in a near-PCO (Projected Circular Orbit) formation: the zero-drift constraint on δa is turned off, the relative orbit size is 1 kilometer, and the deputy's initial phase angle is 0. The chief's osculating initial conditions are semi-major axis 7100 kilometers, eccentricity 0.01, inclination 50 degrees, and all other classical elements 0. J_2 is considered as the only perturbation. The relative position and velocity error magnitudes are shown for the Hoots-element GA-STM as well as for direct differencing of first-order orbit theories due to Hoots [10] and to Kinoshita [6]. In this scenario, the STM shows error characteristics competitive with the direct differencing models, especially for position error.
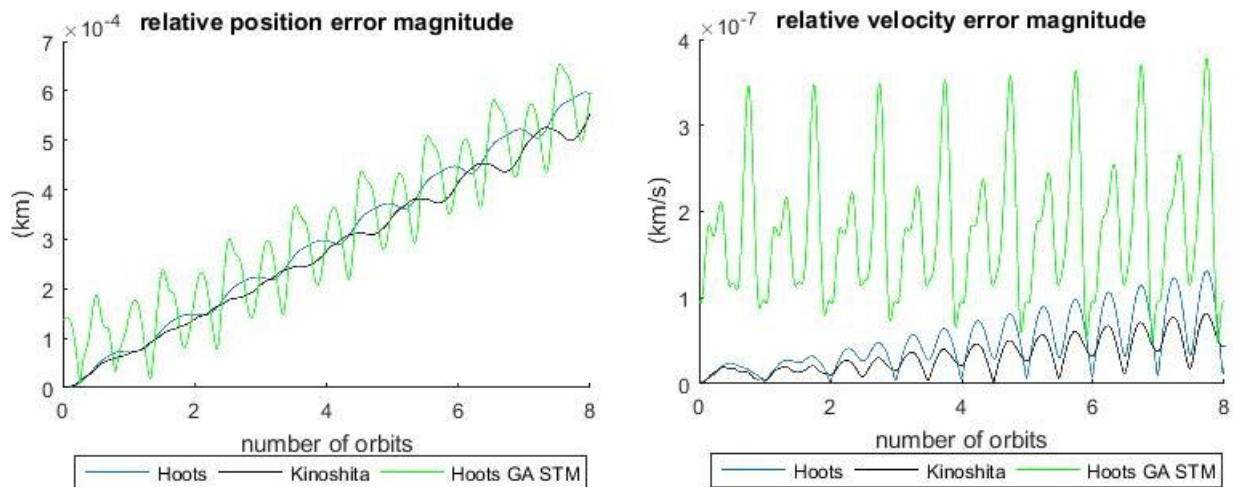
Figure 6. First-order theory comparison: Direct differencing vs. GA-STM

The new version can also be compared against previous versions of the GA-STM formulated in terms of nonsingular elements and equinoctial elements. Figure 7 shows results from a chief satellite in a near-circular low-Earth orbit; the LVLH components and the magnitude of the relative position error are shown for all three STMs, as well as for both versions of direct differencing. For this case, the STM errors are not significantly greater than those for direct differencing.
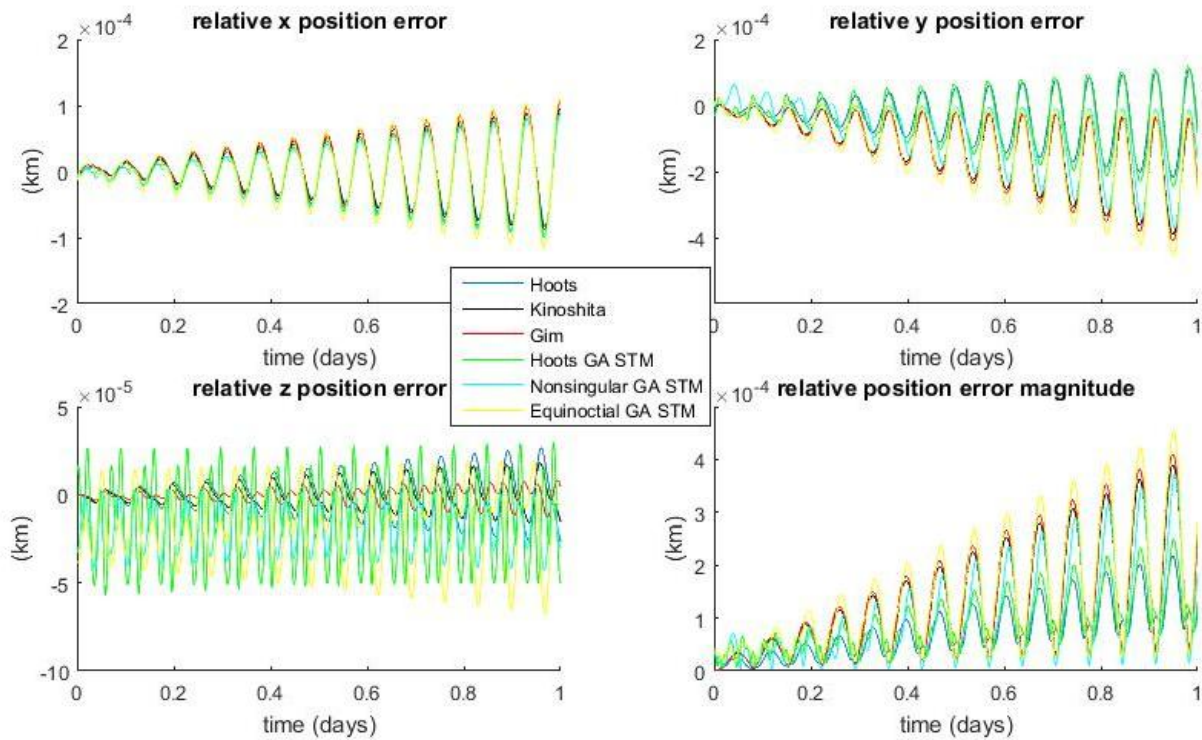
Figure 7. Relative position error for near-circular orbit

Figure 8 shows the same relative position error plots for a different scenario. In this case, the chief's eccentricity is approximately 0.1. Here, the STMs perform slightly worse than the direct differencing models, not an unexpected result.
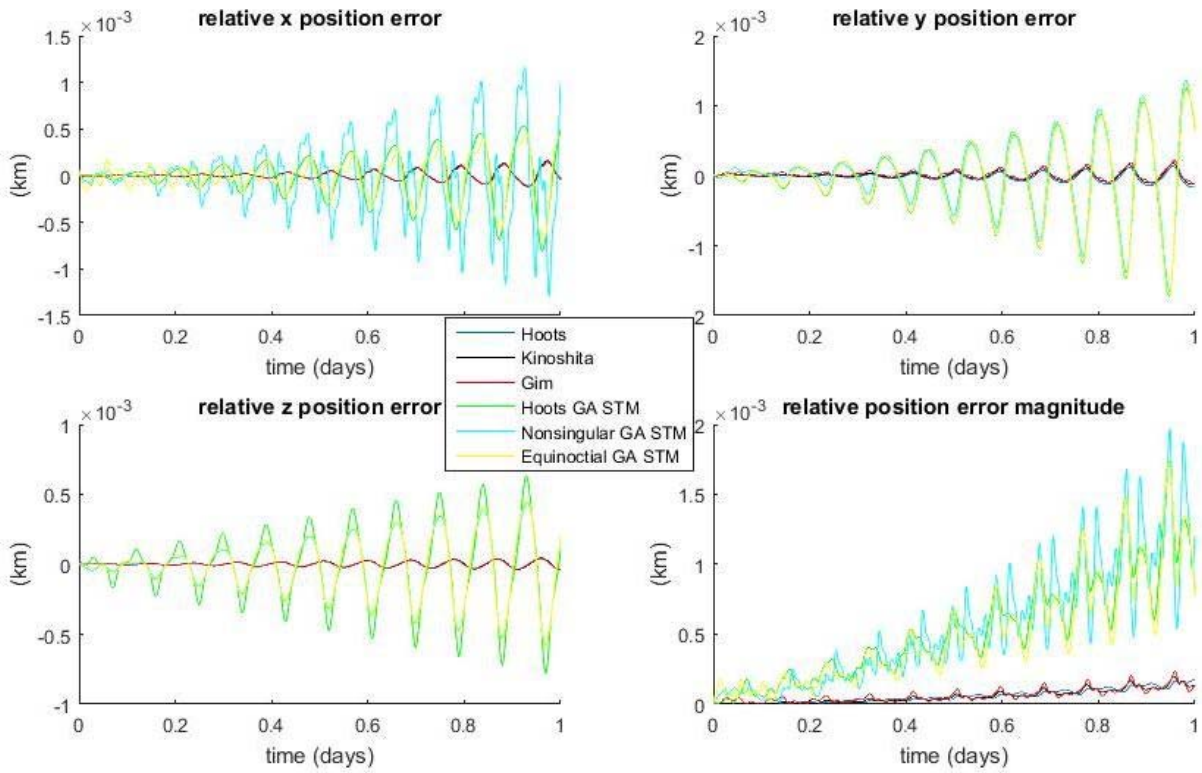
Figure 8. Relative position error for eccentric orbit

Figure 9 shows the relative position error for a formation in geostationary orbit. Because the chief's orbit is equatorial, both Kinoshita theory and the nonsingular-element STM are singular and are not shown.
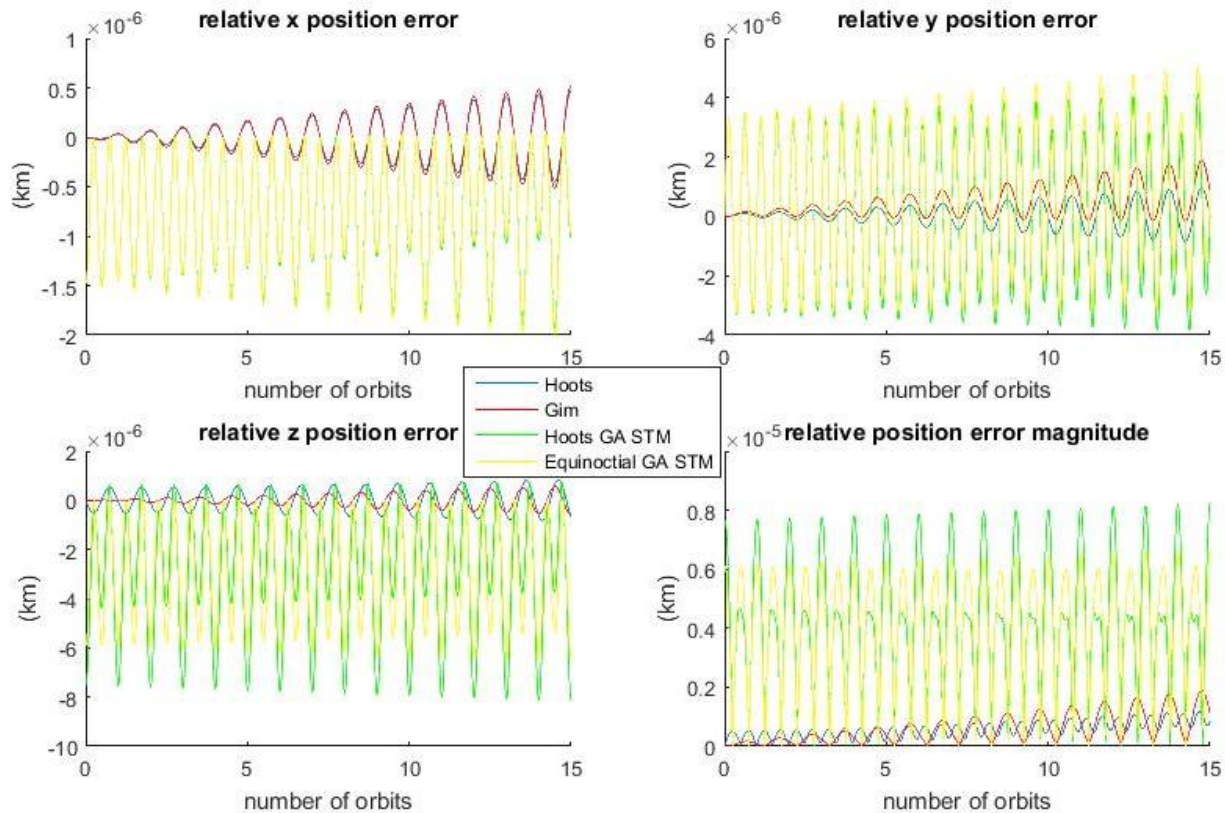
Figure 9. Relative position error for geostationary orbit

Note that in many cases the STM errors are nonzero even at the initial time. In order to propagate the relative orbit accurately with an STM, the relative initial conditions must themselves undergo a linearizing transformation--this transformation introduces an offset at the initial time, but prevents an accumulating error over the course of the propagation.

4.1.3 Numerical Verification using GMAT and a Graphical User Interface (GUI)

The analytic formulae for the second-order short-period effects, the first-order long-period effects and second-order secular effects have been verified for the zonals J_3 and J_4 with the published results. A MATLAB-based code for the relative motion STM, including all the expressions for J_2 effects computed by using Maple, and the generalized analytic formulae for the higher zonals, has been developed. A graphical user interface (GUI) has also been implemented to easily configure and run simulations, as well as analyze results. An interface to National Aeronautics and Space Administration (NASA) GMAT software is also implemented as part of the GUI in order to compare the analytic STM accuracy with the direct numerical propagation using GMAT. Figure 10 shows the screenshot of the Matlab-based Simulation GUI.
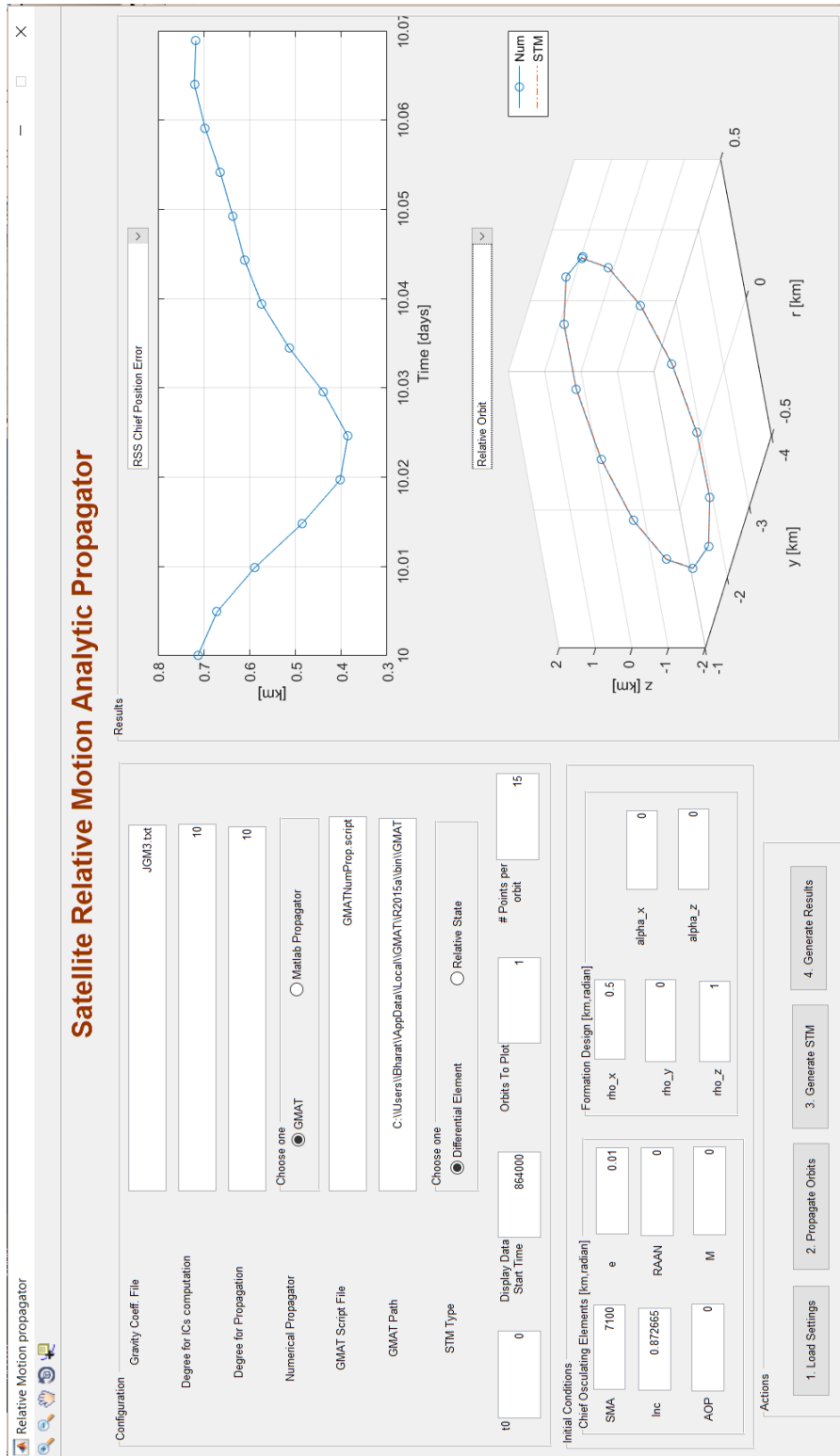
Figure 10. Relative Motion Propagator GUI

59

For comparing the accuracy of the STM, two satellites: chief and deputy, are simulated using the NASA GMAT software with 70×0 JGM-3 gravity model. The mean initial conditions of chief are chosen with a= 7100 km and node angle, perigee angle as well as the mean anomaly all as zero. Two different reference orbits are simulated: eccentricity 0.01 with inclination 50∘ and eccentricity 0 with inclination 0∘. The mean initial conditions of deputy are computed according to a projected circular orbit type formation with a baseline distance of 1 km. The osculating initial conditions of chief and deputy required for numerical propagation are computed analytically using the mean to osculating transformations as described in the previous sections. The orbits of chief and deputy are propagated for ten days in GMAT and the relative position and velocity states in the curvilinear frame are computed. Using the extended GA-STM, the same relative states are also directly propagated for ten days. The maximum degree up to which zonal harmonics are included in the extended GA-STM was successively increased. Figure 11 shows the absolute position and velocity root-sum-square (RSS) error plots for chief satellite with eccentricity 0.01 and inclination 50∘ after ten days of propagation as the maximum degree of the extended GA-STM is increased. Figure 12 shows the relative position errors for a PCO type formation with 1 km of baseline distance for the same chief reference orbit. It is noted that with the maximum degree of the GA-STM J_{20}, the absolute position errors were reduced to less than 1 km and relative position error less than 1 m after ten days of propagation. Figure 13 and 14 shows the absolute and relative errors when the reference orbit is chosen as equatorial and circular. The similar trend in the absolute motion as well as relative motion was observed for this case.
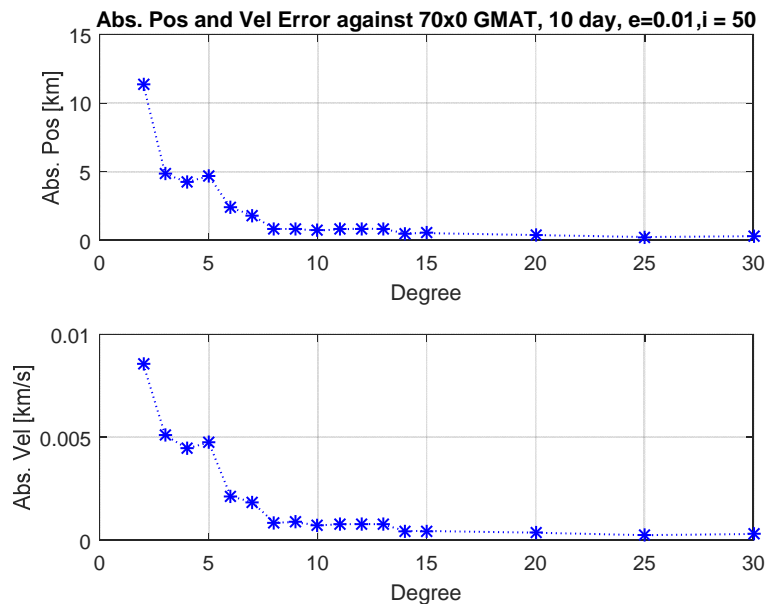

Figure 11. Absolute Position and Velocity Error vs. Degree of the Extended GA-STM.
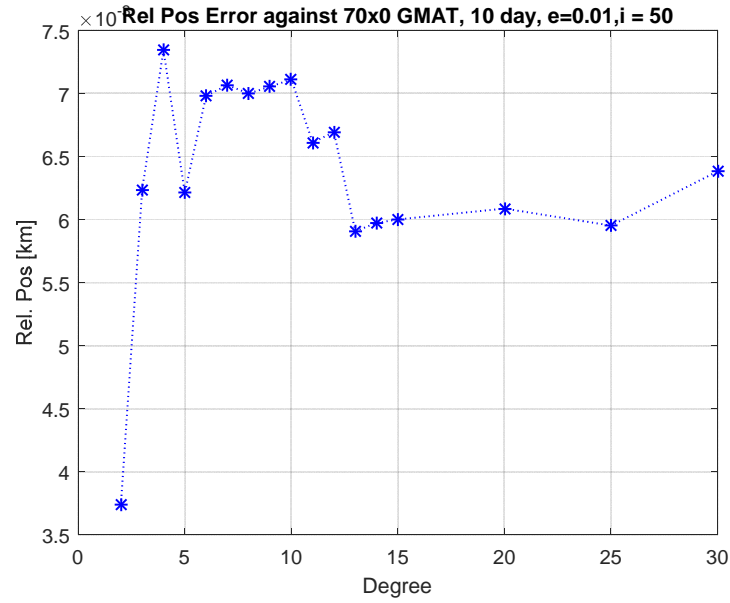
Figure 12. Relative Position Error Versus Degree of the Extended GA-STM
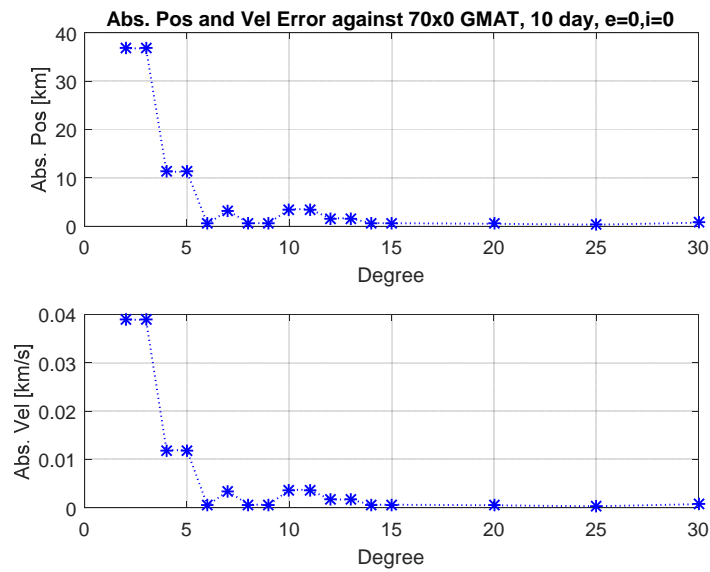

Figure 13. Absolute Position and Velocity Error Versus Degree of the Extended GA-STM for Equatorial Circular Reference Orbit
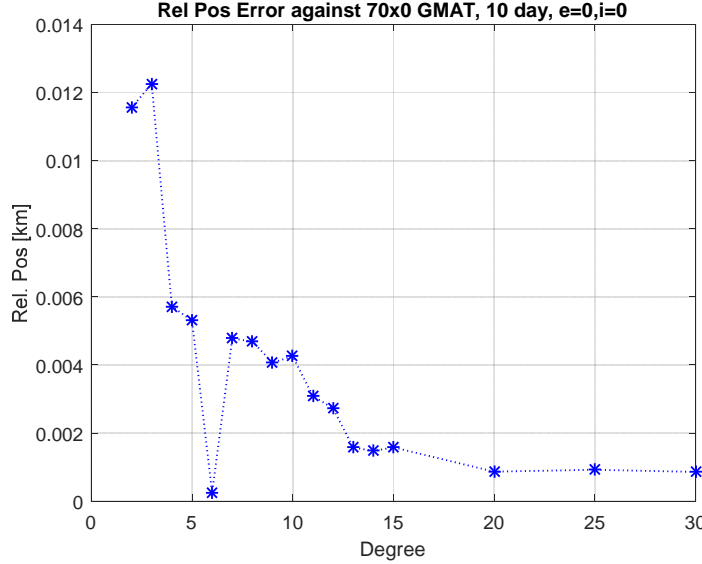
Figure 14. Relative Position Error Versus Degree of the Extended GA-STM for the Equatorial Circular Reference Orbit.

4.2   Non-Earth Gravitational Perturbations

4.2.1   Third Body Perturbations

A representative example for which the lunar perturbation is significant is the NASA Magnetospheric Multiscale (MMS) mission, designed to study magnetic reconnection, charged particle acceleration, and turbulence in key boundary regions of the Earth's magnetosphere. The MMS orbit is highly eccentric and lunar perturbation cannot be ignored. The starting epoch is August 5, 2013. The mean inclination, eccentricity, and right ascension of the lunar orbit are assumed to be 19.65º, 0.0497, and 350.36º, respectively. The lunar position data at 30 minute intervals is taken from the Jet Propulsion Laboratory Horizons website.

The reference orbit is assumed to have the following initial mean elements: a=42095 km, e=0.81818, i=28.5º, Ω=357.857º, ω=298.2253º, and M_0=180º. The initial phase angle α_0 is selected to be zero and the relative orbit size ρ, is 10 km. Because of the high eccentricity, the relative orbit undergoes an expansion near perigee and therefore, ρ as well as the relative orbit element differences do not remain constant along the orbit. The simulation time is 100 days. Earth's gravitational perturbations are not included in the simulations presented in this section.

4.2.1.1 Results for the Reference Orbit

The equations of motion for the chief are propagated and the position and velocities are converted into osculating orbital elements. In Fig. 15, these results are compared with the respective solutions obtained from Eqs. (85).
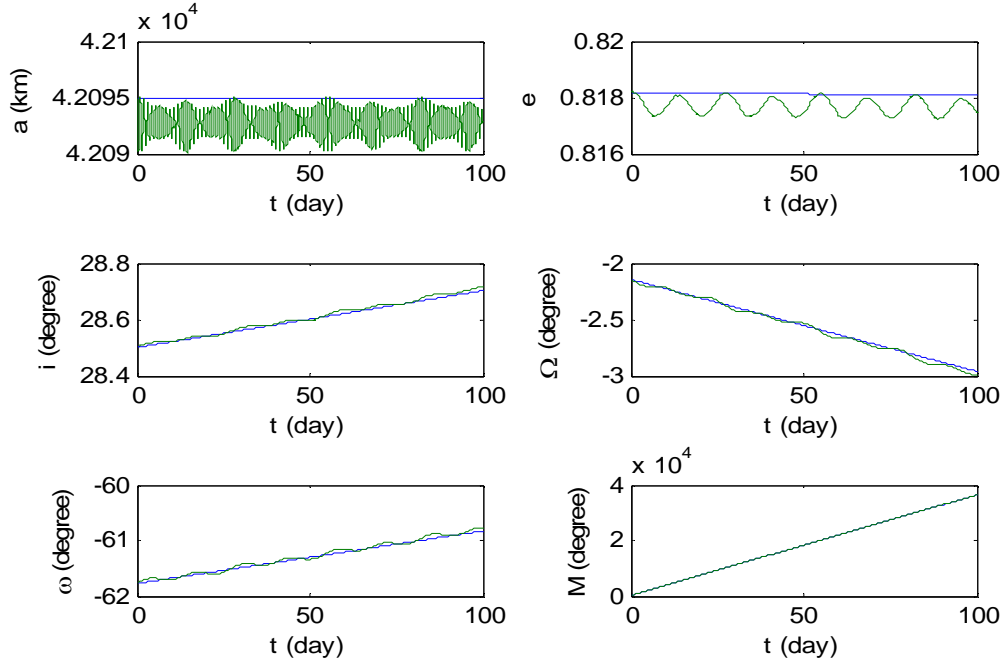
Figure 15. Averaged Lunar Model vs. Nonlinear Model

The blue lines represent the averaged model, while the green lines stand for the nonlinear model in Fig. 15. One can see that there are obvious differences in the semi-major axis and eccentricity for the two models due to the use of the same initial conditions for both the simulation models. The initial conditions for the nonlinear simulation should be corrected to fit the averaged model. Application of the least squares method to correct the initial conditions results in the plots in Fig. 16.

Figure 16. Averaged Lunar Model vs. Nonlinear Model after Correction
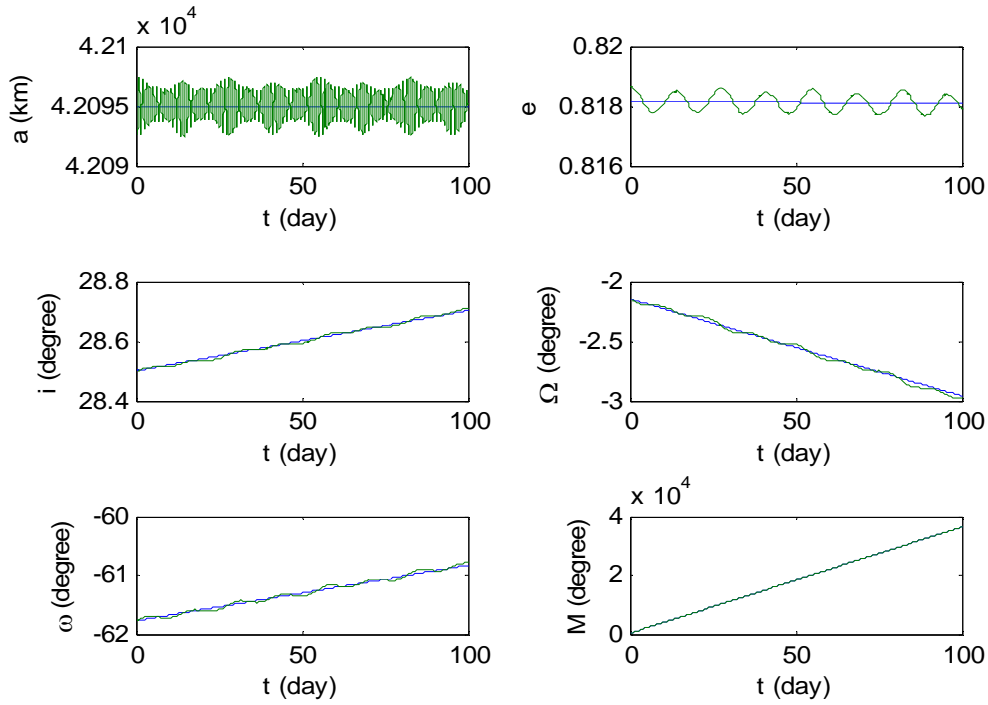
Figure 16 indicates that the averaged model predicts the long-term behavior very well, providing confidence that the effects of the third-body have been incorporated correctly. Only the first term is taken in the infinite series represented in Eq. (81) for the averaged potential. From Fig. 16, we can see the ($n=2$) term dominates the third-body perturbation, akin to the gravitational potential of the Earth, in which J_2 plays the dominant role. Figures 15-16 also show that it is important to include the lunar orbit's inclination in the averaged model for higher accuracy, as concluded in Reference 8.

We compare the nonlinear simulation results with GMAT for further validation, as shown in Fig. 17.
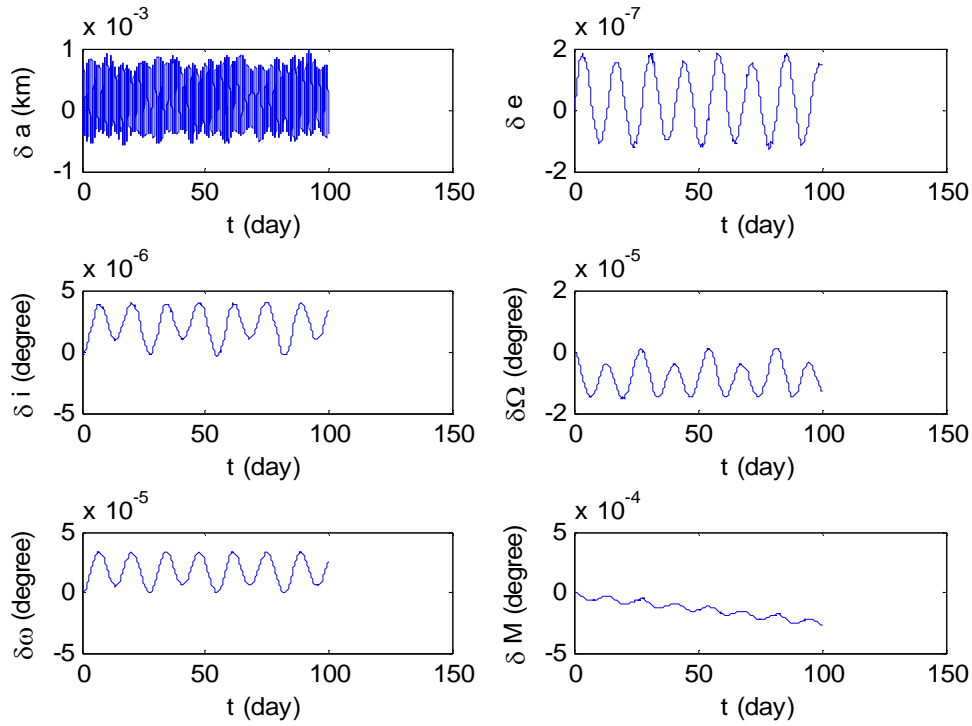
Figure 17. Differences between Nonlinear Simulation and GMAT

GMAT is an open-source space mission design tool to model and optimize spacecraft trajectories in flight regimes ranging from low Earth orbit to lunar, libration point, and deep space missions. GMAT has been developed by a team of NASA, private industry, and public and private contributors. Note that only the lunar perturbations are included in both the simulations.

4.2.1.2 Simulation Results for Relative Motion

The process outlined previously for the simulation of the reference orbit is repeated for the deputy's orbit. In this section, numerical results produced by the extended GA STM are presented. To isolate the third-body effects, we neglect the Earth's gravitational perturbations first. Figures 18-19, respectively, show the errors in relative position with and without modeling the third-body effect.
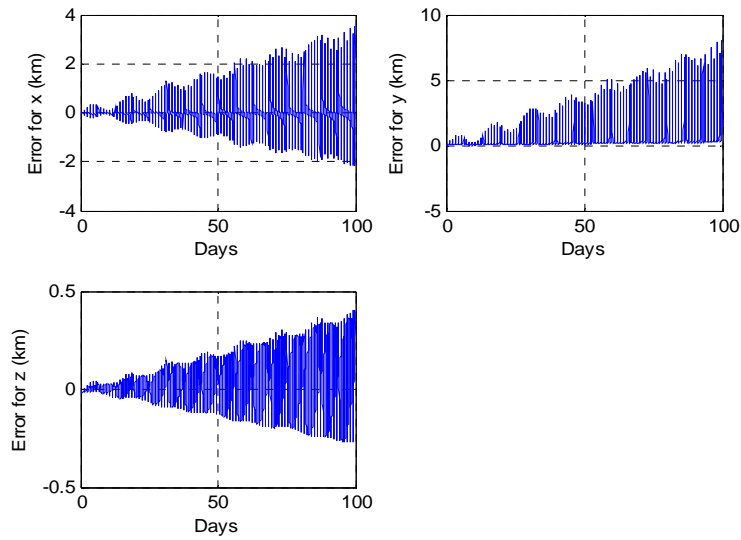
Figure 18. Relative Position Errors, Two-body STM vs. Lunar-perturbed Nonlinear Model
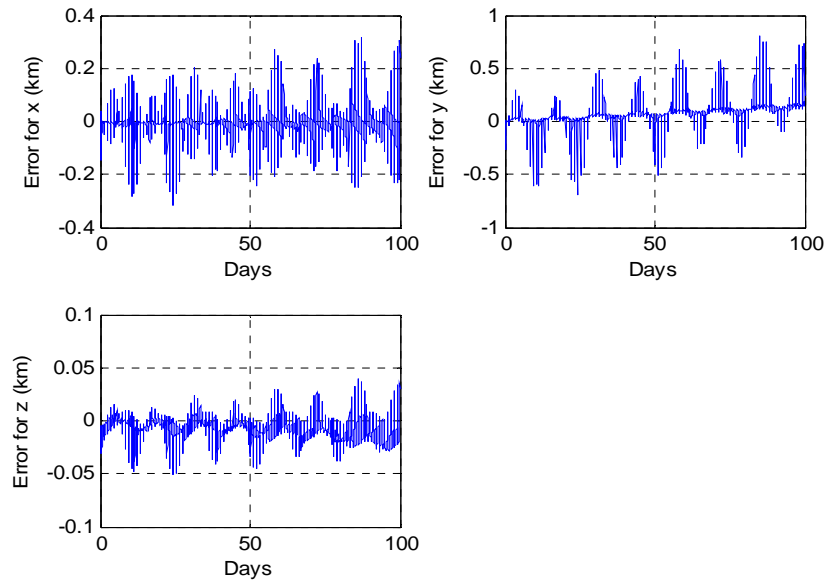
Figure 19. Relative Position Errors, STM includes Averaged Lunar Perturbations

Note that the reference orbit for this example has a large semi-major axis and is also highly eccentric. Figure 18 shows that the in-track component of the relative position error vector has the largest growth, while the smallest error results in the cross-track direction. Comparing Figure 18 with Fig. 19, it is seen that the accuracy greatly improves with the inclusion of the lunar

perturbation model in the GA-STM, especially in the cross-track direction. The residual errors are mostly caused by absence of the short period lunar effects.

The J_2 perturbation is three orders of magnitude larger than that due to the higher-order Earth gravitational perturbations. It is necessary to investigate the combined effects of the J_2 and the third-body perturbations. In the examples presented for error comparisons, the initial conditions for the numerical integration models are determined by the least squares approach.
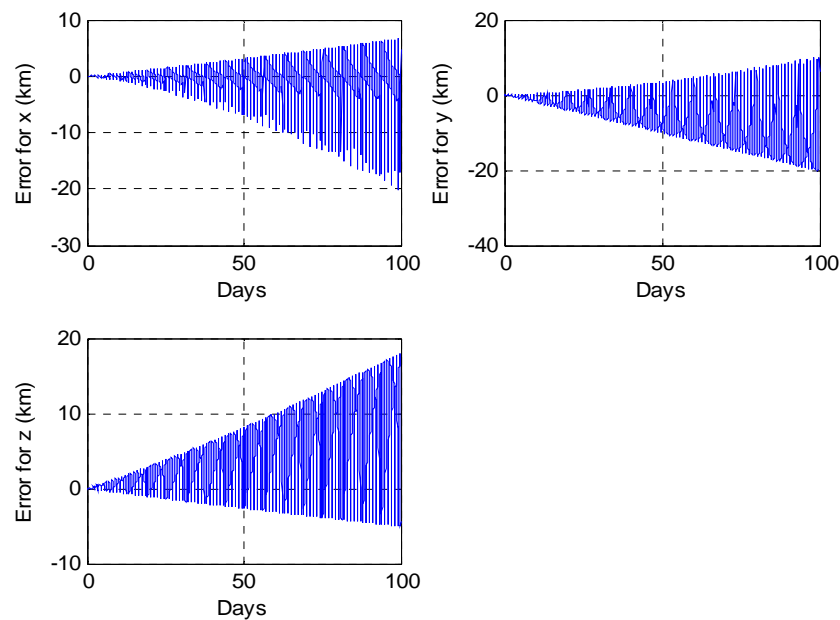
Figure 20. Relative Position Errors, Two-body STM vs. Nonlinear Simulation With J_2

Figure 20 shows the position errors as a result of neglecting J_2, arising from the use of the two-body STM model. A comparison of Figures 18 and 20 confirms that the position error due to the J_2 perturbation is larger than that caused by the Moon; although the semi-major axis of the MMS orbit is large, about 42,000 km.

Figures 21-22 present the improvements obtained from the use of the extended GA STM for propagating relative motion and for the least squares corrections for the initial conditions. The extended GA STM models the J_2 and third-body perturbations. The in-track position error varies significantly between apogee and perigee, proportional to the size of the relative orbit.
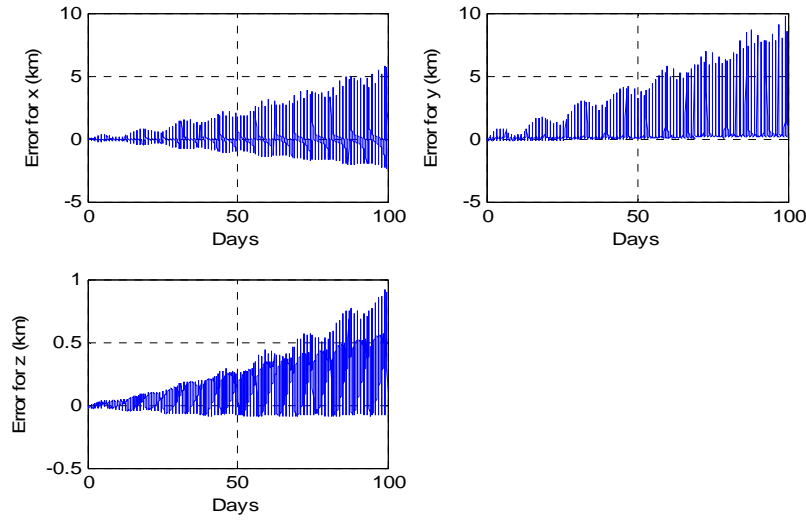
Figure 21. GA STM vs. Nonlinear Simulation including J_2 and Lunar Perturbation
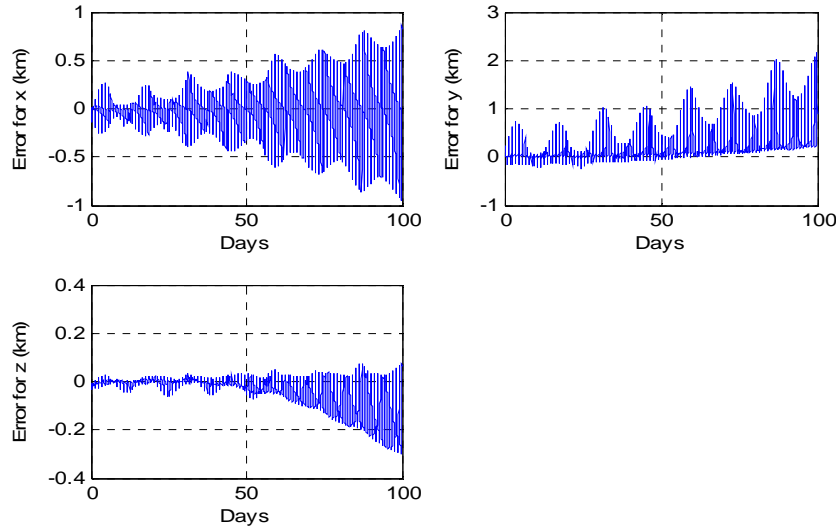
Figure 22. Extended GA STM with Lunar Effect vs. Nonlinear Simulation including J_2 and Lunar Perturbation

4.2.2 SRP Numerical Results

The mean orbit element of the chief satellite is a=43527.7589899 km; e=0.0005671; Ω= 18.88 deg; ω=321.5388 deg; M=38.4719. The cross sectional area is 5.02 m^2 and the satellite mass is 611 kg. The simulation time is 10 days. Only the SRP perturbation is included in the simulations.

The inclination *i* is set as 113 deg so that the satellites will be illuminated all the time to avoid the shadowing effects.

4.2.2.1   *SRP Model Verification*

Figures 23 and 24 show the accuracy of the analytical model, with and without corrections for the initial conditions of the analytical model, respectively. The solid lines stand for the solutions from Eq. (107) and the circles represent the results from Eq. (110). Biases in the semi-major axis and right ascension are observed in Figure 23. Generally, a least squares method is applied to correct the initial conditions to remove these biases. Here we apply the short period corrections of Eq. (111) at the initial time to remove the biases, as shown in Figure 24.
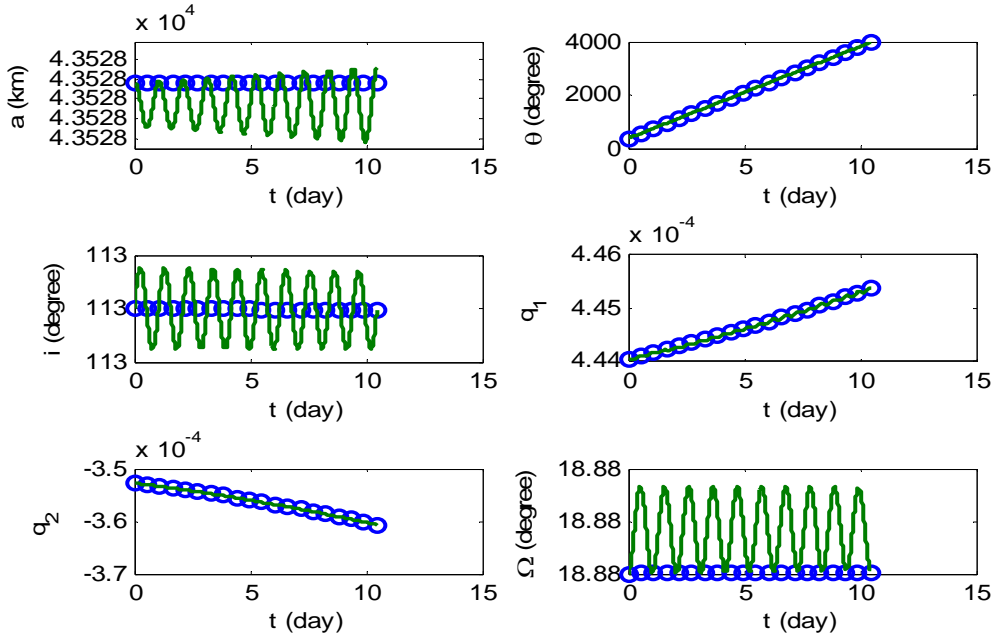
Figure 23. Comparisons Between Numerical and Analytical Simulations Without Corrections for the Initial Conditions of the Analytical Model
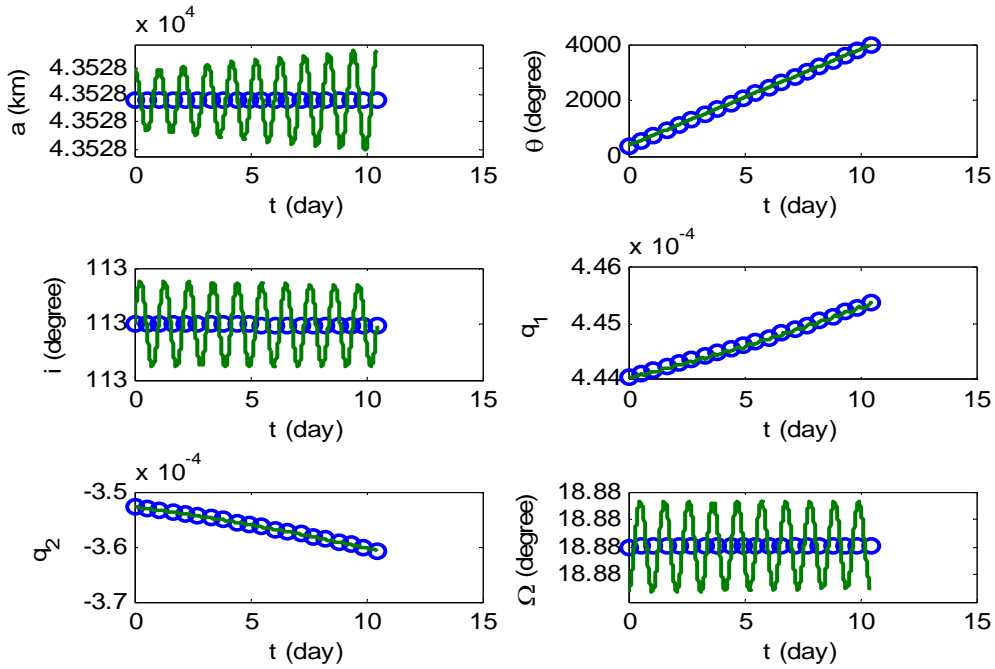
Figure 24. Comparisons Between Numerical and Analytical Simulations With Corrections to the Initial Conditions of the Analytical Model

4.2.2.2 *Relative Errors for Formation of Identical Satellites*

The deputy satellite has the same area and mass as the chief satellite. The mean orbit of the deputy is determined from $\mathbf{e}_0 = \overline{\mathbf{e}}_0 + \Delta\mathbf{e}_0$. The initial phase angle α_0 is selected to be zero and the relative orbit size ρ is 1 km. Using the corrected initial conditions, Eq. (107) is integrated for the chief and deputy satellite, respectively. Then nonlinear relative position and velocity are obtained by the unit sphere approach [18], which are the reference values for evaluating the accuracy of the extend GA STM.

Figures 25 and 26, respectively, show the effects of differential SRP due to orbital element differences for a formation. The relative position error due to the use of a two-body STM is less than 0.06 m in 10 days, and it is reduced to 0.03 m by modeling differential SRP due to orbital element differences. Notice part of the relative errors is from nonlinearity. The theory does not include the effects due to differences in solar areas of the satellites, which is a more significant effect.
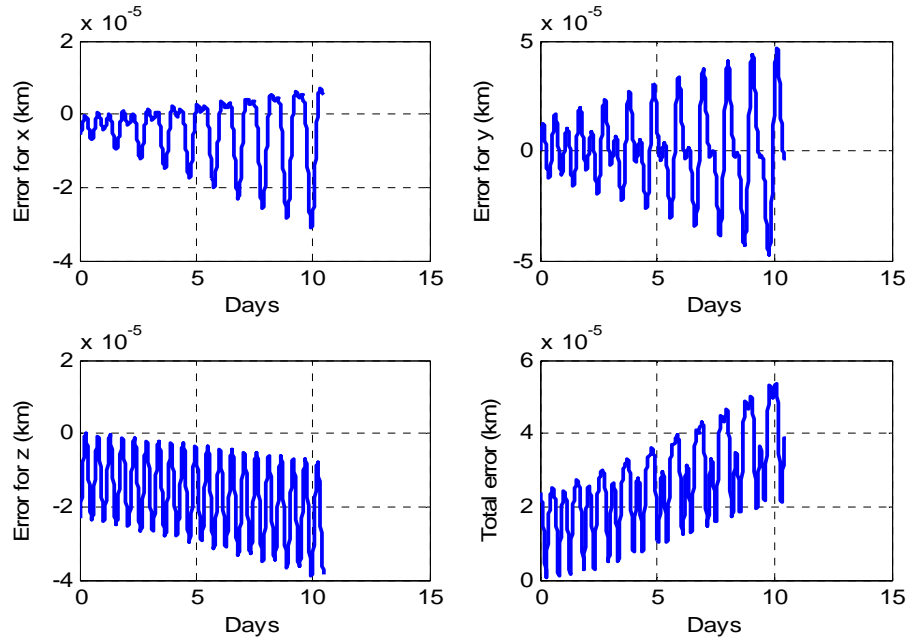
Figure 25. Relative Motion Errors: Two-Body STM Vs Nonlinear Simulation

Figure 26. Relative Motion Errors: STM Including Differential SRP Due to Orbital Element Difference Vs Nonlinear Simulation

4.2.2.3 Relative Position Errors From Differential Area

Now we assume the cross sectional area of the deputy satellite is 5.07 m^2 or about 1% more than that of the chief satellite, as shown in Figures 27-28.

Figure 27. Relative Motion Errors: STM Including Differential SRP Due to Orbital Element Difference Vs Nonlinear Simulation
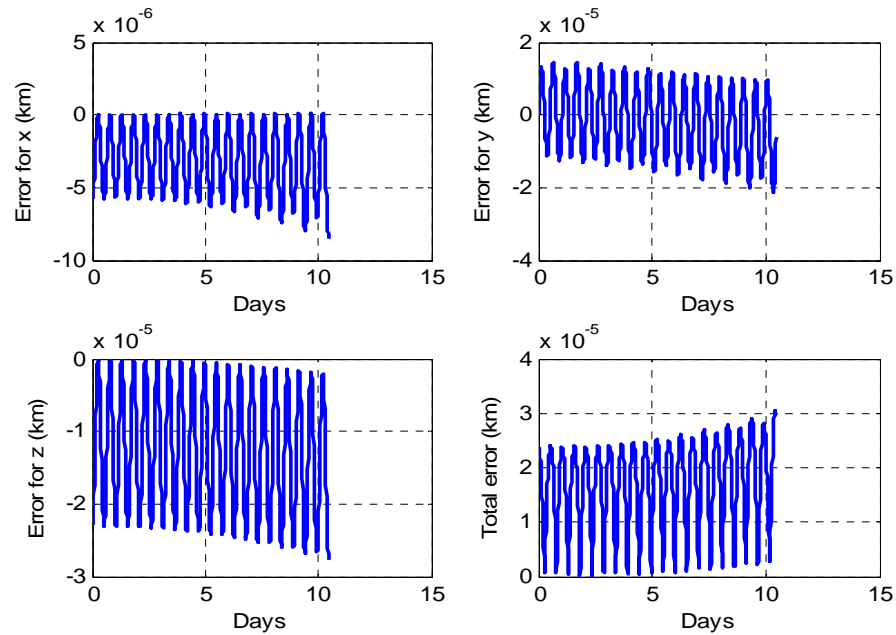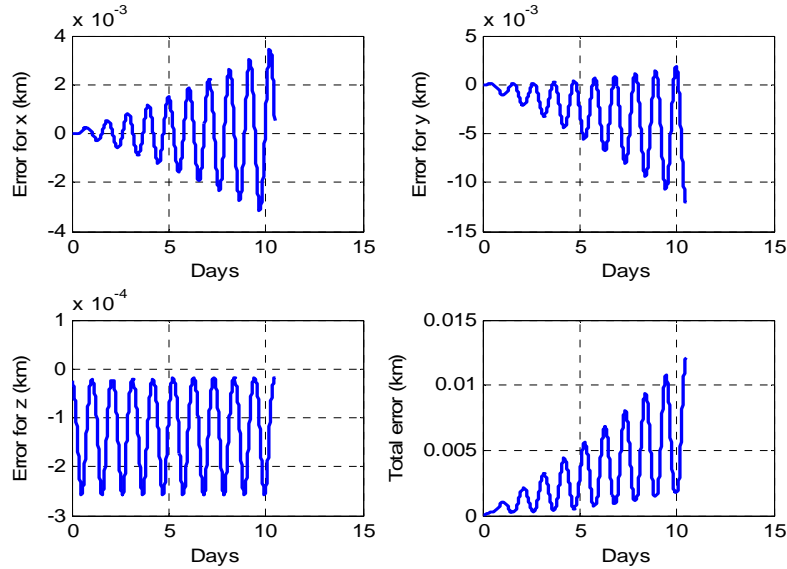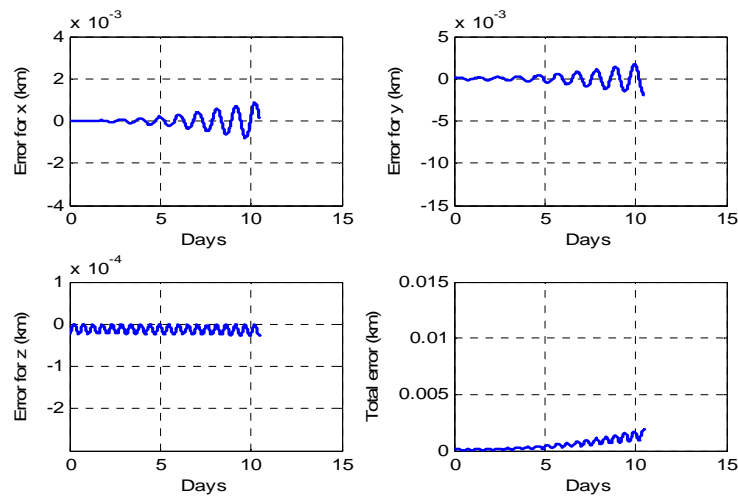

Figure 28. Relative Motion Errors: STM Including Differential SRP Due to Orbital Element And Differential Area Vs Nonlinear Simulation

Figures 27 and 28 show relative motion errors between the solutions of the extended GA STM and nonlinear simulations. The effect of differential area is modeled into the solutions of the extended GA STM in Figure 28 while the differential SRP due to only orbital element difference is included in the solutions of the extended GA STM. Comparing Figure 27 with Figure 28, one can see the relative motion errors due to the effects of differential area are much larger than those due to orbital element differences. The reason is described as follows: taking the normal direction of the acceleration due to SRP as example and differentiating Eqs. (105-106), we have

$$
\begin{aligned}
\delta U_h &= -\frac{Pk}{m}\bar{U}_h \delta A - \frac{Pk}{m} A \delta \bar{U}_h \\
&= -\frac{Pk}{Am}\left(\bar{U}_h \frac{\delta A}{A} + C_1 \delta i + C_2 \delta\Omega \right)
\end{aligned}
\tag{168}
$$

where

$$
\begin{aligned}
C_1 &= \sin\Omega\cos i\cos\lambda_e - \cos\Omega\cos i\sin\lambda_e\cos\varepsilon - \sin i\sin\lambda_e\sin\varepsilon \\
C_2 &= \cos\Omega\sin i\cos\lambda_e + \sin\Omega\sin i\sin\lambda_e\cos\varepsilon
\end{aligned}
$$

From Eq. (112), we have

$$
\begin{aligned}
\delta i &= \delta i_0 + \delta\dot{\bar{i}}\left(t - t_0\right) \\
\delta\Omega &= \delta\Omega_0 + \delta\dot{\bar{\Omega}}\left(t - t_0\right)
\end{aligned}
\tag{169}
$$

The long and secular rates are assumed constants. The estimated values are approximately 10^{-16}/s for the inclination and right ascension right rates at the initial time. Substituting Eq. (112) into Eq. (169), then Eq. (168) after ignoring the rate terms, we have

$$
\delta U_h = -\frac{Pk}{Am}\left(\bar{U}_h \frac{\delta A}{A} + C_1 \frac{\rho}{a_0} \right)
\tag{170}
$$

Equation (170) clearly demonstrates even one percent of the area variation will dominate the differential SRP.

Similar to the drag problems, modeling differential area into the STM is very important as this can be seen in the same scale of Figures 27-28. The root mean square (RMS) is 0.686 m with modeling differential area while it is 4.18 m without modeling differential area into the extended GA STM for one percent difference between the cross sectional areas of the chief and deputy satellite. Table 2 shows the effect of modeling differential area into the STM to deal with the SRP perturbations due to different differential area among the satellites and presents the RMS variations as the percentage of the area difference increases for a 10 day simulation. There is about six times reduction for relative motion errors for the example.

Table 2 RMS Variation With Area Difference

Deputy Area (m^2)	Area Diff (%)	RMS without Diff Area (m)	RMS with Diff Area (m)
5.07	1	4.18	0.69
5.12	2	8.36	1.37
5.17	3	12.54	2.06
5.22	4	16.71	2.74
5.27	5	20.90	3.43

4.2.3 Perturbations due to Drag

The Chief satellite orbit is a=6700km, e=0.004, i=48deg, Ω=0, ω=10 deg, and M=120 deg. The simulation time is 3 days. The satellite is 100 kg and the cross sectional area is 1 m^2. The relative orbit size is 1 km and initial phase angle is zero. The deputy satellite orbit is determined in the usual manner for the PCO. All the initial conditions are obtained by analytical methods.

4.2.3.1 Drag Only Problem

We use the two-body GA STM to get the solutions of relative motion, and integrate nonlinear equations including drag perturbation only for the chief and deputy orbits and get the real relative solutions. The errors are the differences between the former and latter, as shown in Fig. 29. Then we analytically model the drag into the extended GA STM, the corresponding errors are shown in Fig. 30.
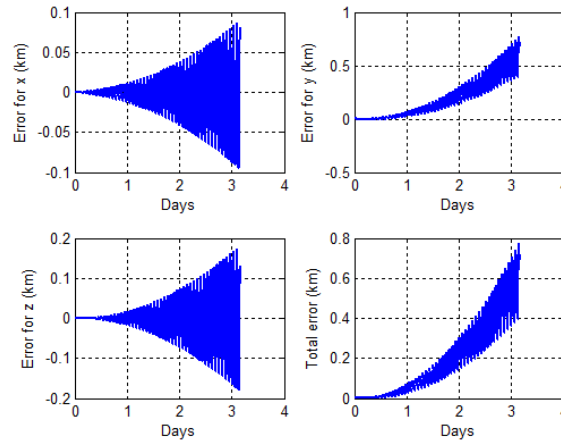
**Figure 29. Relative Position Errors From Two-Body Modeling
For Drag Only Problem**
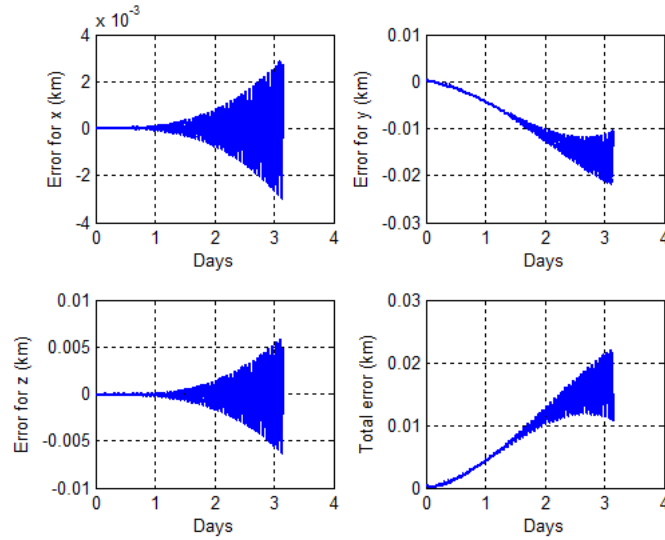
Figure 30. Relative Position Errors From Modeling Drag Into Extended GA STM for Drag Only Problem

There is more than one order of magnitude improvement by including drag in the extended GA STM, as shown in Figs. 29-30. Since the assumption on the constant rates perturbed by drag is inaccurate [44], the accuracy is not high.

The cross sectional areas are the same for the chief and deputy. Now we assume there is one percent difference in the area, i.e. the area of the deputy is 1.01e-6 m^2 and the chief area is still 1.00e-6 m^2. The simulation time is one day, as shown in Figs. 31-32.
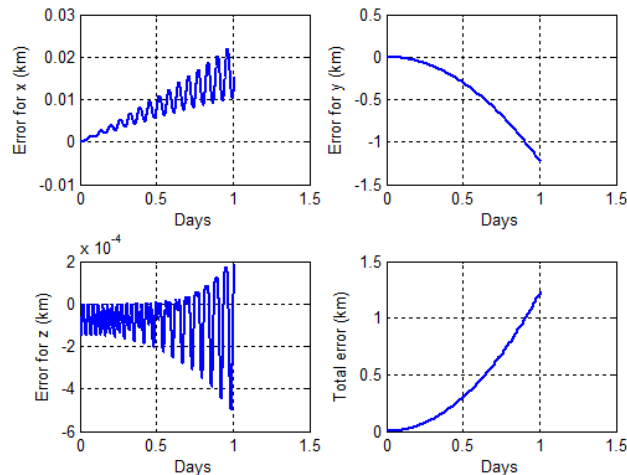
Figure 31. Relative Position Errors Without Modeling Diff. Area Into Extended GA STM
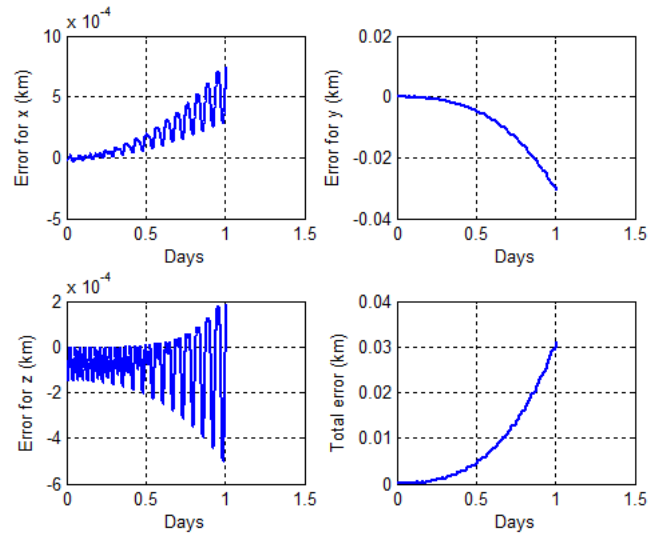
**Figure 32. Relative Position Errors With Modeling Diff. Area
Into Extended GA STM**

Figures 31-32 indicate the differential area has significant effects on the accuracy, especially in the in-track direction. Modeling the differential area into the extended GA STM remarkably alleviates the effect. As the differential area percent increases, it is necessary to modeling the differential area into the extended GA STM, as shown in Fig. 33 for a one day simulation.
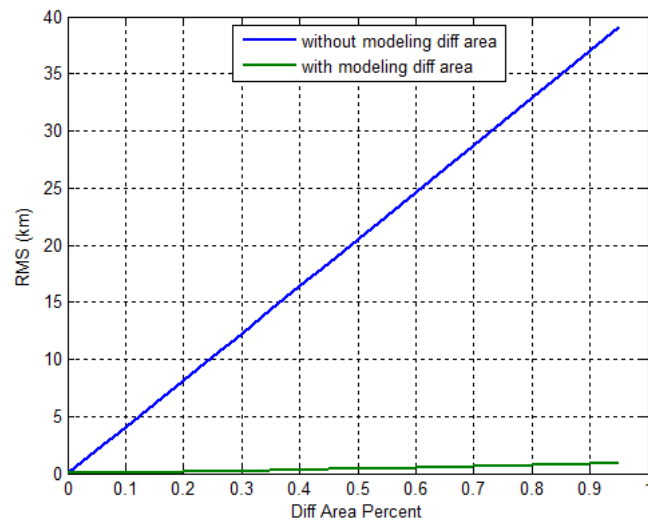
**Figure 33. Effect of Modeling Differential Area in the Extended
GA STM**

Figure 33 demonstrates it is important to introduce the area-mass-ratio variable C_b into the extended GA STM, especially for the perturbations sensitive to the cross sectional area.

4.2.3.2 *Drag and Gravity Combined Perturbations*

Comparing Figs. 29-30 with Figs. 34-35, one can see the effect of the gravity perturbation is about four times more than that of the drag perturbation for this example. The accuracy modeling J_2 is much higher than that modeling the drag perturbations since the mean rates caused by the gravity perturbations are exactly constants.

The accuracy of the extended GA STM is shown in Fig. 36 for the drag and J_2 combined

perturbations.
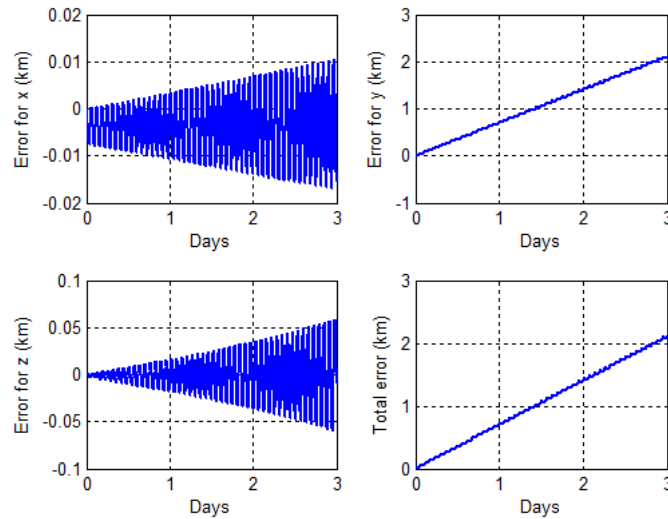
**Figure 34. Relative Position Errors From Two-Body Modeling
For J_2 Only Problem**
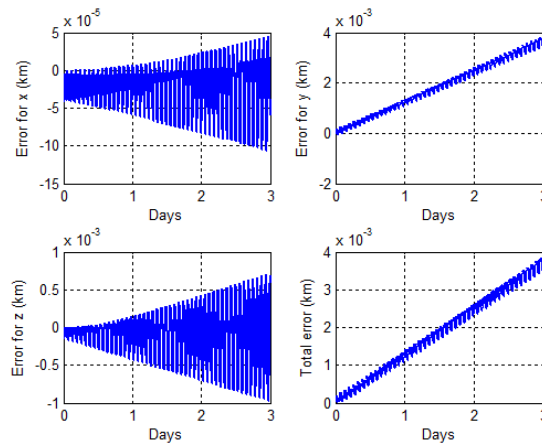
**Figure 35. Relative Position Errors From GA STM For J_2 Only
Problem**
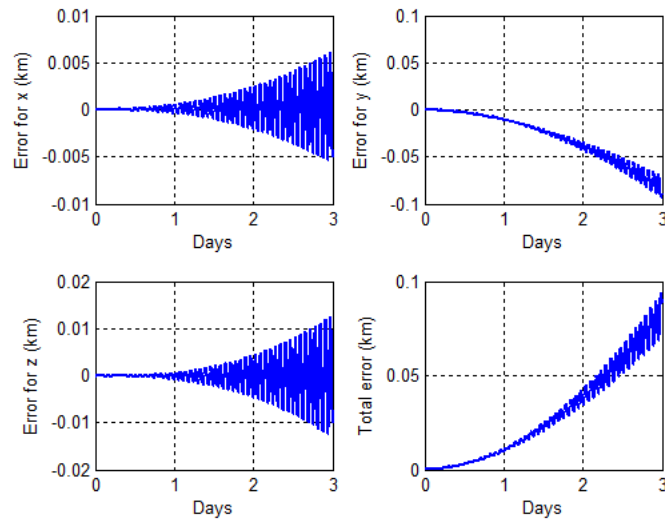
**Figure 36. Relative Position Errors From Modeling Combined
Perturbations Without Height Corrections**

The errors for the combined perturbations are larger than those obtained by a superposition of the individual effects, due to a coupling effect.
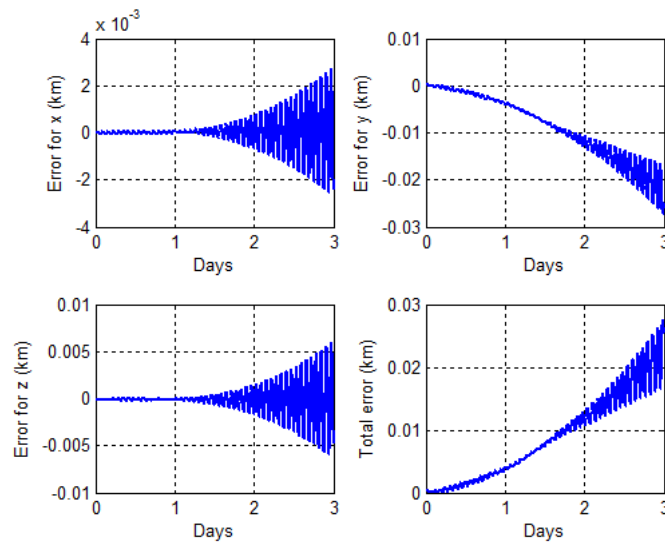
**Figure 37. Relative Position Errors From Modeling Combined
Perturbations With Height Corrections**

Fig. 37 illustrates the coupling effects are greatly reduced by applying the height correction given by Eq. (132). The cross sectional areas are the same for both the chief and deputy for the combined perturbations. Now we want to see the effect of the differential area on the drag and

gravity combined perturbations for one day simulation. Fig. 37 shows the RMS position errors vary with the differential area percent changes.
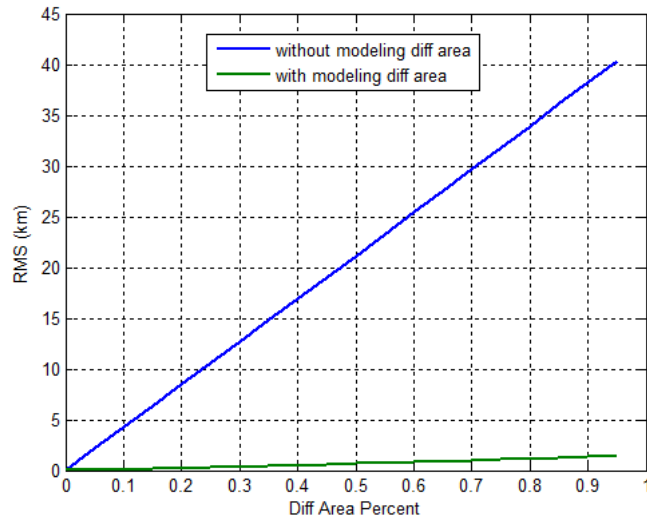
Figure 38. Effect of Modeling Differential Area Into Extended GA STM For Combined Perturbations
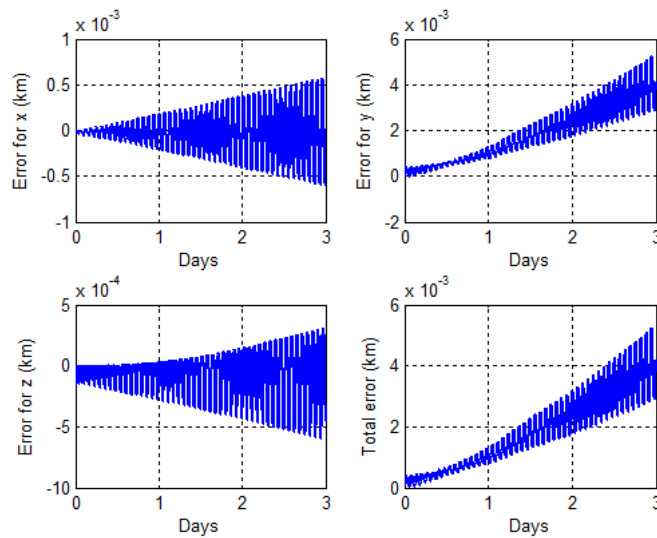
Figure 39. Relative Position Errors From Modeling Drag and
J_2 By Semi-Analytical Method

Fig. 38 indicates there are little changes if the combined perturbations are considered for the effect of the cross sectional area, possibly due to gravity perturbations being insensitive to variation of the area. Figure 39 shows the results of using the semi-analytic STM. Comparing

with Fig. 38, one can see the relative position errors are effectively reduced by using the semi-analytic STM.

4.2.3.3 *Effects of Different Density Models*

We only consider perturbations from drag only. All the simulations are nonlinear. We integrate the equations of motion for the drag only problem for chief and deputy, respectively, and then get relative distances that are compared with the GMAT solutions with the same initial conditions. The density model is the Jacchia-Roberts model in GMAT simulations. We use two kinds of the density models, the first one is the 1976 US standard atmosphere and the second is Harris-Priester density model.[45]

The epoch time for GMAT simulations is April 15, 00:00:00, 2015. Fig. 40 shows the relative distance error from nonlinear two-body simulation and GMAT simulation with Jacchia-Roberts model. Fig. 41 illustrates the relative distance error from nonlinear simulation with 1976 US standard density model and GMAT simulation with the Jacchia-Roberts model. Fig. 42 shows the relative distance error from nonlinear simulation with the Harris-Priester density model and GMAT simulation with Jacchia-Roberts model.

The standard density model only considers a spherical atmosphere while the Harris-Priester density model introduces the effects of oblateness and diurnal bulge. From Figs. 40-42 we can see the nonlinear modeling errors obviously decrease as we use more accurate density models. Assuming we exactly model nonlinear systems by the extended GA STM with the standard density model or Eq. (116), there is about an 0.8 km errors at the end of three day simulation if we compare with Jacchia-Roberts model, as shown in Fig. 41.
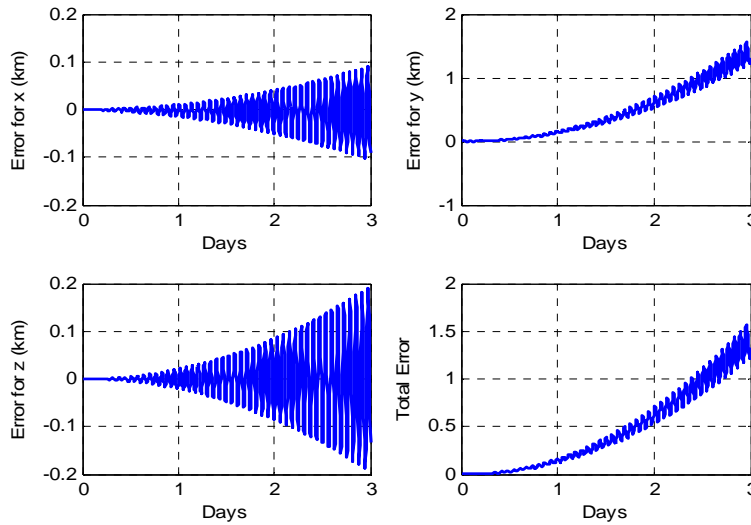
Figure 40. Relative Position Errors By Using Two-Body and Jacchia-Roberts Model
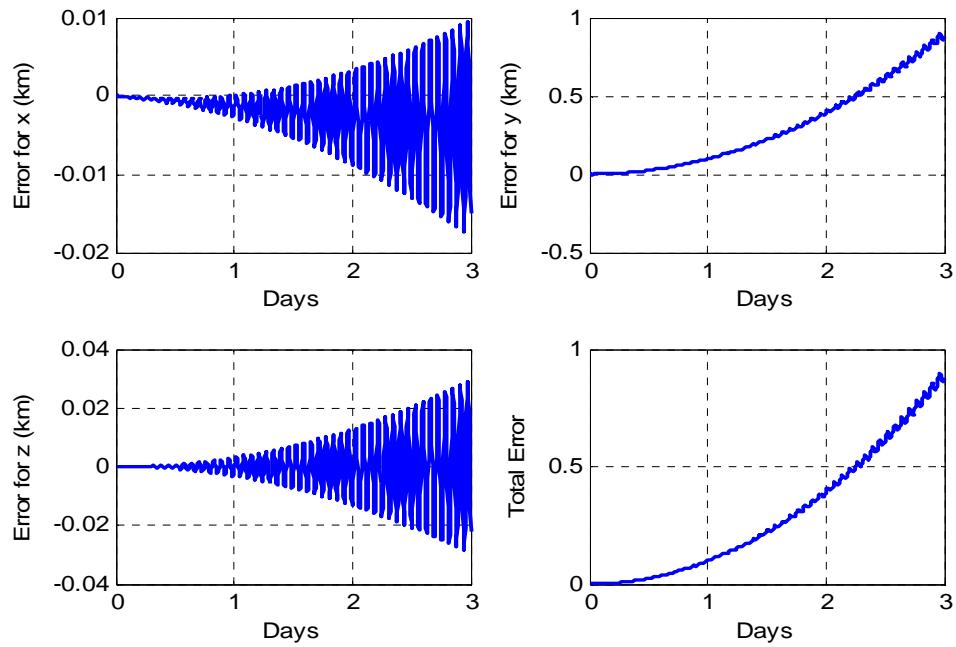
Figure 41. Relative Position Errors By Using Standard Density and Jacchia-Roberts Model
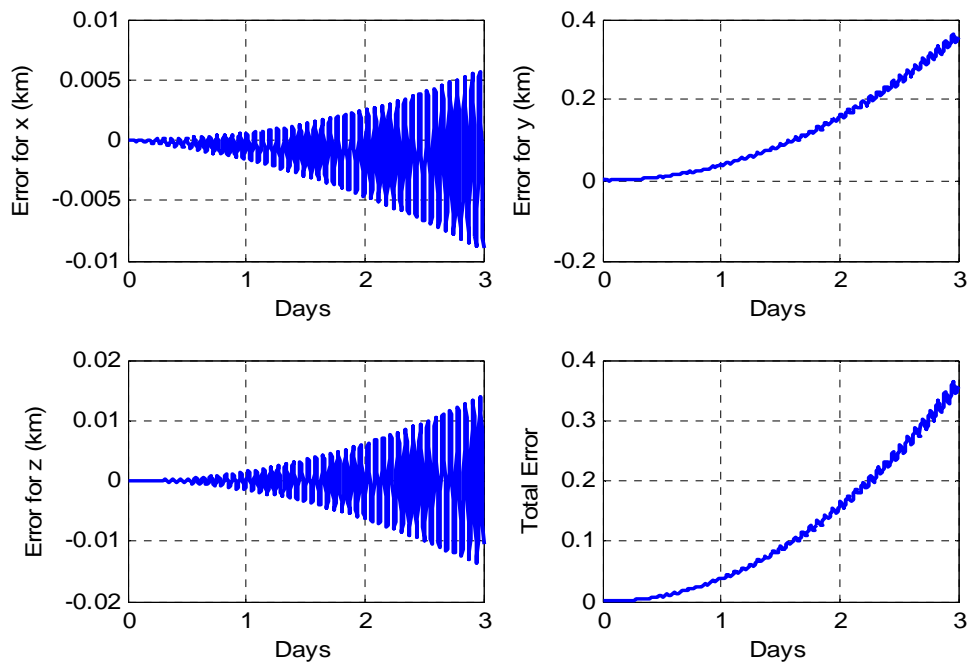
Figure 42. Relative Position Errors by Using Harris-Priester and Jacchia-Roberts Model

4.3   Navigation and Thruster Inaccuracies
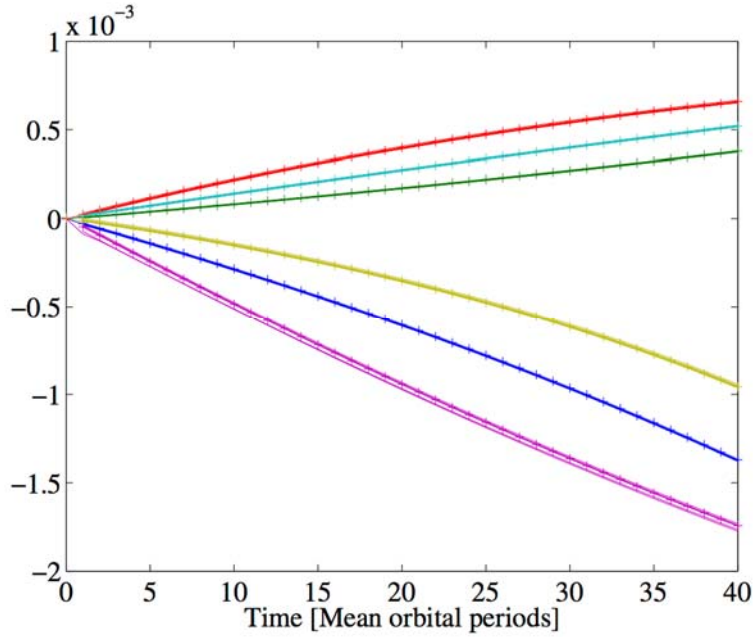
**Figure 43. Time history of $\Phi^{ij}_F/\Phi^{ij} - 1$ (lines) and $m^i - 1$
(crosses) color coded by i (1 = blue, 2 = green, 3 = red, 4 = teal,
5 = purple, 6 = gold) for all j. Values plotted once every orbit
for clarity.**

As a practical example, suppose the true dynamics include zonal terms of the Earth gravity up to
sixth order whereas the approximate dynamics include those only up to second order. Figure 43
is the time history of $\Phi^{ij}_F/\Phi^{ij} - 1$ compared with $\mathbf{m}^i - \mathbf{1}$ over 40 orbital periods for an object
whose orbital elements are

$$(a, e, i, \Omega, \omega, M)$$
$$= (7554.9 \text{ km}, 0.050078, 0.83775 \text{ rad}, 0.34859 \text{ rad}, 0.17984 \text{ rad}, 2.089 \text{ rad})$$

at epoch. We see that the two plots match well for the entire analysis timespan of 3.0256 days.

We further find in Fig. 43 that the difference between values in the two STMs are on the order of
0.1 %, suggesting that a linear function relating STM bias and maximum *a posteriori* state
estimates will sufficiently capture sensitivities between them for many relative navigation
scenarios of interest.

We now demonstrate how the tools developed in this research enable rapid design of relative navigation algorithms. Consider a formation of two spacecraft where the initial orbital elements for the chief are as given and the differences in orbital elements between the chief and deputy at epoch are

$$(\Delta a, \Delta e, \Delta i, \Delta \Omega, \Delta \omega, \Delta M)$$
$$= (0.00055381 \text{ km}, 5.7624 \times 10^{-5}, 1.0515 \times 10^{-5} \text{ rad},$$
$$- 9.2463 \times 10^{-8} \text{ rad}, -4.939 \times 10^{-6} \text{ rad}, 5.0279 \times 10^{-6} \text{ rad}).$$

For this work, we assume the absolute state of the chief is perfectly known and that the true and reference relative trajectories are set equal. This assumption shall be relaxed in future work. The observations are instantaneous range measurements made every 0.081001 seconds, corresponding to approximately 100 measurements over the course of a single orbital period for the chief. Measurement noise is assumed to be Gaussian white noise with a constant standard deviation of 1 meter. The measurements are simulated over 3.0256 days or approximately 40 orbital periods of the chief, resulting in 4001 range measurements total.

A batch processor is run for the true case whose dynamical model includes a 40×40 gravity field. State estimate and covariance biases are then computed for three approximate models which includes a 20×20, 10×10, or 2×0 gravity field. Any deviation from the estimated trajectory based on the true dynamics would indicate extraneous fuel expenditure attributed to dynamical model error. The total deviation $\Delta \hat{X}$ is the sum of the state estimate bias and the deviation in the reference state

$$\Delta \hat{X}(t) = \Delta \hat{x}(t) + \Delta x(t) \tag{171}$$

This vector may be converted into an approximate Δv cost as a consequence of Gauss' planetary equations. Suppose $\Delta \hat{X}(t) = (\delta a, \delta e, \delta i, \delta \Omega, \delta \omega, \delta M)$ are expressed in the mean orbital elements. An osculating-to-mean transformation including first-order J_2 effects such as Brouwer theory [3] will suffice for this computation regardless of dynamical model used. Then, assuming that the sensitivity between the mean and osculating elements are sufficiently close to unity,

$$\begin{cases} \Delta v_h = (h/r) \sqrt{\delta i^2 + \delta \Omega^2 \sin^2 i} \\ \Delta v_{r_p} = -(na/4) \left\{ \left[(1 + e)^2 / \eta \right] (\delta \omega + \delta \Omega \cos i) + \delta M \right\} \\ \Delta v_{r_a} = -(na/4) \left\{ \left[(1 - e)^2 / \eta \right] (\delta \omega + \delta \Omega \cos i) + \delta M \right\} \\ \Delta v_{t_p} = na\eta/4 \left[\delta a/a + \delta e/(1 + e) \right] \\ \Delta v_{t_a} = na\eta/4 \left[\delta a/a - \delta e/(1 - e) \right] \end{cases} \tag{172}$$

where subscripts h, r, and t indicate that the thrust is made along the angular momentum direction, radial direction, or a direction perpendicular to the two, respectively, and subsubscripts p and a indicate that the maneuver is executed at periapsis or apoapsis, respectively.

The state estimate uncertainty, however, may be so high such that $\Delta\widehat{X}$ cannot be distinguished from noise. Here, noise is attributed solely to measurement error, but in subsequent studies, we hope to add the effects of process noise. We would, nonetheless, like to compute another metric characterizing the magnitude of $\Delta\widehat{X}$ with respect to true state deviation estimate $\widehat{x}$; i.e., if $\Delta\widehat{X}$ is much smaller in magnitude compared to representative values of $\widehat{x}$, then it may safely be ignored. We define a non-dimensional distance d, similar to the Mahalanobis distance [49], where $\Delta\widehat{X}$ is normalized by the diagonalized true state estimate covariance $\mathbb{P}$

$$d(t) = \sqrt{\Delta\widehat{X}(t)^{\mathrm{T}}\mathbb{P}(t)^{-1}\Delta\widehat{X}(t)} \tag{173}$$

Thus, a d metric value of 1 would indicate that the magnitude of $\Delta\widehat{X}(t)$ in each coordinate direction is equal to their respective true 1-σ uncertainty level. We choose to ignore the correlations in P as we are not interested in quantifying the direction of $\Delta\widehat{X}(t)$ with respect to the state uncertainty for this particular metric.

We find for this problem that, in under 10 orbits, ΔH_i becomes small such that

$$\Delta\widehat{x} \approx P\boldsymbol{\eta} \approx P\left\{\sum\left[H_i^{\mathrm{T}}R_i^{-1}\Delta\boldsymbol{y}_i\right]\right\} \tag{174}$$

based on Eqs. (160) and (164). $\boldsymbol{\eta}$ is nearly parallel to $\boldsymbol{N} = \sum H_i^{\mathrm{T}}R_i^{-1}\boldsymbol{y_i}$ as the STM term dominates (4). Therefore, after running the true batch processor, one only needs to compute $\Delta\mathbf{y}_i$, which is often available as a closed-form function of the solution flow, and subsequently $\boldsymbol{\eta}$ across approximate dynamical models to evaluate

$$\Delta\widehat{X}(t) \approx \Phi(t; \boldsymbol{x}_0)P\boldsymbol{\eta} + \Delta\Phi(t; \boldsymbol{x}_0)\boldsymbol{x}_0 \tag{175}$$

accurate to order of magnitude. Table 3 corroborates this reasoning based on numerical simulations. That is, the truncated expression Eq. (175) for $\Delta\widehat{X}(t)$ results in the d distance metric computed accurately to at least order of magnitude.

Table 3 compares for each approximate dynamical model, the non-dimensional distance metric d using the truncated form of $\Delta\widehat{X}(t)$ in Eq. (175) (d_{Trunc}) and subsequently substituting into Eq. (173), and by running individual batch processors to compute $\Delta\widehat{X}(t)$ (d_{Full}). Δ is the relative error of the two methods in terms of percentage.

Table 3 Metric Comparison For Various Gravity Models

Gravity	d_{Trunc}	d_{Full}	Δ [%]
20×20	5.0496×10^{-2}	4.6012×10^{-2}	9.7454
10×10	2.8434×10^{-1}	2.8231×10^{-1}	0.7177
2×0	2.5473×10^{0}	5.7479×10^{0}	-55.682

For both the 20×20 and 10×10 models, the total deviation of the state estimate due to inaccurate dynamical modeling is an order of magnitude smaller than the magnitude of the state estimate noise. If we are to implement these in our navigation algorithms, then, it is unlikely that fuel will be spent to correct effects due to unmodeled terms in the geopotential. The same cannot be said, however, for the 2×0 model, as the magnitude of the bias in the state estimate is well over the 3-σ level of the diagonalized state covariance, as indicated by $d_{\text{Full}} = 5.7479$. For the given measurement parameters, then, a 2×0 model may be deemed insufficient as it leads to wasted fuel. On the other hand, the dimensional value of $\Delta \widehat{X}(t)$ throughout the analysis timeframe is, at most, meter-level in position and mm/s-level in velocity. Qualitatively, we expect that correcting such a small state deviation is within the bounds of thruster error. Future work is to directly relate the Δv value based on Eq. (172) and control system errors.

Finally, we note that, if the sensor were precise to 0.1 meters 1-σ, then without running any additional simulations, linearity suggests that d will accordingly increase by approximately an order of magnitude compared to those in Table 3, bringing the bias of the 10×10 model close to 3-σ level of the estimate noise.

We have thus shown how, with the tools developed in this work, one is able to bypass running multiple batch processors per each dynamical model we'd like to test in navigation algorithm design. Further computational gains may be reaped by applying analytical STMs or by computing the STM bias based on a vector scaling function between said models. In order to apply this methodology to a wider range of measurement types and mission scenarios, we are working to develop a way to automatically determine ignorable terms in the linear sensitivity function.

5 CONCLUSIONS

The conclusions of this program sponsored by the Air Force Research Laboratory are:

- A systems approach for the selection of the dynamic model that is based on the accuracy of the relative navigation system and the accuracy of the thrusters has been developed. The methodology simplifies the workflow of selecting the dynamic model and designing navigation systems so that the trade space between navigation system parameters and dynamical model fidelity could be quickly surveyed in lieu of performing massive numerical simulations for numerous scenarios and system parameter variations.
- Including the short period terms of higher order geopotential effects, especially J_2^2, in calculating the relative state initial conditions can reduce the secular error drift.
- Including the secular and long period effects of the lunar perturbations can improve the accuracy of the relative state prediction for high altitude formations.
- The correction of the deputy semi-major axis for negating in-track secular drift has been expanded to include higher order geopotential terms and this expansion will further reduce the drift.
- The GA-STM uses a set of nonsingular variables for non-equatorial orbits and equinoctial elements for near equatorial elements. Other sets of nonsingular variables, such as Hoots variables, were evaluated and compared to those in the GA-STM. In some cases the performance was better and others it was not. No general methodology for evaluating different sets of variables was found.

The recommendations from this project are:

- The system methodology for selecting the dynamic model and relative navigations system based on relative navigation requirements and thruster accuracy should be used to reduce the analysis required in making these selections in formation design.
- To help reduce secular drift the higher order geopotential short period terms should be included in the calculation of the relative state initial conditions.
- The extensive analysis performed in this project has revealed the need for Air Force Research Laboratory to have a detailed formation system simulation that includes all relevant perturbing forces, control forces and modules for thruster control, and modules for different types of relative navigation.

REFERENCES

[1]   D.W. Gim and K.T. Alfriend, "State Transition Matrix of Relative Motion for the Perturbed Non-Circular Reference Orbit," *Journal of Guidance, Control, and Dynamics*, Vol. 26, No. 6, 2003, pp. 956–971.

[2]   GMAT Development Team, "GMAT User Guide," http://gmat.gsfc.nasa.gov, NASA, 2013, Accessed 9 Aug 2016.

[3]   D. Brouwer, "Solution of the Problem of Artificial Satellite Theory without Drag," *The Astronomical Journal*, Vol. 64, No. 11, 1959, pp. 378–397.

[4]   A. Deprit, "Canonical transformations depending on a small parameter," *Celes. Mech.*, Vol. 1 (1969), 12–30.

[5]   W.M. Kaula, *Theory of Satellite Geodesy,* Blaisdell Publishing Co., Waltham, 1966 (republished by Dover, New York, 2000), Chapter Three.

[6]   H. Kinoshita, "Third-Order Solution of an Artificial Satellite Theory," Smithsonian Astrophysical Observatory, Special Report 379, 1977.

[7]   H. Yan, S.R. Vadali and K.T. Alfriend, "State Transition Matrix for Relative Motion Including General Gravitational Perturbations," AAS 15-339, AAS/AIAA Space Flight Mechanics Meeting, Williamsburg, VA, Jan 11-14, 2015.

[8]   B. D. Saedeleer, "Complete Zonal Problem of the Artificial Satellite: Generic Compact Analytic First Order In Closed Form," *Celestial Mechanics and Dynamical Astronomy*, Vol. 91, No. 3-4, 2005, pp. 239–268.

[9]   B. Mahajan, S. R. Vadali, and K. T. Alfriend, "Analytic Solution for Satellite Relative Motion with Zonal Gravity Perturbations," AAS 15-705, *AAS/AIAA Astrodynamics Specialist Conference*, Vail, CO, August 2015.

[10]   Hoots, F. R., "Reformulation of the Brouwer Geopotential Theory for Improved Computational Efficiency," *Celestial Mechanics*, Vol. 24, No. 4, 1981, pp. 367-375.

[11]   Y. Kozai, "On the Effects of the Sun and the Moon upon the Motion of a Close Earth Satellite," Smithsonian Astrophysical Observatory Special Report 22 (Part 2), 1959.

[12]   P. Musen, A. Bailie and E. Upton, "Development of the Lunar and Solar Perturbations in the Motion of an Artificial Satellite," NASA-TN D494, Washington, D.C., 1961.

[13]   G. E. O. Giacaglia,"Lunar Perturbations of Artificial Satellites of the Earth," *Celestial Mechanics and Dynamical Astronomy*, Vol. 9, April 1974, pp. 239–267.

[14]   D. Vallado, *Fundamentals of Astrodynamics and Applications,* New York, NY: McGraw-Hill, 1997, Chapter Eight.

[15]   P. J. Cefola, and R. Broucke, "On the Formulation of the Gravitational Potential in Terms of Equinoctial Variables," AIAA 13th Aerospace Sciences Meeting, Pasadena, CA, January 20-22, 1975.

[16]   A. F. B. A. Prado, "Third-Body Perturbation in Orbits Around Natural Satellites," *Journal of Guidance, Control, & Dynamics*, Vol. 26, January–February 2003, pp. 33–40.

[17]   C. W. T. Roscoe, "Satellite Formation Design in Orbits of High Eccentricity for Missions with Performance Criteria Specified over a Region of Interest," Dissertation, Texas A&M University, December 2012,

[18]   H. Yan, S. R. Vadali and K. T. Alfriend, "State Transition Matrix for Relative Motion Including Higher Order Gravity Perturbations," 2013 AAS/AIAA Astrodynamics Specialist Conference in Hilton Head, SC, August 11-15, 2013**.**

[19]   R.C. Domingos, R.V. Moraes and A.F.B.A. Prado, Third-Body Perturbation in the Case of Elliptic Orbits for the Disturbing Body, *Mathematical Problems in Engineering*, Volume 2008, Hindawi Publishing Corporation.

[20]   X. Liu, H. Baoyin and X. Ma, "Long-term Perturbations Due to a Disturbing Body in Elliptic Inclined Orbit," *Astrophysics and Space Science*, No. 2, Vol. 339, June 2012, pp 295-304.

[21]   C. W. T. Roscoe, S. R. Vadali and K. T. Alfriend, "Third-Body Perturbation Effects on Satellite Formation," *The Journal of the Astronautical Sciences*, Vol 60, Issue 3, 2013, pp. 408-433.

[22]   Wie, B., *Space Vehicle Dynamics and Control*, 2nd edition AIAA Education Series, Published by AIAA, Reston, VA, 2008.

[23]   X. Zeng, K.T. Alfriend, S.R. Vadali, H. Baoyin and S. Gong, "Time-Optimal Trajectory Design for a Dual-Satellite Sailcraft Interstellar Mission with Probe Release," 23th AAS/AIAA Space Flight Mechanics Meeting, Kauai, Hawaii, February 10, 2013.

[24]   T.W. Williams and Z.S. Wang, "Uses of Solar Radiation Pressure for Satellite Formation Flight," *International Journal of Robust and Nonlinear Control*, Vol 12, Jan. 2002, pp. 163-183.

[25]   S. Varma, and K.D. Kumar, "Multiple Satellite Formation Flying using Differential Solar Radiation Pressure," *AIAA/AAS Astrodynamics Specialist Conference*, Toronto, Ontario Canada, 2 August 2010.

[26]   S. Gong, J. Li and H. Baoyin, H, "Solar Radiation Pressure Used for Formation Flying Control around the Sun-Earth Libration Point," *Applied Mathematics and Mechanics*, Vol. 30, No.8, 2009, pp. 1009–1016.

[27]   J.A. Paris, *The Effects of Using Solar Radiation Pressure to Alleviate Fuel Requirements for Orbit Changing and Maintenance of the DSCS II F-13 Satellite*, Master thesis, Air Force Institute of Technology, AFIT/GA/ENY/006-M08, Wright Patterson AFB, OH, 2006.

[28]   J.C. Yang, *Spacecraft Orbit Dynamics and Control*, China Astronautic Publishing House, Beijing, China, 1995.

[29]   D. Brouwer and G. Hori, "Theoretical Evaluation of Atmospheric Drag Effects in the Motion of an Artificial Satellite," *The Astronomical Journal*, Vol. 66, No. 5, 1961, pp. 193-225.

[30]   F.R. Hoots and R.G. France, "An Analytical Satellite Theory Using Gravity and a Dynamic Atmosphere," *Celestial Mechanics*, 40, 1987, pp 1-17.

[31]   M.H. Lane, "The Development of an Artificial Satellite Theory Using a Power-Law Atmospheric Density Representation," AIAA Paper 65-35, AIAA 2nd Aerospace Science Meeting, New York, NY, 1965.

[32]   C.L. Leonard, W.M. Hollister and E.V. Bergman, "Orbital Formation keeping with Differential Drag," *Journal of Guidance, Control and Dynamics*, Vol. 12, No.1, 1989, pp. 108-113.

[33]   R. Bevilacqua and M. Romano, "Rendezvous Maneuvers of Multiple Spacecraft Using Differential Drag Under J_2 Perturbations," *Journal of Guidance, Control and Dynamics*, Vol. 31, No. 6, 2008, pp. 1595-1607.

[34]   S.A. Schweighart and R.J. Sedwick, "High-Fidelity Linearized J_2 Model for Satellite Formation Flight," *Journal of Guidance, Control and Dynamics*, Vol. 25, No. 6, 2002, pp. 1073-1080.

[35] T. Reid and A.K. Misra, "Formation Flight of Satellites in The Presence of Atmospheric Drag," *Journal of Aerospace Engineering, Sciences, and Applications*, Vol. 3, January-April 2011, pp. 64-91.

[36] K.D. Kumar, A.K. Misra, S. Varma, T. Reid and F. Bellefeuille, "Maintenance of Satellite Formations Using Environmental Forces," *Acta Astronautica*, Vol. 102, September 2014, pp. 341-354.

[37] D. Mishne, "Formation Control of Satellites Subject to Drag Variations and J_2 Perturbations," *Journal of Guidance, Control and Dynamics*, Vol. 27, No. 4, July-August 2004, pp. 685-692.

[38] M. Humi and T. Carter, "Rendezvous Equations in a Central-Force Field with Linear Drag," *Journal of Guidance, Control and Dynamics*, Vol. 25, No. 1, 2002, pp. 74-79.

[39] T. Carter and M. Humi, "Clohessy-Wiltshire Equations Modified to Include Quadratic Drag," *Journal of Guidance, Control and Dynamics*, Vol. 25, No. 6, 2002, pp. 1058-1063.

[40] G.B. Palmerini, S. Sgubini and G. Taini, "Spacecraft Orbit Control Using Air Drag," Paper IAC-05 C.1.6.10, 56th International Astronautical Congress of the International Astronautical Federation, Fukuoka, Japan, Oct. 2005.

[41] G.B. Palmerini and S. Sgubini, "Control Effort Evaluation for Low-Altitude Formation Flying," IEEE Aerospace Conference, Big Sky, MT, 2006.

[42] A. J. Green, "Orbit Determination and Prediction Processes for Low Altitude Satellites," CSDL-T 703, PhD Thesis, Department of Aeronautics and Astronautics, MIT, Cambridge, MA, Dec 1979.

[43] R.S. Pimm, "Long-Term Orbital Trajectory Determination by Super-position of Gravity and Drag Perturbations," AAS Paper 71-376, AASIAIAA Astrodynamics Specialist Conference, Ft Lauderdale, FL, Aug 17, 1971.

[44] D. Lutsky and C. Uphoff, "Short-Periodic Variations and Second-Order Numerical Averaging," AlAA Paper No. 75-11, AIAA 13th Aerospace Sciences Meeting, Jan. 1975, Pasadena, CA.

[45] J.L. Arsenault, K.C. Ford and P.E. Koskela, "Orbit Determination Using Analytical Partial Derivatives of Perturbed Motion," *AIAA Journal*, Vol. 8, No. 1, 1970, pp. 4-12.

[46] I. Park, K. Fujimoto, and D. J. Scheeres, "Effect of dynamical accuracy for uncertainty propagation of   perturbed Keplerian motion," *Journal of Guidance, Control, and Dynamics*, 38(12):2287–2300, 2015.

[47] H. P. Schaub and K. T. Alfriend, "Impulsive feedback control to establish specific mean orbit elements of   spacecraft formations," *Journal of Guidance, Control, and Dynamics*, 24(4):739–745, 2001.

[48] B. D. Tapley, B. E. Schutz, and G. H. Born, *Statistical Orbit Determination,* Elsevier Academic Press, Burlington, MA, 2004. pp. 159-284.

[49] P. C. Mahalanobis, "On the generalized distance in statistics," *Proceedings of the National Institute of Sciences of India*, 2(1):49–55, 1936.

APPENDIX A. FORMULAE FOR ZONAL HARMONICS

A.1 Expansion Formulae

The following formulae are helpful in computing closed-form expressions for the integrals given in Eq. (6). These formulae include the definition of Legendre polynomials and formulae for converting powers of trigonometric functions into sums of their arguments.

$$P_n(x) = \frac{1}{2^n} \sum_{j=0}^{\lfloor \frac{n}{2} \rfloor} \frac{(-1)^j (2n-2j)!}{j!\,(n-j)!\,(n-2j)!} x^{n-2j} \tag{A.1}$$

$$\left(\frac{a}{r}\right)^{n-1} = \sum_{k=0}^{n-1} \binom{n-1}{k} \frac{e^k \cos^k(f)}{\eta^{2(n-1)}} \tag{A.2}$$

$$\sin^{2n}(x) = \frac{1}{2^{2n}} \sum_{j=0}^{n-1} (-1)^{n-j} 2 \binom{2n}{j} \cos(2(n-j)x) + \binom{2n}{n}$$

$$\sin^{2n-1}(x) = \frac{1}{2^{2n-2}} \sum_{j=0}^{n-1} (-1)^{n+j-1} \binom{2n-1}{j} \sin((2n-2j-1)x)$$

$$\cos^{2n}(x) = \frac{1}{2^{2n}} \sum_{k=0}^{n-1} 2 \binom{2n}{k} \cos(2(n-k)x) + \binom{2n}{n} \tag{A.3}$$

$$\cos^{2n-1}(x) = \frac{1}{2^{2n-2}} \sum_{k=0}^{n-1} \binom{2n-1}{k} \cos((2n-2k-1)x)$$

A.2 Intermediate Terms for Short-Period Corrections

The following intermediate terms are used in the analytic formulae for short-period contributions due to an arbitrary zonal harmonic with degree greater than two.

$$f_{LG} = \frac{\partial f}{\partial L} + \frac{\partial f}{\partial G} = -\sqrt{\frac{1-\eta}{1+\eta}} \frac{\sin(f)}{\eta} \left(\frac{2 + e\cos(f)}{\sqrt{\mu a}} \right) \tag{A.4}$$

$$\frac{\partial f}{\partial l} = \frac{(1 + e\cos(f))^2}{\eta^3} \tag{A.5}$$

$$\frac{\partial f}{\partial e} = \frac{(2 + e\cos(f))\sin(f)}{\eta^2} \tag{A.6}$$

$$\frac{\partial \mathcal{W}_2}{\partial e} = (2n-1)\frac{e}{\eta^2}\mathcal{W}_2 + \delta'_n(a,e) \sum_{j=0}^{\lfloor \frac{n}{2} \rfloor} \beta_{j,n}(i) \sum_{k=1}^{n-1} \frac{(n-k)\alpha_{k-1,n}(e)}{2^k} \tag{A.7}$$

$$\mathcal{W}_2^i = \sin(i)\frac{\partial \mathcal{W}_2}{\partial i} = \cos(i)\left(\mathcal{W}_2(n-2j)\right) \tag{A.8}$$

$$\begin{aligned}
\frac{\partial \mathcal{W}_3}{\partial f} = \lambda_n \binom{n-2j}{\frac{n}{2}-j} \sum_{s=0}^{\lfloor \frac{k-1}{2} \rfloor} 2\binom{k}{s}\cos(k-2s)f \\
+ \sum_{p=0}^{\lfloor \frac{n-1}{2} \rfloor - j} \gamma_{p,j,n} \left\{ \sum_{s=0}^{\lfloor \frac{k-1}{2} \rfloor} \binom{k}{s}(\cos[\sin]((k-2s+c)f+cg)) \right. \\
\left. + \sum_{\substack{s=0 \\ s\neq s^*}}^{\lfloor \frac{k-1}{2} \rfloor} \binom{k}{s}(\cos[-\sin]((k-2s-c)f-cg)) + \lambda_k \binom{k}{\frac{k}{2}}\cos[\sin](cf+cg) \right\}
\end{aligned} \tag{A.9}$$

$$\begin{aligned}
\frac{\partial \mathcal{W}_3}{\partial g} = \sum_{p=0}^{\lfloor \frac{n-1}{2} \rfloor - j} \gamma_{p,j,n} \left\{ \sum_{s=0}^{\lfloor \frac{k-1}{2} \rfloor} \binom{k}{s}\left(\frac{\cos[\sin]((k-2s+c)f+cg)}{k-2s+c}\right)c \right. \\
\left. - \sum_{\substack{s=0 \\ s\neq s^*}}^{\lfloor \frac{k-1}{2} \rfloor} \binom{k}{s}\left(\frac{\cos[-\sin]((k-2s-c)f-cg)}{k-2s-c}\right)c + \lambda_k \binom{k}{\frac{k}{2}}\cos[\sin](cf+cg) \right\}
\end{aligned} \tag{A.10}$$

$$\begin{aligned}
K_{2,n}^{LGH} = \frac{\partial K_{2,n}}{\partial L} + \frac{\partial K_{2,n}}{\partial G} + \frac{\partial K_{2,n}}{\partial H} \\
= \delta_n(a,e)\sum_{j=0}^{\lfloor \frac{n}{2} \rfloor} \beta_{j,n}(i) \sum_{\text{even[odd] } k=0}^{n-1} \frac{\alpha_{k,n}(e)}{2^k}\frac{1}{G}\left\{ -2(n+1) - (n-2j)\frac{\cos(i)}{2\cos^2\left(\frac{i}{2}\right)} \right\} \\
\times \left\{ \lambda_n \binom{n-2j}{\frac{n}{2}-j}\binom{k}{\frac{k}{2}} + \sum_{p=0}^{\lfloor \frac{n-1}{2} \rfloor - j} \gamma_{p,j,n}\binom{k}{\frac{k-(n-2j-2p)}{2}}(\cos[\sin](n-2j-2p)g) \right\}
\end{aligned} \tag{A.11}$$

$$K_{2,n}^{eGH} = e\frac{\partial K_{2,n}}{\partial G} + e\frac{\partial K_{2,n}}{\partial H}$$

$$= \delta_n(a,e) \sum_{j=0}^{\lfloor\frac{n}{2}\rfloor} \beta_{j,n}(i) \sum_{\text{even[odd] } k=0}^{n-1} \frac{\alpha_{k,n}(e)}{2^k} \frac{1}{G} \left\{ -e(2n-1) - \frac{k\eta^2}{e} - e(n-2j)\frac{\cos(i)}{2\cos^2\left(\frac{i}{2}\right)} \right\}$$

$$\times \left\{ \lambda_n \binom{n-2j}{\frac{n}{2}-j}\binom{k}{\frac{k}{2}} + \sum_{p=0}^{\lfloor\frac{n-1}{2}\rfloor-j} \gamma_{p,j,n} \binom{k}{\frac{k-(n-2j-2p)}{2}} (\cos[\sin](n-2j-2p)g) \right\}$$

$$\text{(A.12)}$$

$$\frac{\partial K_{2,n}}{\partial g} = \delta_n(a,e) \sum_{j=0}^{\lfloor\frac{n}{2}\rfloor} \beta_{j,n}(i) \sum_{\text{even[odd] } k=0}^{n-1} \frac{\alpha_{k,n}(e)}{2^k}$$

$$\times \left\{ \sum_{p=0}^{\lfloor\frac{n-1}{2}\rfloor-j} \gamma_{p,j,n} \binom{k}{\frac{k-(n-2j-2p)}{2}} (n-2j-2p)(-\sin[\cos](n-2j-2p)g) \right\}$$

$$\text{(A.13)}$$

$$\mathcal{W}_1^{lge} = \frac{\partial \mathcal{W}_1}{\partial l}\frac{\partial e}{\partial L} + \frac{\partial \mathcal{W}_1}{\partial g}\frac{\partial e}{\partial G}$$

$$= \frac{a}{2\mu\eta}\left(4\cos(f) + e\cos(2f) + e\frac{2\eta^2+3\eta+3}{1+\eta} \right) K_{2,n}$$

$$- \frac{a\eta}{\mu}(f-l)\left\{ \delta_n(a,e) \sum_{j=0}^{\lfloor\frac{n}{2}\rfloor} \beta_{j,n}(i) \sum_{\text{even[odd] } k=1}^{n-1} \frac{\alpha_{k-1,n}(e)}{2^k}\frac{n-k}{k} \right. \qquad \text{(A.14)}$$

$$\left. \sum_{p=0}^{\lfloor\frac{n-1}{2}\rfloor-j} \gamma_{p,j,n}\binom{k}{\frac{k-(n-2j-2p)}{2}}(n-2j-2p)(-\sin[\cos](n-2j-2p)g) \right\}$$

$$\mathcal{W}_{23}^{lge} = \mathcal{W}_2\frac{\partial \mathcal{W}_3}{\partial f}\frac{\partial f}{\partial l}\frac{\partial e}{\partial L} + \mathcal{W}_2\frac{\partial \mathcal{W}_3}{\partial g}\frac{\partial e}{\partial G}$$

$$= \delta_n'(a,e) \sum_{j=0}^{\lfloor\frac{n}{2}\rfloor} \beta_{j,n}(i) \left\{ \frac{1}{2\eta\sqrt{\mu a}}(4\cos(f)+e\cos(2f)+3e)\sum_{p=0}^{\lfloor\frac{n-1}{2}\rfloor-j} \gamma_{p,j,n}\cos[\sin](cf+cg) \right.$$

$$\left. + \sum_{k=1}^{n-1} \frac{\alpha_{k-1,n}(e)}{2^k}\frac{n-k}{k}\frac{\eta^2}{\sqrt{\mu a}}\left(\frac{\partial \mathcal{W}_3}{\partial f}\frac{\partial f}{\partial l} - \frac{1}{\eta}\frac{\partial \mathcal{W}_3}{\partial g} \right) \right\}$$

$$\text{(A.15)}$$

APPENDIX B. Φ MATRIX FOR THIRD BODY PERTURBATIONS

Derivatives for *a*

$$\frac{\partial a}{\partial a_0} = 1$$

$$\frac{\partial a}{\partial i_0} = \frac{\partial a}{\partial \theta_0} = \frac{\partial a}{\partial q_{10}} = \frac{\partial a}{\partial q_{20}} = \frac{\partial a}{\partial \Omega_0} = 0$$

(B.1)

Derivatives for θ_0

$$\frac{\partial \theta}{\partial a_0} = \left[\frac{\partial \dot{\lambda}}{\partial a_0}(t - t_0) - \frac{\partial G}{\partial q_1}\frac{\partial q_1}{\partial a_0} - \frac{\partial G}{\partial q_2}\frac{\partial q_2}{\partial a_0} \right] \Big/ \left(\frac{\partial G}{\partial \theta} \right)$$

$$\frac{\partial \theta}{\partial \theta_0} = \left(\frac{\partial G}{\partial \theta_0} \right) \Big/ \left(\frac{\partial G}{\partial \theta} \right)$$

$$\frac{\partial \theta}{\partial i_0} = \left[\frac{\partial \dot{\lambda}}{\partial i_0}(t - t_0) - \frac{\partial G}{\partial q_1}\frac{\partial q_1}{\partial i_0} - \frac{\partial G}{\partial q_2}\frac{\partial q_2}{\partial i_0} \right] \Big/ \left(\frac{\partial G}{\partial \theta} \right)$$

$$\frac{\partial \theta}{\partial q_{10}} = \left[\frac{\partial \dot{\lambda}}{\partial q_{10}}(t - t_0) - \frac{\partial G}{\partial q_1}\frac{\partial q_1}{\partial q_{10}} - \frac{\partial G}{\partial q_2}\frac{\partial q_2}{\partial q_{10}} \right] \Big/ \left(\frac{\partial G}{\partial \theta} \right)$$

(B.2)

$$\frac{\partial \theta}{\partial q_{20}} = \left[\frac{\partial \dot{\lambda}}{\partial q_{20}}(t - t_0) - \frac{\partial G}{\partial q_1}\frac{\partial q_1}{\partial q_{20}} - \frac{\partial G}{\partial q_2}\frac{\partial q_2}{\partial q_{20}} \right] \Big/ \left(\frac{\partial G}{\partial \theta} \right)$$

$$\frac{\partial \theta}{\partial \Omega_0} = 0$$

Derivatives for *i*

$$\frac{\partial i}{\partial a_0} = \frac{\partial \dot{i}}{\partial a_0}\left(t - t_0\right)$$

$$\frac{\partial i}{\partial \theta_0} = 0$$

$$\frac{\partial i}{\partial i_0} = 1 + \frac{\partial \dot{i}}{\partial i_0}\left(t - t_0\right)$$

$$\frac{\partial i}{\partial q_{10}} = \frac{\partial \dot{i}}{\partial q_{10}}\left(t - t_0\right)$$

$$\frac{\partial i}{\partial q_{20}} = \frac{\partial \dot{i}}{\partial q_{20}}\left(t - t_0\right)$$

$$\frac{\partial i}{\partial \Omega_0} = \frac{\partial \dot{i}}{\partial \Omega_0}\left(t - t_0\right)$$

(B.3)

Derivatives for *q₂*

$$\frac{\partial q_1}{\partial a_0} = K_1 K_3 \frac{\partial \dot{\omega}}{\partial a_0} + K_2 \frac{\partial\left(\dfrac{\dot{e}}{e}\right)}{\partial a_0}$$

$$\frac{\partial q_1}{\partial \theta_0} = 0$$

$$\frac{\partial q_1}{\partial i_0} = K_1 K_3 \frac{\partial \dot{\omega}}{\partial i_0} + K_2 \frac{\partial\left(\dfrac{\dot{e}}{e}\right)}{\partial i_0}$$

(B.4)

$$\frac{\partial q_1}{\partial q_{10}} = K_1 K_3 \frac{\partial \dot{\omega}}{\partial q_{10}} + K_2 \frac{\partial\left(\dfrac{\dot{e}}{e}\right)}{\partial q_{10}} + K_3 \cos \Delta\omega$$

$$\frac{\partial q_1}{\partial q_{20}} = K_1 K_3 \frac{\partial \dot{\omega}}{\partial q_{20}} + K_2 \frac{\partial\left(\dfrac{\dot{e}}{e}\right)}{\partial q_{20}} - K_3 \sin \Delta\omega$$

$$\frac{\partial q_1}{\partial \Omega_0} = K_1 K_3 \frac{\partial \dot{\omega}}{\partial \Omega_0} + K_2 \frac{\partial\left(\dfrac{\dot{e}}{e}\right)}{\partial \Omega_0}$$

Derivatives for *q₂*

$$\frac{\partial q_2}{\partial a_0} = K_2 K_3 \frac{\partial \dot{\omega}}{\partial a_0} - K_1 \frac{\partial \left(\frac{\dot{e}}{e} \right)}{\partial a_0}$$

$$\frac{\partial q_2}{\partial \theta_0} = 0$$

$$\frac{\partial q_2}{\partial i_0} = K_2 K_3 \frac{\partial \dot{\omega}}{\partial i_0} - K_1 \frac{\partial \left(\frac{\dot{e}}{e} \right)}{\partial i_0}$$

$$\frac{\partial q_2}{\partial q_{10}} = K_2 K_3 \frac{\partial \dot{\omega}}{\partial q_{10}} - K_1 \frac{\partial \left(\frac{\dot{e}}{e} \right)}{\partial q_{10}} + K_3 \sin \Delta \omega \qquad \text{(B.5)}$$

$$\frac{\partial q_2}{\partial q_{20}} = K_2 K_3 \frac{\partial \dot{\omega}}{\partial q_{20}} - K_1 \frac{\partial \left(\frac{\dot{e}}{e} \right)}{\partial q_{20}} + K_3 \cos \Delta \omega$$

$$\frac{\partial q_2}{\partial \Omega_0} = K_2 K_3 \frac{\partial \dot{\omega}}{\partial \Omega_0} - K_1 \frac{\partial \left(\frac{\dot{e}}{e} \right)}{\partial \Omega_0}$$

Derivatives for Ω

$$\frac{\partial \Omega}{\partial a_0} = \frac{\partial \dot{\Omega}}{\partial a_0} (t - t_0)$$

$$\frac{\partial \Omega}{\partial \theta_0} = 0$$

$$\frac{\partial \Omega}{\partial i_0} = \frac{\partial \dot{\Omega}}{\partial i_0} (t - t_0)$$

$$\frac{\partial \Omega}{\partial q_{10}} = \frac{\partial \dot{\Omega}}{\partial q_{10}} (t - t_0) \qquad \text{(B.6)}$$

$$\frac{\partial \Omega}{\partial q_{20}} = \frac{\partial \dot{\Omega}}{\partial q_{20}} (t - t_0)$$

$$\frac{\partial \Omega}{\partial \Omega_0} = 1 + \frac{\partial \dot{\Omega}}{\partial \Omega_0} (t - t_0)$$

where

$$G = \lambda - \lambda\left(t_0\right) = M\left(t_0\right) + \omega\left(t_0\right) + \left(\dot{M} + \dot{\omega}\right)\left(t - t_0\right)$$
$$K_1 = \left(-q_{10} \sin \Delta\omega + q_{20} \cos \Delta\omega\right)$$
$$K_2 = \left(q_{10} \cos \Delta\omega + q_{20} \sin \Delta\omega\right) \tag{B.7}$$
$$K_3 = 1 + \frac{\dot{e}}{e}\left(t - t_0\right)$$

APPENDIX C. Φ AND *D* MATRIX FOR SRP PERTURBATIONS

C.1   Φ Matrix

Derivatives of *a*

$$a = a_0$$

$$\frac{\partial a}{\partial a_0} = 1 \tag{C.1}$$

$$\frac{\partial a}{\partial \theta_0} = \frac{\partial a}{\partial i_0} = \frac{\partial a}{\partial q_{10}} = \frac{\partial a}{\partial q_{20}} = \frac{\partial a}{\partial \Omega_0} = \frac{\partial a}{\partial C_B} = 0$$

Derivatives of *θ*

$$\frac{\partial \theta}{\partial a_0} = \left(\frac{\partial \lambda}{\partial a_0} - \frac{\partial G}{\partial q_1}\frac{\partial q_1}{\partial a_0} - \frac{\partial G}{\partial q_2}\frac{\partial q_2}{\partial a_0} \right) \bigg/ \frac{\partial G}{\partial \theta}$$

$$\frac{\partial \theta}{\partial \theta_0} = - \frac{\partial G}{\partial \theta_0} \bigg/ \frac{\partial G}{\partial \theta}$$

$$\frac{\partial \theta}{\partial i_0} = \left(\frac{\partial \lambda}{\partial i_0} - \frac{\partial G}{\partial q_1}\frac{\partial q_1}{\partial i_0} - \frac{\partial G}{\partial q_2}\frac{\partial q_2}{\partial i_0} \right) \bigg/ \frac{\partial G}{\partial \theta}$$

$$\frac{\partial \theta}{\partial q_{10}} = \left(\frac{\partial \lambda}{\partial q_{10}} - \frac{\partial G}{\partial q_{10}} - \frac{\partial G}{\partial q_1}\frac{\partial q_1}{\partial q_{10}} - \frac{\partial G}{\partial q_2}\frac{\partial q_2}{\partial q_{10}} \right) \bigg/ \frac{\partial G}{\partial \theta} \tag{C.2}$$

$$\frac{\partial \theta}{\partial q_{20}} = \left(\frac{\partial \lambda}{\partial q_{20}} - \frac{\partial G}{\partial q_{10}} - \frac{\partial G}{\partial q_1}\frac{\partial q_1}{\partial q_{20}} - \frac{\partial G}{\partial q_2}\frac{\partial q_2}{\partial q_{20}} \right) \bigg/ \frac{\partial G}{\partial \theta}$$

$$\frac{\partial \theta}{\partial \Omega_0} = \left(\frac{\partial \lambda}{\partial i_0} - \frac{\partial G}{\partial q_1}\frac{\partial q_1}{\partial \Omega_0} - \frac{\partial G}{\partial q_2}\frac{\partial q_2}{\partial \Omega_0} \right) \bigg/ \frac{\partial G}{\partial \theta}$$

$$\frac{\partial \theta}{\partial C_B} = \left(\frac{\partial \lambda}{\partial C_B} - \frac{\partial G}{\partial q_1}\frac{\partial q_1}{\partial C_B} - \frac{\partial G}{\partial q_2}\frac{\partial q_2}{\partial C_B} \right) \bigg/ \frac{\partial G}{\partial \theta}$$

Derivatives of i

$$i = i_0 + \dot{i}_0 \Delta t$$

$$\frac{\partial i}{\partial a_0} = \frac{3PkC_B}{4na_0^2} \bar{U}_h q_{10} \Delta t$$

$$\frac{\partial i}{\partial \theta_0} = 0$$

$$\frac{\partial i}{\partial i_0} = 1 + \frac{3PkC_B q_{10}}{2na_0} \frac{\partial \bar{U}_h}{\partial i_0} \Delta t$$

$$\frac{\partial i}{\partial q_{10}} = \frac{3}{2na_0} PkC_B \bar{U}_h \Delta t \qquad\qquad (C.3)$$

$$\frac{\partial i}{\partial q_{20}} = 0$$

$$\frac{\partial i}{\partial \Omega_0} = \frac{3PkC_B q_{10}}{2na_0} \frac{\partial \bar{U}_h}{\partial \Omega_0} \Delta t$$

$$\frac{\partial i}{\partial C_B} = \frac{3Pk}{2na_0} \bar{U}_h q_1 \Delta t$$

Derivatives of q_q

$$q_1 = q_{10} + \dot{q}_{10} \Delta t$$

$$\frac{\partial q_1}{\partial a_0} = -\frac{3}{4na_0^2} PkC_B \bar{U}_t \Delta t$$

$$\frac{\partial q_1}{\partial \theta_0} = 0$$

$$\frac{\partial q_1}{\partial i_0} = -\frac{3}{2na_0} PkC_B \frac{\partial \bar{U}_t}{\partial i_0} \Delta t$$

$$\frac{\partial q_1}{\partial q_{10}} = 1 \qquad\qquad (C.4)$$

$$\frac{\partial q_1}{\partial q_{20}} = 0$$

$$\frac{\partial q_1}{\partial \Omega_0} = -\frac{3}{2na_0} PkC_B \frac{\partial \bar{U}_t}{\partial \Omega_0} \Delta t$$

$$\frac{\partial q_1}{\partial C_B} = -\frac{3Pk}{2na_0} \bar{U}_t \Delta t$$

Derivatives of q_2

$$q_2 = q_{20} + \dot{q}_{20}\Delta t$$

$$\frac{\partial q_2}{\partial a_0} = \frac{3}{4na_0^2}PkC_B\bar{U}_r\Delta t$$

$$\frac{\partial q_2}{\partial \theta_0} = 0$$

$$\frac{\partial q_2}{\partial i_0} = \frac{3}{2na_0}PkC_B\frac{\partial \bar{U}_r}{\partial i_0}\Delta t$$

$$\frac{\partial q_2}{\partial q_{10}} = 0 \tag{C.5}$$

$$\frac{\partial q_2}{\partial q_{20}} = 1$$

$$\frac{\partial q_2}{\partial \Omega_0} = \frac{3}{2na_0}PkC_B\frac{\partial \bar{U}_r}{\partial \Omega_0}\Delta t$$

$$\frac{\partial q_2}{\partial C_B} = \frac{3Pk}{2na_0}\bar{U}_r\Delta t$$

Derivatives of Ω

$$\Omega = \Omega_0 + \dot{\Omega}_0\Delta t$$

$$\frac{\partial \Omega}{\partial a_0} = \frac{3}{4na_0^2\sin i_0}PkC_B\bar{U}_h q_{20}\Delta t$$

$$\frac{\partial \Omega}{\partial \theta_0} = 0$$

$$\frac{\partial \Omega}{\partial i_0} = -\frac{3PkC_B q_{20}}{2na_0\sin i_0}\left(\bar{U}_h\cot i_0 - \frac{\partial \bar{U}_h}{\partial i_0}\right)$$

$$\frac{\partial \Omega}{\partial q_{10}} = 0 \tag{C.6}$$

$$\frac{\partial \Omega}{\partial q_{20}} = \frac{3}{2na_0\sin i_0}PkC_B\bar{U}_h\Delta t$$

$$\frac{\partial \Omega}{\partial \Omega_0} = 1 + \frac{3}{2na_0\sin i_0}PkC_B q_{20}\frac{\partial \bar{U}_h}{\partial \Omega_0}$$

$$\frac{\partial \Omega}{\partial C_B} = \frac{3Pk}{2na_0\sin i_0}\bar{U}_h q_2\Delta t$$

where

$$\frac{\partial \lambda}{\partial a_0} = -\frac{3n}{2a_0}\Delta t - \frac{3PkC_B}{4na_0^2}\left(\bar{U}_r q_{10} + \bar{U}_t q_{20} + \bar{U}_h q_{20}\cot i_0\right)\Delta t$$

$$\frac{\partial \lambda}{\partial i_0} = -\frac{3PkC_B}{2na_0}\left(\frac{\partial \bar{U}_r}{\partial i_0}q_{10} + \frac{\partial \bar{U}_t}{\partial i_0}q_{20} - \frac{1}{\sin^2 i}\bar{U}_h q_{20} + \frac{\partial \bar{U}_h}{\partial i_0}q_{20}\cot i_0\right)\Delta t$$

$$\frac{\partial \lambda}{\partial q_{10}} = -\frac{3}{2na_0}PkC_B\bar{U}_r\Delta t$$

$$\frac{\partial \lambda}{\partial q_{20}} = -\frac{3}{2na_0}PkC_B\left(\bar{U}_t + \bar{U}_h\cot i_0\right)\Delta t$$ (C.7)

$$\frac{\partial \lambda}{\partial \Omega_0} = -\frac{3}{2na_0}PkC_B\left(\frac{\partial \bar{U}_r}{\partial \Omega_0}q_{10} + \frac{\partial \bar{U}_t}{\partial \Omega_0}q_{20} + \frac{\partial \bar{U}_h}{\partial \Omega_0}q_{20}\cot i_0\right)\Delta t$$

$$\frac{\partial \lambda}{\partial C_B} = -\frac{3Pk}{2na_0}\left(\bar{U}_r q_{10} + \bar{U}_t q_{20} + \bar{U}_h q_{20}\cot i_0\right)\Delta t$$

Derivatives of C_B

$$\frac{\partial C_B}{\partial a_0} = \frac{\partial C_B}{\partial \theta_0} = \frac{\partial C_B}{\partial i_0} = \frac{\partial C_B}{\partial q_{10}} = \frac{\partial C_B}{\partial q_{20}} = 0$$

$$\frac{\partial C_B}{\partial C_{B0}} = 1$$ (C.8)

C.2   *D* Matrix

Derivatives of δa

$$a_\lambda = -\frac{2PkC_B}{n^2}\left[\left(-\sin\lambda - q_1\sin 2\lambda + q_2\cos 2\lambda\right)\bar{U}_r + \left(\cos\lambda + q_2\sin 2\lambda + q_1\cos 2\lambda\right)\bar{U}_t\right]$$

$$\frac{\partial\delta a}{\partial a} = -\frac{6PkC_B}{n^2 a}\left[\left(\cos\lambda + \frac{1}{2}q_1\cos 2\lambda + \frac{1}{2}q_2\sin 2\lambda\right)\bar{U}_r + \left(\sin\lambda - \frac{1}{2}q_2\cos 2\lambda + \frac{1}{2}q_1\sin 2\lambda\right)\bar{U}_t\right]$$

$$\frac{\partial\delta a}{\partial\theta} = a_\lambda\frac{\partial\lambda}{\partial\theta}$$

$$\frac{\partial\delta a}{\partial i} = -\frac{2PkC_B}{n^2}\left[\left(\cos\lambda + \frac{1}{2}q_1\cos 2\lambda + \frac{1}{2}q_2\sin 2\lambda\right)\frac{\partial\bar{U}_r}{\partial i} + \left(\sin\lambda - \frac{1}{2}q_2\cos 2\lambda + \frac{1}{2}q_1\sin 2\lambda\right)\frac{\partial\bar{U}_t}{\partial i}\right]$$

$$\frac{\partial\delta a}{\partial q_1} = -\frac{PkC_B}{n^2}\left(\bar{U}_r\cos 2\lambda + \bar{U}_t\sin 2\lambda\right) + a_\lambda\frac{\partial\lambda}{\partial q_1}$$

$$\frac{\partial\delta a}{\partial q_2} = -\frac{PkC_B}{n^2}\left(\bar{U}_r\sin 2\lambda - \bar{U}_t\cos 2\lambda\right) + a_\lambda\frac{\partial\lambda}{\partial q_2}$$

$$\frac{\partial\delta a}{\partial\Omega} = -\frac{2PkC_B}{n^2}\left[\left(\cos\lambda + \frac{1}{2}q_1\cos 2\lambda + \frac{1}{2}q_2\sin 2\lambda\right)\frac{\partial\bar{U}_r}{\partial\Omega} + \left(\sin\lambda - \frac{1}{2}q_2\cos 2\lambda + \frac{1}{2}q_1\sin 2\lambda\right)\frac{\partial\bar{U}_t}{\partial\Omega}\right]$$

$$\frac{\partial\delta a}{\partial C_B} = -\frac{2Pk}{n^2}\left[\left(\cos\lambda + \frac{1}{2}q_1\cos 2\lambda + \frac{1}{2}q_2\sin 2\lambda\right)\bar{U}_r + \left(\sin\lambda - \frac{1}{2}q_2\cos 2\lambda + \frac{1}{2}q_1\sin 2\lambda\right)\bar{U}_t\right]$$

(C.9)

Derivatives of $\delta\theta$

$$\frac{\partial \delta\theta}{\partial a} = \left(1 + 2q_1 \cos\lambda + 2q_2 \sin\lambda\right)\frac{\partial \delta\lambda}{\partial a} + 2\sin\lambda\frac{\partial \delta q_1}{\partial a} - 2\cos\lambda\frac{\partial \delta q_2}{\partial a}$$

$$\frac{\partial \delta\theta}{\partial \theta} = \left(1 + 2q_1 \cos\lambda + 2q_2 \sin\lambda\right)\frac{\partial \delta\lambda}{\partial \theta} + 2\sin\lambda\frac{\partial \delta q_1}{\partial \theta} - 2\cos\lambda\frac{\partial \delta q_2}{\partial \theta}$$

$$+2\left(-q_1 \sin\lambda + q_2 \cos\lambda\right)\frac{\partial \lambda}{\partial \theta}\delta\lambda + 2\cos\lambda\frac{\partial \lambda}{\partial \theta}\delta q_1 + 2\sin\lambda\frac{\partial \lambda}{\partial \theta}\delta q_2$$

$$\frac{\partial \delta\theta}{\partial i} = \left(1 + 2q_1 \cos\lambda + 2q_2 \sin\lambda\right)\frac{\partial \delta\lambda}{\partial a} + 2\sin\lambda\frac{\partial \delta q_1}{\partial i} - 2\cos\lambda\frac{\partial \delta q_2}{\partial i}$$

$$\frac{\partial \delta\theta}{\partial q_1} = \left(1 + 2q_1 \cos\lambda + 2q_2 \sin\lambda\right)\frac{\partial \delta\lambda}{\partial q_1} + 2\sin\lambda\frac{\partial \delta q_1}{\partial q_1} - 2\cos\lambda\frac{\partial \delta q_2}{\partial q_1} + 2\delta\lambda\cos\lambda \qquad \text{(C.10)}$$

$$\frac{\partial \delta\theta}{\partial q_2} = \left(1 + 2q_1 \cos\lambda + 2q_2 \sin\lambda\right)\frac{\partial \delta\lambda}{\partial q_2} + 2\sin\lambda\frac{\partial \delta q_1}{\partial q_2} - 2\cos\lambda\frac{\partial \delta q_2}{\partial q_2} + 2\delta\lambda\sin\lambda$$

$$\frac{\partial \delta\theta}{\partial \Omega} = \left(1 + 2q_1 \cos\lambda + 2q_2 \sin\lambda\right)\frac{\partial \delta\lambda}{\partial \Omega} + 2\sin\lambda\frac{\partial \delta q_1}{\partial \Omega} - 2\cos\lambda\frac{\partial \delta q_2}{\partial \Omega}$$

$$\frac{\partial \delta\theta}{\partial C_B} = \left(1 + 2q_1 \cos\lambda + 2q_2 \sin\lambda\right)\frac{\partial \delta\lambda}{\partial C_B} + 2\sin\lambda\frac{\partial \delta q_1}{\partial C_B} - 2\cos\lambda\frac{\partial \delta q_2}{\partial C_B}$$

Derivatives of δi

$$i_\lambda = -\frac{PkC_B\bar{U}_h}{2n^2a}\left(2\cos\lambda + q_1\cos 2\lambda + q_2\sin 2\lambda\right)$$

$$\frac{\partial\delta i}{\partial a} = -\frac{PkC_B\bar{U}_h}{n^2a^2}\left(2\sin\lambda + \frac{1}{2}q_1\sin 2\lambda - \frac{1}{2}q_2\cos 2\lambda\right)$$

$$\frac{\partial\delta i}{\partial\theta} = i_\lambda\frac{\partial\lambda}{\partial\theta}$$

$$\frac{\partial\delta i}{\partial i} = -\frac{PkC_B}{2n^2a}\left(2\sin\lambda + \frac{1}{2}q_1\sin 2\lambda - \frac{1}{2}q_2\cos 2\lambda\right)\frac{\partial\bar{U}_h}{\partial i}$$

$$\frac{\partial\delta i}{\partial q_1} = -\frac{PkC_B\bar{U}_h}{4n^2a}\sin 2\lambda + i_\lambda\frac{\partial\lambda}{\partial q_1}$$

$$\frac{\partial\delta i}{\partial q_2} = \frac{PkC_B\bar{U}_h}{4n^2a}\cos 2\lambda + i_\lambda\frac{\partial\lambda}{\partial q_2}$$

$$\frac{\partial\delta i}{\partial\Omega} = -\frac{PkC_B}{2n^2a}\left(2\sin\lambda + \frac{1}{2}q_1\sin 2\lambda - \frac{1}{2}q_2\cos 2\lambda\right)\frac{\partial\bar{U}_h}{\partial\Omega}$$

$$\frac{\partial\delta i}{\partial C_B} = -\frac{Pk\bar{U}_h}{2n^2a}\left(2\sin\lambda + \frac{1}{2}q_1\sin 2\lambda - \frac{1}{2}q_2\cos 2\lambda\right)$$

(C.11)

Derivatives of δq_1

$$q_{1\lambda} = -\frac{PkC_B}{4n^2a}\Big[\big(2\sin 2\lambda + q_1\sin\lambda + 5q_2\cos\lambda - 3q_1\sin 3\lambda + 3q_2\cos 3\lambda\big)\bar{U}_r$$
$$+\big(2\cos 2\lambda + 3q_2\sin\lambda - 3q_1\cos\lambda + 3q_2\sin 3\lambda + 3q_1\cos 3\lambda\big)\bar{U}_t\Big]$$

$$\frac{\partial\delta q_1}{\partial a} = -\frac{PkC_B}{2n^2a^2}\Big[\big(-\cos 2\lambda - q_1\cos\lambda + 5q_2\sin\lambda + q_1\cos 3\lambda + q_2\sin 3\lambda\big)\bar{U}_r$$
$$+\big(\sin 2\lambda - 3q_2\cos\lambda - 3q_1\sin\lambda - q_2\cos 3\lambda + q_1\sin 3\lambda\big)\bar{U}_t\Big] + q_2\cos i\frac{\partial\delta\Omega}{\partial a}$$

$$\frac{\partial\delta q_1}{\partial\theta} = q_{1\lambda}\frac{\partial\lambda}{\partial\theta} + q_2\cos i\frac{\partial\delta\Omega}{\partial\theta}$$

$$\frac{\partial\delta q_1}{\partial i} = -\frac{PkC_B}{4n^2a}\Big[\big(-\cos 2\lambda - q_1\cos\lambda + 5q_2\sin\lambda + q_1\cos 3\lambda + q_2\sin 3\lambda\big)\frac{\partial\bar{U}_r}{\partial i}$$
$$+\big(\sin 2\lambda - 3q_2\cos\lambda - 3q_1\sin\lambda - q_2\cos 3\lambda + q_1\sin 3\lambda\big)\frac{\partial\bar{U}_t}{\partial i}\Big]$$

$$+q_2\cos i\frac{\partial\Omega}{\partial i} - q_2\sin i\delta\Omega$$

$$\frac{\partial\delta q_1}{\partial q_1} = -\frac{PkC_B}{4n^2a}\Big[\big(-\cos\lambda + \cos 3\lambda\big)\bar{U}_r + \big(-3\sin\lambda + \sin 3\lambda\big)\bar{U}_t\Big] + q_{1\lambda}\frac{\partial\lambda}{\partial q_1} + q_2\cos i\frac{\partial\delta\Omega}{\partial q_1}$$

$$\frac{\partial\delta q_1}{\partial q_2} = -\frac{PkC_B}{4n^2a}\Big[\big(5\sin\lambda + \sin 3\lambda\big)\bar{U}_r - \big(3\cos\lambda + \cos 3\lambda\big)\bar{U}_t\Big] + q_{1\lambda}\frac{\partial\lambda}{\partial q_2} + q_2\cos i\frac{\partial\delta\Omega}{\partial q_2} + \cos i\delta\Omega$$

$$\frac{\partial\delta q_1}{\partial\Omega} = -\frac{PkC_B}{4n^2a}\Big[\big(-\cos 2\lambda - q_1\cos\lambda + 5q_2\sin\lambda + q_1\cos 3\lambda + q_2\sin 3\lambda\big)\frac{\partial\bar{U}_r}{\partial\Omega}$$
$$+\big(\sin 2\lambda - 3q_2\cos\lambda - 3q_1\sin\lambda - q_2\cos 3\lambda + q_1\sin 3\lambda\big)\frac{\partial\bar{U}_t}{\partial\Omega}\Big] + q_2\cos i\frac{\partial\delta\Omega}{\partial\Omega}$$

$$\frac{\partial\delta q_1}{\partial a} = -\frac{Pk}{4n^2a}\Big[\big(-\cos 2\lambda - q_1\cos\lambda + 5q_2\sin\lambda + q_1\cos 3\lambda + q_2\sin 3\lambda\big)\bar{U}_r$$
$$+\big(\sin 2\lambda - 3q_2\cos\lambda - 3q_1\sin\lambda - q_2\cos 3\lambda + q_1\sin 3\lambda\big)\bar{U}_t\Big] + q_2\cos i\frac{\partial\delta\Omega}{\partial C_B}$$

(C.12)

Derivatives of δq_2

$$q_{2\lambda} = -\frac{PkC_B}{4n^2a}\Big[\big(2\cos 2\lambda + 3q_2\sin\lambda - 3q_1\cos\lambda + 3q_2\sin 3\lambda + 3q_1\cos 3\lambda\big)\bar{U}_r$$
$$+\big(2\sin 2\lambda - 5q_1\sin\lambda - q_2\cos\lambda + 3q_1\sin 3\lambda - 3q_2\cos 3\lambda\big)\bar{U}_t\Big]$$

$$\frac{\partial\delta q_2}{\partial a} = -\frac{PkC_B}{2n^2a^2}\Big[\big(\sin 2\lambda - 3q_2\cos\lambda - 3q_1\sin\lambda - q_2\cos 3\lambda + q_1\sin 3\lambda\big)\bar{U}_r$$
$$+\big(-\cos 2\lambda + 5q_1\cos\lambda - q_2\sin\lambda - q_1\cos 3\lambda - q_2\sin 3\lambda\big)\bar{U}_t\Big] - q_1\cos i\frac{\partial\delta\Omega}{\partial a}$$

$$\frac{\partial\delta q_2}{\partial\theta} = q_{2\lambda}\frac{\partial\lambda}{\partial\theta} - q_1\cos i\frac{\partial\delta\Omega}{\partial\theta}$$

$$\frac{\partial\delta q_2}{\partial i} = -\frac{PkC_B}{4n^2a}\Big[\big(\sin 2\lambda - 3q_2\cos\lambda - 3q_1\sin\lambda - q_2\cos 3\lambda + q_1\sin 3\lambda\big)\frac{\partial\bar{U}_r}{\partial i}$$
$$+\big(-\cos 2\lambda + 5q_1\cos\lambda - q_2\sin\lambda - q_1\cos 3\lambda - q_2\sin 3\lambda\big)\frac{\partial\bar{U}_t}{\partial i}\Big]$$

$$-q_1\cos i\frac{\partial\delta\Omega}{\partial i} + q_1\sin i\delta\Omega$$

$$\frac{\partial\delta q_2}{\partial q_1} = -\frac{PkC_B}{4n^2a}\Big[\big(-3\sin\lambda + \sin 3\lambda\big)\bar{U}_r + \big(5\cos\lambda - \cos 3\lambda\big)\bar{U}_t\Big]$$
$$+q_{2\lambda}\frac{\partial\lambda}{\partial q_1} - \cos i\delta\Omega - q_1\cos i\frac{\partial\delta\Omega}{\partial q_1}$$

$$\frac{\partial\delta q_2}{\partial q_2} = \frac{PkC_B}{4n^2a}\Big[\big(3\cos\lambda + \cos 3\lambda\big)\bar{U}_r + \big(\sin\lambda + \sin 3\lambda\big)\bar{U}_t\Big] + q_{2\lambda}\frac{\partial\lambda}{\partial q_2} - q_1\cos i\frac{\partial\delta\Omega}{\partial q_2}$$

$$\frac{\partial\delta q_2}{\partial\Omega} = -\frac{PkC_B}{4n^2a}\Big[\big(\sin 2\lambda - 3q_2\cos\lambda - 3q_1\sin\lambda - q_2\cos 3\lambda + q_1\sin 3\lambda\big)\frac{\partial\bar{U}_r}{\partial\Omega}$$
$$+\big(-\cos 2\lambda + 5q_1\cos\lambda - q_2\sin\lambda - q_1\cos 3\lambda - q_2\sin 3\lambda\big)\frac{\partial\bar{U}_t}{\partial\Omega}\Big] - q_1\cos i\frac{\partial\delta\Omega}{\partial\Omega}$$

$$\frac{\partial\delta q_2}{\partial C_B} = -\frac{Pk}{4n^2a}\Big[\big(\sin 2\lambda - 3q_2\cos\lambda - 3q_1\sin\lambda - q_2\cos 3\lambda + q_1\sin 3\lambda\big)\bar{U}_r$$
$$+\big(-\cos 2\lambda + 5q_1\cos\lambda - q_2\sin\lambda - q_1\cos 3\lambda - q_2\sin 3\lambda\big)\bar{U}_t\Big] - q_1\cos i\frac{\partial\delta\Omega}{\partial C_B} \qquad (C.13)$$

Derivatives of $\delta\Omega$

$$\Omega_\lambda = \frac{PkC_B\bar{U}_h}{2n^2a\sin i}\left(-2\sin\lambda - q_1\sin 2\lambda + q_2\cos 2\lambda\right)$$

$$\frac{\partial\delta\Omega}{\partial a} = \frac{PkC_B\bar{U}_h}{n^2a^2\sin i}\left(2\cos\lambda + \frac{1}{2}q_1\cos 2\lambda + \frac{1}{2}q_2\sin 2\lambda\right)$$

$$\frac{\partial\delta\Omega}{\partial\theta} = \Omega_\lambda\frac{\partial\lambda}{\partial\theta}$$

$$\frac{\partial\delta\Omega}{\partial i} = \frac{PkC_B}{2n^2a\sin i}\left(-\bar{U}_h\cot i + \frac{\partial\bar{U}_h}{\partial i}\right)\left(2\cos\lambda + \frac{1}{2}q_1\cos 2\lambda + \frac{1}{2}q_2\sin 2\lambda\right)$$

$$\frac{\partial\delta\Omega}{\partial q_1} = \frac{PkC_B\bar{U}_h}{4n^2a\sin i}\cos 2\lambda + \Omega_\lambda\frac{\partial\lambda}{\partial q_1} \qquad\qquad\text{(C.14)}$$

$$\frac{\partial\delta\Omega}{\partial q_2} = \frac{PkC_B\bar{U}_h}{4n^2a\sin i}\sin 2\lambda + \Omega_\lambda\frac{\partial\lambda}{\partial q_2}$$

$$\frac{\partial\delta\Omega}{\partial\Omega} = \frac{PkC_B}{2n^2a\sin i}\left(2\cos\lambda + \frac{1}{2}q_1\cos 2\lambda + \frac{1}{2}q_2\sin 2\lambda\right)\frac{\partial\bar{U}_h}{\partial\Omega}$$

$$\frac{\partial\delta\Omega}{\partial C_B} = \frac{Pk\bar{U}_h}{2n^2a\sin i}\left(2\cos\lambda + \frac{1}{2}q_1\cos 2\lambda + \frac{1}{2}q_2\sin 2\lambda\right)$$

where

106

$$\lambda_\lambda = \frac{PkC_B}{n^2a}\Big[\big(\cos\lambda + 2q_1\cos 2\lambda + 2q_2\sin 2\lambda\big)\bar{U}_r - \big(-\sin\lambda + 2q_2\cos 2\lambda - 2q_1\sin 2\lambda\big)\bar{U}_t\Big]$$

$$\frac{\partial\delta\lambda}{\partial a} = \frac{2PkC_B}{n^2a^2}\Big[\big(\sin\lambda + q_1\sin 2\lambda - q_2\cos 2\lambda\big)\bar{U}_r - \big(\cos\lambda + q_2\sin 2\lambda + q_1\cos 2\lambda\big)\bar{U}_t\Big]$$
$$\qquad - \frac{\partial\delta\Omega}{\partial a}\cos i$$

$$\frac{\partial\delta\lambda}{\partial\theta} = \lambda_\lambda\frac{\partial\lambda}{\partial\theta} - \frac{\partial\delta\Omega}{\partial\theta}\cos i$$

$$\frac{\partial\delta\lambda}{\partial i} = \frac{PkC_B}{n^2a}\Big[\big(\sin\lambda + q_1\sin 2\lambda - q_2\cos 2\lambda\big)\frac{\partial\bar{U}_r}{\partial i} - \big(\cos\lambda + q_2\sin 2\lambda + q_1\cos 2\lambda\big)\frac{\partial\bar{U}_t}{\partial i}\Big]$$
$$\qquad + \delta\Omega\sin i - \cos i\frac{\partial\delta\Omega}{\partial i}$$

$$\frac{\partial\delta\lambda}{\partial q_1} = \frac{PkC_B}{n^2a}\big(\bar{U}_r\sin 2\lambda - \bar{U}_t\cos 2\lambda\big) + \lambda_\lambda\frac{\partial\lambda}{\partial q_1} - \cos i\frac{\partial\delta\Omega}{\partial q_1}$$

$$\frac{\partial\delta\lambda}{\partial q_2} = -\frac{PkC_B}{n^2a}\big(\bar{U}_r\cos 2\lambda + \bar{U}_t\sin 2\lambda\big) + \lambda_\lambda\frac{\partial\lambda}{\partial q_2} - \cos i\frac{\partial\delta\Omega}{\partial q_2}$$

$$\frac{\partial\delta\lambda}{\partial\Omega} = \frac{PkC_B}{n^2a}\Big[\big(\sin\lambda + q_1\sin 2\lambda - q_2\cos 2\lambda\big)\frac{\partial\bar{U}_r}{\partial\Omega} - \big(\cos\lambda + q_2\sin 2\lambda + q_1\cos 2\lambda\big)\frac{\partial\bar{U}_t}{\partial\Omega}\Big]$$
$$\qquad - \cos i\frac{\partial\delta\Omega}{\partial\Omega}$$

$$\frac{\partial\delta\lambda}{\partial C_B} = \frac{Pk}{n^2a}\Big[\big(\sin\lambda + q_1\sin 2\lambda - q_2\cos 2\lambda\big)\bar{U}_r - \big(\cos\lambda + q_2\sin 2\lambda + q_1\cos 2\lambda\big)\bar{U}_t\Big]$$
$$\qquad - \frac{\partial\delta\Omega}{\partial C_B}\cos i$$

(C.15)

Derivatives of δC_B

$$\frac{\partial\delta C_B}{\partial a} = \frac{\partial\delta C_B}{\partial\theta} = \frac{\partial\delta C_B}{\partial i} = \frac{\partial\delta C_B}{\partial q_1} = \frac{\partial\delta C_B}{\partial q_2} = \frac{\partial\delta C_B}{\partial C_B} = 0 \qquad\text{(C.16)}$$

where

$$\frac{\partial \bar{U}_r}{\partial i} = 0$$

$$\frac{\partial \bar{U}_r}{\partial \Omega} = -\sin \Omega \cos \lambda_e + \cos \Omega \sin \lambda_e \cos \varepsilon$$

$$\frac{\partial \bar{U}_t}{\partial i} = \sin \Omega \sin i \cos \lambda_e - \cos \Omega \sin i \sin \lambda_e \cos \varepsilon + \cos i \sin \lambda_e \sin \varepsilon$$

$$\frac{\partial \bar{U}_t}{\partial \Omega} = -\cos \Omega \cos i \cos \lambda_e - \sin \Omega \cos i \sin \lambda_e \cos \varepsilon$$

$$\frac{\partial \bar{U}_h}{\partial i} = \sin \Omega \cos i \cos \lambda_e - \cos \Omega \cos i \sin \lambda_e \cos \varepsilon - \sin i \sin \lambda_e \sin \varepsilon$$

$$\frac{\partial \bar{U}_h}{\partial \Omega} = \cos \Omega \sin i \cos \lambda_e + \sin \Omega \sin i \sin \lambda_e \cos \varepsilon$$

(C.17)

APPENDIX D. Φ AND *D* MATRIX FOR DRAG PERTURBATIONS
D.1 Φ Matrix

Derivatives for *a*

$$a = a_0 + \dot{a}\Delta t$$

$$\frac{\partial a}{\partial a_0} = 1 - anC_DC_B\rho_p\left(a\frac{\partial f_1}{\partial a_0} + \frac{1}{2}f_1\right)\Delta t - a^2nC_DC_Bf_1\frac{\partial \rho_p}{\partial a_0}\Delta t$$

$$\frac{\partial a}{\partial \theta_0} = 0$$

$$\frac{\partial a}{\partial i_0} = 0$$

$$\frac{\partial a}{\partial q_{10}} = -a^2nC_DC_B\rho_p\frac{\partial f_1}{\partial e_0}\frac{\partial e_0}{\partial q_{10}}\Delta t - a^2nC_DC_Bf_1\frac{\partial \rho_p}{\partial q_{10}}\Delta t \qquad \text{(D.1)}$$

$$\frac{\partial a}{\partial q_{20}} = -a^2nC_DC_B\rho_p\frac{\partial f_1}{\partial e_0}\frac{\partial e_0}{\partial q_{20}}\Delta t - a^2nC_DC_Bf_1\frac{\partial \rho_p}{\partial q_{20}}\Delta t$$

$$\frac{\partial a}{\partial \Omega_0} = 0$$

$$\frac{\partial a}{\partial C_{B0}} = -a^2nC_D\rho_Pf_1\Delta t$$

Derivatives for *i*

$$i = i_0$$

$$\frac{\partial i}{\partial i_0} = 1 \qquad \text{(D.2)}$$

$$\frac{\partial i}{\partial a_0} = \frac{\partial i}{\partial \theta_0} = \frac{\partial i}{\partial q_{10}} = \frac{\partial i}{\partial q_{20}} = \frac{\partial i}{\partial \Omega_0} = \frac{\partial i}{\partial C_{B0}} = 0$$

Derivatives for q_1

$$q_1 = e\cos\omega = \left(e_0 + \dot{e}\Delta t\right)\cos\omega_0 = \left(1 + \frac{\dot{e}}{e_0}\Delta t\right)q_{10} = \left(1 + f_3\Delta t\right)q_{10}$$

$$\frac{\partial q_1}{\partial a_0} = q_{10}\Delta t \frac{\partial f_3}{\partial a_0}$$

$$\frac{\partial q_1}{\partial \theta_0} = 0$$

$$\frac{\partial q_1}{\partial i_0} = 0$$

(D.3)

$$\frac{\partial q_1}{\partial q_{10}} = 1 + f_3\Delta t + q_{10}\Delta t \frac{\partial f_3}{\partial e_0}\frac{\partial e_0}{\partial q_{10}}$$

$$\frac{\partial q_1}{\partial q_{20}} = q_{10}\Delta t \frac{\partial f_3}{\partial e_0}\frac{\partial e_0}{\partial q_{20}}$$

$$\frac{\partial q_1}{\partial \Omega_0} = 0$$

$$\frac{\partial q_1}{\partial C_{B0}} = -anC_D\eta^2\rho_P f_4 q_{10}\Delta t$$

Derivatives for q_2

$$q_2 = e\sin\omega = \left(e_0 + \dot{e}\Delta t\right)\sin\omega_0 = \left(1 + \frac{\dot{e}}{e_0}\Delta t\right)q_{20} = \left(1 + f_3\Delta t\right)q_{20}$$

$$\frac{\partial q_2}{\partial a_0} = q_{20}\Delta t\frac{\partial f_3}{\partial a_0}$$

$$\frac{\partial q_2}{\partial \theta_0} = 0$$

$$\frac{\partial q_2}{\partial i_0} = 0$$

$$\frac{\partial q_2}{\partial q_{10}} = q_{20}\Delta t\frac{\partial f_3}{\partial e_0}\frac{\partial e_0}{\partial q_{10}}$$

$$\frac{\partial q_2}{\partial q_{20}} = 1 + f_3\Delta t + q_{20}\Delta t\frac{\partial f_3}{\partial e_0}\frac{\partial e_0}{\partial q_{20}}$$

$$\frac{\partial q_2}{\partial \Omega_0} = 0$$

$$\frac{\partial q_2}{\partial C_{B0}} = -anC_D\eta^2\rho_P f_4 q_{20}\Delta t$$

(D.4)

Derivatives for Ω

$$\Omega = \Omega_0$$

$$\frac{\partial \Omega}{\partial \Omega_0} = 1$$

$$\frac{\partial \Omega}{\partial a_0} = \frac{\partial \Omega}{\partial \theta_0} = \frac{\partial \Omega}{\partial i_0} = \frac{\partial \Omega}{\partial q_{10}} = \frac{\partial \Omega}{\partial q_{20}} = \frac{\partial \Omega}{\partial C_{B0}} = 0$$

(D.5)

Derivatives for θ

$$\frac{\partial \theta}{\partial a_0} = \left(\frac{\partial \dot{\lambda}}{\partial a_0} \Delta t - \frac{\partial G}{\partial q_1} \frac{\partial q_1}{\partial a_0} - \frac{\partial G}{\partial q_2} \frac{\partial q_2}{\partial a_0} \right) \Big/ \frac{\partial G}{\partial \theta}$$

$$\frac{\partial \theta}{\partial \theta_0} = \frac{\partial G}{\partial \theta_0} \Big/ \frac{\partial G}{\partial \theta}$$

$$\frac{\partial \theta}{\partial i_0} = \left(\frac{\partial \dot{\lambda}}{\partial i_0} \Delta t - \frac{\partial G}{\partial q_1} \frac{\partial q_1}{\partial i_0} - \frac{\partial G}{\partial q_2} \frac{\partial q_2}{\partial i_0} \right) \Big/ \frac{\partial G}{\partial \theta}$$

$$\frac{\partial \theta}{\partial q_{10}} = \left(\frac{\partial \dot{\lambda}}{\partial q_{10}} \Delta t - \frac{\partial G}{\partial q_{10}} - \frac{\partial G}{\partial q_1} \frac{\partial q_1}{\partial q_{10}} - \frac{\partial G}{\partial q_2} \frac{\partial q_2}{\partial q_{10}} \right) \Big/ \frac{\partial G}{\partial \theta} \qquad \text{(D.6)}$$

$$\frac{\partial \theta}{\partial q_{20}} = \left(\frac{\partial \dot{\lambda}}{\partial q_{20}} \Delta t - \frac{\partial G}{\partial q_{10}} - \frac{\partial G}{\partial q_1} \frac{\partial q_1}{\partial q_{20}} - \frac{\partial G}{\partial q_2} \frac{\partial q_2}{\partial q_{20}} \right) \Big/ \frac{\partial G}{\partial \theta}$$

$$\frac{\partial \theta}{\partial \Omega_0} = 0$$

$$\frac{\partial \theta}{\partial C_{B0}} = 0$$

where

$$f_1 = \left[I_0 + 2eI_1 + \tfrac{3}{4}e^2 \left(I_0 + I_2 \right) \right] \exp\left(-\beta ae \right)$$

$$f_2 = \left[I_1 + \tfrac{1}{2}e\left(I_0 + I_2 \right) + \tfrac{1}{8}e^2 \left(3I_1 + I_3 \right) \right] \exp\left(-\beta ae \right) \qquad \text{(D.7)}$$

$$f_3 = -ank\eta^2 \rho_p \frac{f_2}{e} = -ank\eta^2 \rho_p f_4$$

$$f_4 = \tfrac{1}{2} \left[\left(1 + a\beta \right) I_0 + \left(1 - a\beta \right) I_2 + \tfrac{1}{4}e\left(3I_1 + I_3 \right) \right] \exp\left(-\beta ae \right)$$

Derivatives of f_1, f_3, f_4

$$\frac{\partial f_1}{\partial a} = \beta e \left[-I_0 + I_1 + 2\left(eI_0 - I_1/\beta a - eI_1 \right) + \tfrac{3}{4}e\left(2eI_1 - eI_0 - eI_2 - 2I_2/\beta a \right) \right] \exp\left(-\beta ae \right)$$

$$= \beta e f_{11} \qquad \text{(D.8)}$$

$$\frac{\partial f_1}{\partial e} = a\beta f_{11} + \left[2I_1 + \tfrac{3}{2}e\left(I_0 + I_2 \right) \right] \exp\left(-\beta ae \right)$$

$$\frac{\partial f_3}{\partial a} = \tfrac{1}{2} n C_D C_B \eta^2 \rho_p f_4 - a n C_D C_B \eta^2 \rho_p \frac{\partial f_4}{\partial a} - a n C_D C_B \eta^2 f_4 \frac{\partial \rho_p}{\partial a}$$

$$\frac{\partial f_3}{\partial e} = 2 a n C_D C_B e \rho_p f_4 - a n C_D C_B \eta^2 \rho_p \frac{\partial f_4}{\partial e} - a n C_D C_B \eta^2 f_4 \frac{\partial \rho_p}{\partial e} \tag{D.9}$$

$$\frac{\partial f_4}{\partial a} = \tfrac{1}{2}[\left(1 - e + \tfrac{3}{4} e^2 - \beta a e\right) \beta I_0 + \left(2\beta - \tfrac{3}{4} a^{-1} - \tfrac{3}{4} \beta e\right) e I_1 +$$

$$\left(\beta - 2 a^{-1} + \tfrac{1}{4} \beta e^2 - \beta e + \beta^2 a e\right) I_2 - \tfrac{1}{4}\left(3 a^{-1} + \beta e\right) e I_3] \exp(-\beta a e)$$

$$\frac{\partial f_4}{\partial e} = \tfrac{1}{2}[\left(-\tfrac{1}{4} \beta a e + \tfrac{1}{4} \beta^2 a^2 e + \tfrac{3}{4} e - \beta a - 1\right) \beta a I_0 + \left(2 - \tfrac{3}{4} e\right) \beta a I_1 - \tfrac{1}{2}\left(\tfrac{1}{2} \beta a e + 1\right) I_3 \tag{D.10}$$

$$+ \left(\tfrac{1}{3} \beta a e - \tfrac{1}{3} \beta^2 a^2 e + \tfrac{1}{4} e + \beta a - 1\right) \beta a I_2 - \tfrac{1}{12}\left(1 - \beta a\right) \beta^2 a^2 e I_4] \exp(-\beta a e)$$

D.2 *D* Matrix

Derivatives of δa

$$\frac{\partial \delta a}{\partial a} = \left(\frac{\partial \delta a_1}{\partial a} + \frac{\partial \delta a_1}{\partial \rho_p} \frac{\partial \delta \rho_p}{\partial a}\right) \delta a_2 + \frac{\partial \delta a_2}{\partial a} \delta a_1$$

$$\frac{\partial \delta a}{\partial \theta} = \delta a_1 \frac{\partial \delta a_2}{\partial \lambda} \frac{\partial \lambda}{\partial \theta}$$

$$\frac{\partial \delta a}{\partial i} = 0$$

$$\frac{\partial \delta a}{\partial q_1} = \left(\frac{\partial \delta a_1}{\partial q_1} + \frac{\partial \delta a_1}{\partial \rho_p} \frac{\partial \delta \rho_p}{\partial q_1}\right) \delta a_2 + \left(\frac{\partial \delta a_2}{\partial q_1} + \frac{\partial \delta a_2}{\partial \lambda} \frac{\partial \lambda}{\partial q_1}\right) \delta a_1 \tag{D.11}$$

$$\frac{\partial \delta a}{\partial q_2} = \left(\frac{\partial \delta a_1}{\partial q_2} + \frac{\partial \delta a_1}{\partial \rho_p} \frac{\partial \delta \rho_p}{\partial q_2}\right) \delta a_2 + \left(\frac{\partial \delta a_2}{\partial q_2} + \frac{\partial \delta a_2}{\partial \lambda} \frac{\partial \lambda}{\partial q_2}\right) \delta a_1$$

$$\frac{\partial \delta a}{\partial \Omega} = 0$$

$$\frac{\partial \delta a}{\partial C_B} = -a^2 C_D \rho_P \exp(-\xi e) \delta a_2$$

where

$$\delta a = \delta a_1 \delta a_2$$

$$\delta a_1 = -a^2 C_D C_B \rho_p \exp(-\xi e) \tag{D.12}$$

$$\delta a_2 = (\xi + 3)(q_1 \sin\lambda - q_2 \cos\lambda) + \frac{1}{8}\xi^2(q_1^2 - q_2^2)\sin 2\lambda - \frac{1}{4}\xi^2 q_1 q_2 \cos 2\lambda$$

$$\frac{\partial \delta a_1}{\partial a} = aC_D C_B \rho_p \exp(-\xi e)(\xi e - 2)$$

$$\frac{\partial \delta a_1}{\partial q_1} = a^2 C_D C_B \rho_p \xi \exp(-\xi e)\cos\omega$$

$$\frac{\partial \delta a_1}{\partial q_2} = a^2 C_D C_B \rho_p \xi \exp(-\xi e)\sin\omega$$

$$\frac{\partial \delta a_1}{\partial \rho_p} = -a^2 C_D C_B \exp(-\xi e) \tag{D.13}$$

$$\frac{\partial \delta \rho_p}{\partial a} = -\frac{\rho_0}{H}\exp\left(-\frac{r_p - r_0}{H}\right)(1 - e)$$

$$\frac{\partial \delta \rho_p}{\partial q_1} = \rho_0 \xi \exp\left(-\frac{r_p - r_0}{H}\right)\cos\omega$$

$$\frac{\partial \delta \rho_p}{\partial q_2} = \rho_0 \xi \exp\left(-\frac{r_p - r_0}{H}\right)\sin\omega$$

$$\frac{\partial \delta a_2}{\partial a} = \frac{1}{H}(q_1 \sin\lambda - q_2 \cos\lambda) + \frac{\xi}{4H}(q_1^2 - q_2^2)\sin 2\lambda - \frac{\xi}{2H}q_1 q_2 \cos 2\lambda$$

$$\frac{\partial \delta a_2}{\partial \lambda} = (\xi + 3)(q_1 \cos\lambda + q_2 \sin\lambda) + \frac{\xi^2}{4}(q_1^2 - q_2^2)\cos 2\lambda + \frac{\xi^2}{2}q_1 q_2 \sin 2\lambda$$

$$\frac{\partial \lambda}{\partial \theta} = \frac{1}{1 + 2q_1 \cos\lambda + 2q_2 \sin\lambda} \tag{D.14}$$

$$H = \frac{1}{\beta}$$

Derivatives of δi

$$\frac{\partial \delta i}{\partial a} = \frac{\partial \delta i}{\partial \theta} = \frac{\partial \delta i}{\partial i} = \frac{\partial \delta i}{\partial q_1} = \frac{\partial \delta i}{\partial q_2} = \frac{\partial \delta i}{\partial \Omega} = \frac{\partial \delta i}{\partial C_B} = 0 \tag{D.15}$$

Derivatives of δq_1

$$\frac{\partial \delta q_1}{\partial a} = \left(\frac{\partial \delta q_{11}}{\partial a} + \frac{\partial \delta q_{11}}{\partial \rho_p} \frac{\partial \delta \rho_p}{\partial a} \right) \delta q_{12} + \frac{\partial \delta q_{12}}{\partial a} \delta q_{11}$$

$$\frac{\partial \delta q_1}{\partial \theta} = \delta q_{11} \frac{\partial \delta q_{12}}{\partial \lambda} \frac{\partial \lambda}{\partial \theta}$$

$$\frac{\partial \delta q_1}{\partial i} = 0$$

$$\frac{\partial \delta q_1}{\partial q_1} = \left(\frac{\partial \delta q_{11}}{\partial q_1} + \frac{\partial \delta q_{11}}{\partial \rho_p} \frac{\partial \delta \rho_p}{\partial q_1} \right) \delta q_{12} + \left(\frac{\partial \delta q_{12}}{\partial q_1} + \frac{\partial \delta q_{12}}{\partial \lambda} \frac{\partial \lambda}{\partial q_1} \right) \delta q_{11} \qquad \text{(D.16)}$$

$$\frac{\partial \delta q_1}{\partial q_2} = \left(\frac{\partial \delta q_{11}}{\partial q_2} + \frac{\partial \delta q_{11}}{\partial \rho_p} \frac{\partial \delta \rho_p}{\partial q_2} \right) \delta q_{12} + \left(\frac{\partial \delta q_{12}}{\partial q_2} + \frac{\partial \delta q_{12}}{\partial \lambda} \frac{\partial \lambda}{\partial q_2} \right) \delta q_{11}$$

$$\frac{\partial \delta q_1}{\partial \Omega} = 0$$

$$\frac{\partial \delta q_1}{\partial C_B} = -\frac{1}{2} a C_D \rho_P \exp(-\xi e) \delta q_{12}$$

where

$$\delta q_1 = \delta q_{11} \delta q_{12}$$

$$\delta q_{11} = -\frac{1}{2} a C_D C_B \rho_p \exp(-\xi e)$$

$$\delta q_{12} = \left(2 + \frac{3}{4} \xi^2 q_1^2 + \frac{1}{4} \xi^2 q_2^2 \right) \sin \lambda - \frac{1}{2} \xi^2 q_1 q_2 \cos \lambda + \qquad \text{(D.17)}$$

$$\frac{1}{2}(\xi + 3)(q_1 \sin 2\lambda - q_2 \cos 2\lambda) + \frac{1}{12} \xi^2 (q_1^2 - q_2^2) \sin 3\lambda - \frac{1}{6} \xi^2 q_1 q_2 \cos 3\lambda$$

$$\frac{\partial \delta q_{11}}{\partial a} = -\frac{1}{2} C_D C_B \rho_p \exp(-\xi e)(1 - \xi e)$$

$$\frac{\partial \delta q_{11}}{\partial q_1} = \frac{1}{2} a C_D C_B \rho_p \xi \exp(-\xi e) \cos \omega$$

$$\frac{\partial \delta q_{11}}{\partial q_2} = \frac{1}{2} a C_D C_B \rho_p \xi \exp(-\xi e) \sin \omega \qquad \text{(D.18)}$$

$$\frac{\partial \delta q_{11}}{\partial \rho_p} = -\frac{1}{2} a C_D C_B \exp(-\xi e)$$

$$\frac{\partial \delta q_{12}}{\partial a} = \left(\frac{3}{2}q_1^2 + \frac{1}{2}q_2^2\right)\frac{\xi}{H}\sin\lambda - \frac{\xi}{H}q_1 q_2 \cos\lambda +$$

$$\frac{1}{2H}\left(q_1 \sin 2\lambda - q_2 \cos 2\lambda\right) + \frac{1}{6}\frac{\xi}{H}\left(q_1^2 - q_2^2\right)\sin 3\lambda - \frac{1}{3}\frac{\xi}{H}q_1 q_2 \cos 3\lambda$$

$$\frac{\partial \delta q_{12}}{\partial \lambda} = \left(2 + \frac{3}{4}\xi^2 q_1^2 + \frac{1}{4}\xi^2 q_2^2\right)\cos\lambda + \frac{1}{2}\xi^2 q_1 q_2 \sin\lambda +$$

$$\left(\xi + 3\right)\left(q_1 \cos 2\lambda + q_2 \sin 2\lambda\right) + \frac{1}{4}\xi^2\left(q_1^2 - q_2^2\right)\cos 3\lambda + \frac{1}{2}\xi^2 q_1 q_2 \sin 3\lambda$$

$$\frac{\partial \delta q_{12}}{\partial q_1} = \frac{\xi^2}{2}\left(3q_1 \sin\lambda - q_2 \cos\lambda\right) + \frac{\xi+3}{2}\sin 2\lambda + \frac{\xi^2}{6}\left(q_1 \sin 3\lambda - q_2 \cos 3\lambda\right)$$

$$\frac{\partial \delta q_{12}}{\partial q_2} = \frac{\xi^2}{2}\left(q_2 \sin\lambda - q_1 \cos\lambda\right) - \frac{\xi+3}{2}\cos 2\lambda - \frac{\xi^2}{6}\left(q_2 \sin 3\lambda + q_1 \cos 3\lambda\right)$$

(D.19)

Derivatives of δq_2

$$\frac{\partial \delta q_2}{\partial a} = \left(\frac{\partial \delta q_{21}}{\partial a} + \frac{\partial \delta q_{21}}{\partial \rho_p} \frac{\partial \delta \rho_p}{\partial a} \right) \delta q_{22} + \frac{\partial \delta q_{12}}{\partial a} \delta q_{21}$$

$$\frac{\partial \delta q_2}{\partial \theta} = \delta q_{21} \frac{\partial \delta q_{22}}{\partial \lambda} \frac{\partial \lambda}{\partial \theta}$$

$$\frac{\partial \delta q_2}{\partial i} = 0$$

$$\frac{\partial \delta q_2}{\partial q_1} = \left(\frac{\partial \delta q_{21}}{\partial q_1} + \frac{\partial \delta q_{21}}{\partial \rho_p} \frac{\partial \delta \rho_p}{\partial q_1} \right) \delta q_{22} + \left(\frac{\partial \delta q_{22}}{\partial q_1} + \frac{\partial \delta q_{22}}{\partial \lambda} \frac{\partial \lambda}{\partial q_1} \right) \delta q_{21} \qquad \text{(D.20)}$$

$$\frac{\partial \delta q_2}{\partial q_2} = \left(\frac{\partial \delta q_{21}}{\partial q_2} + \frac{\partial \delta q_{21}}{\partial \rho_p} \frac{\partial \delta \rho_p}{\partial q_2} \right) \delta q_{22} + \left(\frac{\partial \delta q_{22}}{\partial q_2} + \frac{\partial \delta q_{22}}{\partial \lambda} \frac{\partial \lambda}{\partial q_2} \right) \delta q_{21}$$

$$\frac{\partial \delta q_2}{\partial \Omega} = 0$$

$$\frac{\partial \delta q_2}{\partial C_B} = -\frac{1}{2} a C_D \rho_P \exp(-\xi e) \delta q_{22}$$

Derivatives of $\delta \Omega$

$$\frac{\partial \delta \Omega}{\partial a} = \frac{\partial \delta \Omega}{\partial \theta} = \frac{\partial \delta \Omega}{\partial i} = \frac{\partial \delta \Omega}{\partial q_1} = \frac{\partial \delta \Omega}{\partial q_2} = \frac{\partial \delta \Omega}{\partial \Omega} = \frac{\partial \delta \Omega}{\partial C_B} = 0 \qquad \text{(D.21)}$$

Derivatives of $\delta\theta$

$$\frac{\partial\delta\theta}{\partial a} = \left(1 + 2q_1\cos\lambda + 2q_2\sin\lambda\right)\frac{\partial\delta\lambda}{\partial a} + 2\sin\lambda\frac{\partial\delta q_1}{\partial a} - 2\cos\lambda\frac{\partial\delta q_2}{\partial a}$$

$$\frac{\partial\delta\theta}{\partial\theta} = \left(1 + 2q_1\cos\lambda + 2q_2\sin\lambda\right)\frac{\partial\delta\lambda}{\partial\theta} + 2\sin\lambda\frac{\partial\delta q_1}{\partial\theta} - 2\cos\lambda\frac{\partial\delta q_2}{\partial\theta}$$

$$+ 2\left(-q_1\sin\lambda + q_2\cos\lambda\right)\frac{\partial\lambda}{\partial\theta}\delta\lambda + 2\cos\lambda\frac{\partial\lambda}{\partial\theta}\delta q_1 + 2\sin\lambda\frac{\partial\lambda}{\partial\theta}\delta q_2$$

$$\frac{\partial\delta\theta}{\partial i} = \left(1 + 2q_1\cos\lambda + 2q_2\sin\lambda\right)\frac{\partial\delta\lambda}{\partial a} + 2\sin\lambda\frac{\partial\delta q_1}{\partial i} - 2\cos\lambda\frac{\partial\delta q_2}{\partial i}$$

$$\frac{\partial\delta\theta}{\partial q_1} = \left(1 + 2q_1\cos\lambda + 2q_2\sin\lambda\right)\frac{\partial\delta\lambda}{\partial q_1} + 2\sin\lambda\frac{\partial\delta q_1}{\partial q_1} - 2\cos\lambda\frac{\partial\delta q_2}{\partial q_1} + 2\delta\lambda\cos\lambda \qquad \text{(D.22)}$$

$$\frac{\partial\delta\theta}{\partial q_2} = \left(1 + 2q_1\cos\lambda + 2q_2\sin\lambda\right)\frac{\partial\delta\lambda}{\partial q_2} + 2\sin\lambda\frac{\partial\delta q_1}{\partial q_2} - 2\cos\lambda\frac{\partial\delta q_2}{\partial q_2} + 2\delta\lambda\sin\lambda$$

$$\frac{\partial\delta\theta}{\partial\Omega} = \left(1 + 2q_1\cos\lambda + 2q_2\sin\lambda\right)\frac{\partial\delta\lambda}{\partial\Omega} + 2\sin\lambda\frac{\partial\delta q_1}{\partial\Omega} - 2\cos\lambda\frac{\partial\delta q_2}{\partial\Omega}$$

$$\frac{\partial\delta\theta}{\partial C_B} = \left(1 + 2q_1\cos\lambda + 2q_2\sin\lambda\right)\frac{\partial\delta\lambda}{\partial C_B} + 2\sin\lambda\frac{\partial\delta q_1}{\partial C_B} - 2\cos\lambda\frac{\partial\delta q_2}{\partial C_B}$$

where

$$\frac{\partial\delta\lambda}{\partial a} = \left(\frac{\partial\delta\lambda_1}{\partial a} + \frac{\partial\delta\lambda_1}{\partial\rho_p}\frac{\partial\delta\rho_p}{\partial a}\right)\delta\lambda_2 + \frac{\partial\delta\lambda_2}{\partial a}\delta\lambda_1$$

$$\frac{\partial\delta\lambda}{\partial\theta} = \delta\lambda_1\frac{\partial\delta\lambda_2}{\partial\lambda}\frac{\partial\lambda}{\partial\theta}$$

$$\frac{\partial\delta\lambda}{\partial i} = 0$$

$$\frac{\partial\delta\lambda}{\partial q_1} = \left(\frac{\partial\delta\lambda_1}{\partial q_1} + \frac{\partial\delta\lambda_1}{\partial\rho_p}\frac{\partial\delta\rho_p}{\partial q_1}\right)\delta\lambda_2 + \left(\frac{\partial\delta\lambda_2}{\partial q_1} + \frac{\partial\delta\lambda_2}{\partial\lambda}\frac{\partial\lambda}{\partial q_1}\right)\delta\lambda_1 \qquad \text{(D.23)}$$

$$\frac{\partial\delta\lambda}{\partial q_2} = \left(\frac{\partial\delta\lambda_1}{\partial q_2} + \frac{\partial\delta\lambda_1}{\partial\rho_p}\frac{\partial\delta\rho_p}{\partial q_2}\right)\delta\lambda_2 + \left(\frac{\partial\delta\lambda_2}{\partial q_2} + \frac{\partial\delta\lambda_2}{\partial\lambda}\frac{\partial\lambda}{\partial q_2}\right)\delta\lambda_1$$

$$\frac{\partial\delta\lambda}{\partial\Omega} = 0$$

$$\frac{\partial\delta\lambda}{\partial C_B} = \frac{1}{2}aC_D\rho_P\exp\left(-\xi e\right)\delta\lambda_2$$

and

$$\delta\lambda = \delta\lambda_1 \delta\lambda_2$$

$$\delta\lambda_1 = \frac{1}{2} a C_D C_B \rho_p \exp\left(-\xi e\right) \tag{D.24}$$

$$\delta\lambda_2 = q_1 \cos\lambda + q_2 \sin\lambda$$

$$\frac{\partial \delta\lambda_1}{\partial a} = \frac{1}{2} C_D C_B \rho_p \exp\left(-\xi e\right)\left(1 - \xi e\right)$$

$$\frac{\partial \delta\lambda_1}{\partial q_1} = -\frac{1}{2} a C_D C_B \rho_p \xi \exp\left(-\xi e\right) \cos\omega$$

$$\frac{\partial \delta\lambda_1}{\partial q_2} = -\frac{1}{2} a C_D C_B \rho_p \xi \exp\left(-\xi e\right) \sin\omega \tag{D.25}$$

$$\frac{\partial \delta\lambda_1}{\partial \rho_p} = \frac{1}{2} a C_D C_B \exp\left(-\xi e\right)$$

$$\frac{\partial \delta\lambda_2}{\partial a} = 0$$

$$\frac{\partial \delta\lambda_2}{\partial \lambda} = -q_1 \sin\lambda + q_2 \cos\lambda$$

$$\frac{\partial \delta\lambda_2}{\partial q_1} = \cos\lambda \tag{D.26}$$

$$\frac{\partial \delta\lambda_2}{\partial q_2} = \sin\lambda$$

LIST OF ACRONYMS, ABBREVIATIONS, AND SYMBOLS

Acronym/ Abbreviation	Description
AMR	Area-to mass ratio
GA-STM	Gim Alfriend-State Transition Matrix
GMAT	Goddard General Mission Analysis Tool
GNC	Guidance, navigation, and control
GUI	Graphical User Interface
LEO	Low earth orbit
LVLH	Local vertical local horizontal
MMS	Magnetospheric Multiscale
NASA	National Aeronautics and Space Administration
PCO	Projected Circular Orbit
RMS	Root mean square
SRP	Solar radiation pressure
STM	State Transition Matrix

DISTRIBUTION LIST

DTIC/OCP
8725 John J. Kingman Rd, Suite 0944
Ft Belvoir, VA 22060-6218   1 cy

AFRL/RVIL
Kirtland AFB, NM 87117-5776   2 cys

Official Record Copy
AFRL/RVSV/T. Alan Lovell   1 cy

(This page intentionally left blank)